Cyclometalated Ruthenium(II) Complexes and their Incorporation into the Metal-Organic Framework UiO-67 for Photocatalytic CO_2 Reduction

Dissertation for the Degree of

Philosophiae Doctor

Eirik Mydske Thoresen

Department of Chemistry

Faculty of Mathematics and Natural Sciences

University of Oslo

2018

Series of dissertations submitted to the
Faculty of Mathematics and Natural Sciences, University of Oslo
No. 2031

ISSN 1501-7710

Cover: Hanne Baadsgaard Utigard.
Print production: Reprosentralen, University of Oslo.

Vissi d'arte, vissi d'amore

Preface

This PhD thesis is the outcome of four years of research carried out at, and financed by, the Department of Chemistry at the University of Oslo. During this period, I have also passed 35 ECTS credits worth of courses and have been teaching in an undergraduate course in general chemistry.

I am grateful to have had the possibility to study fascinating scientific topics at such a high quality research institution. It is truly a good day at work when you discover that you finally created that new molecule you have been aiming for, or when the material you have developed shows some very promising properties. I have learned a wide range of different synthetic and characterization methods that combined offer many possibilities for future research. On my trips to conferences in Sweden, Germany, and the United States, I have had the pleasure to meet and discuss research with scientists from around the world.

None of this would have been possible without all the talented and helpful people at the department, especially in the catalysis group. My supervisors Mohamed Amedjkouh and Mats Tilset have been inspiring and supportive, and their doors have always been open for me whether I have had small or big conundrums to discuss. Many thanks go out to Per-Anders Stensby Hansen, for help with the UV-Vis measurements, Kristian Blindheim Lausund, for help with SEM and EDS, and Emil Sebastian Gutterød, for help with the GC. Thanks to Isabelle, Greig, Jakob, and Stefan for giving me valuable feedback on the thesis.

During these years, I have shared office with a bunch of great people which, each in their own way, made every day interesting: Giuseppe, Isabelle, Jakob, Kim, Carlo, Matías, and the master students on visit from Bari: Francesca, Marta, Alessia, and Alessandra. Siete le migliori!

Thanks to all the fantastic people in Skala Operakor for the joy of blasting out massive Verdi choir pieces and other hits every Monday.

Finally, I would like to thank my family and friends for their support and encouragement through the years and for being who they are.

Eirik Mydske Thoresen

Blindern, August 2018

Table of Contents

List of Publications

Paper I: *Cyclometalated Ruthenium Complexes with Carboxylated Ligands from a Combined Experimental/Computational Perspective*. Eirik Mydske Thoresen, David Balcells, Sigurd Øien-Ødegaard, Knut Tormodssønn Hylland, Mats Tilset, and Mohamed Amedjkouh. *Dalton Trans.* **2018,** *47* (8), 2589-2601.

Paper II: *Strongly Visible Light-Absorbing Metal-Organic Frameworks Functionalized by Cyclometalated Ruthenium(II) Complexes*. Eirik Mydske Thoresen, Mats Tilset, Karl Petter Lillerud, Sigurd Øien-Ødegaard, Gurpreet Kaur, and Mohamed Amedjkouh. *Preliminary manuscript*.

The Author's Contribution

Paper I: Performed synthesis of all samples, except diethyl 2,2'-bipyridine-5,5'-dicarboxylate. Performed all NMR, MS, and UV-Vis measurements. Growth of single crystals. Preparation of manuscript and figures, except single crystal structures and a figure related to TD-DFT (Fig. 5).

Paper II: Performed synthesis of all samples, except the pristine UiO-67 and UiO-67-bpy. Developed the postsynthetic methods. Performed all PXRD, nitrogen sorption, TGA-DSC, digestion/NMR, SEM, EDS, DR-UV-Vis measurements. Preparation of manuscript and figures, except single crystal structures.

List of Oral and Poster Contributions at Conferences

Metal organic frameworks (MOFs) with functionalized linkers as photosensitizers for photocatalytic CO2 reduction. Eirik Mydske Thoresen, Mats Tilset, Karl Petter Lillerud, and Mohamed Amedjkouh. **Poster** presented at the 30th Organic Chemistry Winter Meeting (OKV 30), January 2015, Skeikampen, Norway.

Metal organic frameworks (MOFs) with functionalized linkers as photosensitizers for photocatalytic CO2 reduction. Eirik Mydske Thoresen, Mats Tilset, Karl Petter Lillerud, and Mohamed Amedjkouh. **Poster** presented at the 3rd Nordic Meeting on Organometallic Chemistry, March 2015, Lund, Sweden.

Functionalized linkers as photosensitizers in UiO-67 MOFs for photocatalytic CO2 reduction. Eirik Mydske Thoresen, Mats Tilset, Karl Petter Lillerud, and Mohamed Amedjkouh. **Poster** presented at the 1st European Conference on Metal Organic Frameworks and Porous Polymers (EuroMOF 2015), October 2015, Potsdam, Germany.

Novel Ruthenium Functionalized Linkers for Photosensitization of Metal-Organic Frameworks. Eirik Mydske Thoresen, Mohamed Amedjkouh, Mats Tilset, Karl Petter Lillerud, Sigurd Øien-Ødegaard, and David Balcells. **Oral presentation** at the 5th International Conference on Metal-Organic Frameworks and Open Framework Compounds, September 2016, Long Beach, California, USA.

Scope

The primary objective of this PhD thesis was originally to develop metal-organic frameworks (MOFs) as catalysts for CO_2 activation. This objective was rapidly specified to become photocatalytic reduction of CO_2. Ru(II) complexes with bipyridine based ligands were chosen as the moieties for introducing photoactive properties to the MOFs, as these complexes were known in the literature as effective photosensitizers. Inspired by dye sensitized solar cells (DSSCs), cyclometalated Ru(II) complexes were targeted to achieve broad band visible light absorbance.

Moreover, the project plan included the development of other metal complexes, based on e.g. Mn, that could work as CO_2 reduction catalysts in synergy with the Ru(II) photosensitizers. However, it became apparent that the synthesis and characterization of the Ru(II) complexes unlocked a wider scientific scope than originally planned.

UiO-67 was chosen as the MOF to be functionalized with Ru(II) complexes due to its high thermal and chemical stability, its appropriateness for accommodating metal complexes with bipyridine based ligands, and the knowledge in the research group on this material. The introduction of the complexes into UiO-67 also became a rather extensive study since three different functionalization methods were examined for the different Ru(II) complexes.

In the end of the project, some initial studies on the photocatalytic properties of the Ru(II)-functionalized MOFs were conducted. Since this type of studies were a novelty in the research group, method development based on the scientific literature was necessary.

Hence, the three main parts of this thesis, in which chapters 1 and 3 are clearly divided, are

I. Synthesis and characterization of cyclometalated Ru(II) complexes
II. Incorporation of the Ru(II) complexes into UiO-67
III. Photocatalytic CO_2 reduction

Parts I and II are much more comprehensive than part III, which consists of preliminary experiments that require future development.

List of Abbreviations

BET	Brunauer-Emmett-Teller (theory of specific surface area determination)
bpy	2,2'-Bipyridine
DCM	Dichloromethane
debpy	Diethyl 2,2'-bipyridine-5,5'-dicarboxylate
deppy	Ethyl 6-(4-(ethoxycarbonyl)phenyl)pyridine-3-carboxylate
DMF	Dimethylformamide
DSSC	Dye Sensitized Solar Cell
EDS	Energy Dispersive X-ray Spectroscopy
GC	Gas Chromatography
H_2bpdc	Biphenyl-4,4'-dicaboxylic acid
H_2bpydc	2,2'-Bipyridine-5,5'-dicarboxylic acid
HOMO	Highest Occupied Molecular Orbital
HR-MS	High Resolution Mass Spectrometry
LUMO	Lowest Unoccupied Molecular Orbital
MLCT	Metal to Ligand Charge Transfer
MOF	Metal-Organic Framework
NMR	Nuclear Magnetic Resonance
PMLS	Premade Linker Synthesis
ppy	2-Phenylpyridine
PSF	Postsynthetic Functionalization
PSLE	Postsynthetic Linker Exchange
PXRD	Powder X-ray Diffraction
SBU	Secondary Building Unit
SC-XRD	Single Crystal X-ray Diffraction
SEM	Scanning Electron Microscopy
TD-DFT	Time Dependent Density Functional Theory
TEOA	Triethanolamine
TGA-DSC	Thermogravimetric Analysis – Differential Scanning Calorimetry
TON	Turnover Number
TOF	Turnover Frequency
UV-Vis	Ultraviolet-Visible

1. Introduction

1.1. Photosensitizers

The sun is the most important energy source for our planet, providing plants with the energy needed to grow, and to convert carbon dioxide and water into sugar and oxygen via photosynthesis. Due to the increasing global demand for energy in usable forms such as electricity and fuels, the development of technologies for harvesting and converting sunlight is an important and expanding field of science. Solar cells offer a direct way of producing electricity from sunlight. They are based on either inorganic semiconductor materials (mainly silicon), or a combination of inorganic and organic materials, like in dye sensitized solar cells (DSSCs), introduced by Grätzel and co-workers.[1-2] In the DSSCs, TiO_2 particles are usually covered with photoactive molecules or metal complexes that absorb light to excite an electron. The excited electron is then transferred into the conduction band of the semiconductor. These photoactive species are called *photosensitizers* and are parallels to the natural chlorophyll molecules, albeit designed to work optimally for a specific technology. Such photosensitizers have also been developed for use in chemical reactions, where they harvest light energy to drive chemical reactions.[3-5] This is one form of photocatalysis, an important branch of chemistry that allows direct use of sunlight in a multitude of processes, such as storing chemical energy in compounds that could later be utilized for consumption of this energy. Such compounds are called *solar fuels* and are sustainable and environmentally friendlier alternatives to fossil fuels.[6-7] Typical solar fuels are hydrogen that is produced by reducing protons, or organic compounds such as methanol that is produced by reducing carbon dioxide. The latter kind of solar fuels also offer a way to recycle carbon dioxide, which is an important contributor to the greenhouse effect and the resulting global warming.

The types of photosensitizers used for photocatalysis span a wide range of molecular structures, both purely organic molecules and metal complexes. In particular, Ru(II) complexes with polypyridine based ligands constitute a thoroughly investigated series of photosensitizers because of their intense metal-to-ligand charge transfer (MLCT) transitions. These complexes have been studied as photosensitizers in homogeneous photocatalysis,[3-5, 8] DSSCs, and metal-organic frameworks (MOFs, see section 1.2).[1, 9-13] Although such Ru(II) polypyridine complexes are effective light harvesters, they mainly absorb in the UV (ultraviolet) and the blue part of the visible region. Since most of the radiation from the sun is within the visible and IR

(infrared) range of the spectrum, while UV accounts for only ca. 4 % (Figure 1),[14] it is interesting to increase the absorbance of such photosensitizers in the lower energy region.

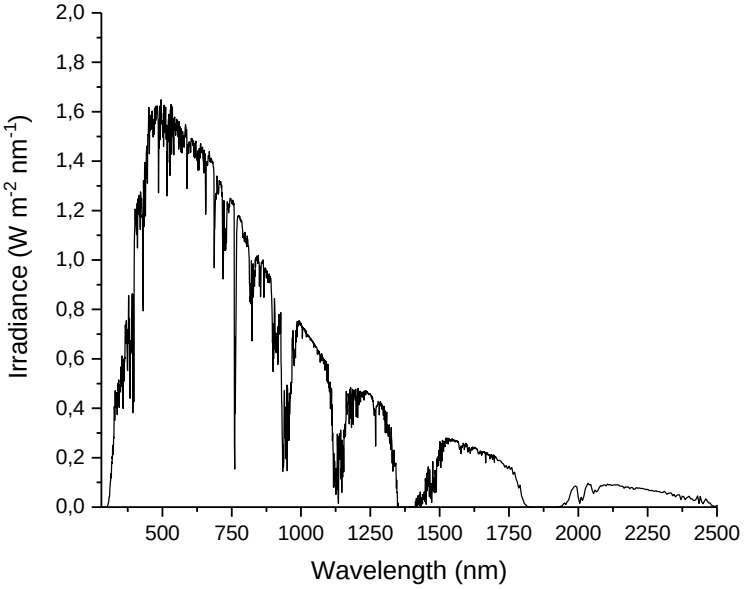

Figure 1. Solar irradiance spectrum at earth's surface. Plotted using data from "Reference Solar Spectral Irradiance: Air Mass 1.5", National Renewable Energy Laboratory.[14]

There are several strategies to achieve a bathochromic shift (a shift toward lower energy) of the absorbance bands of Ru(II) based photosensitizers, such as functionalization with large aromatic or conjugated groups.[15-17] Another strategy is to modify the coordination environment of the central ruthenium atom. Cyclometalated Ru(II) complexes have become a promising class of photosensitizers.[16-23] In this thesis, the term *cyclometalated complex* refers to a structure in which there is a σ bond between the metal (Ru) and a carbon atom as part of a *metallacycle* (Figure 2).[24]

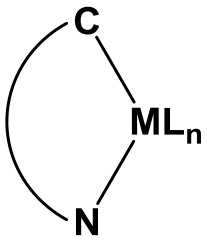

Figure 2. Schematic representation of a cyclometalated complex in which M, C, and N are parts of a metallacycle.[24]

When compared to the commonly used $Ru(bpy)_3^{2+}$ (bpy = 2,2'-bipyridine) based complexes, where the ligands coordinate the metal through Ru-N bonds only, these cyclometalated Ru(II) complexes show significantly improved absorption of visible light.[18] This improvement is the result of two key electronic properties: Firstly, a reduced HOMO-LUMO (Highest Occupied Molecular Orbital – Lowest Unoccupied Molecular Orbital) energy gap leads to a bathochromic shift of the absorption bands. Secondly, the loss of degeneracy of electronic energy levels, which arises from the reduced molecular symmetry, leads to more individual electronic transitions and a broadening of the absorption profile.[18] Cyclometalated Ru(II) complexes have mainly been developed for DSSCs. The group of Berlinguette has been an important contributor to the development of this field (and an inspiration for this thesis),[16-20, 23] and some of their reported structures are shown in Figure 3.

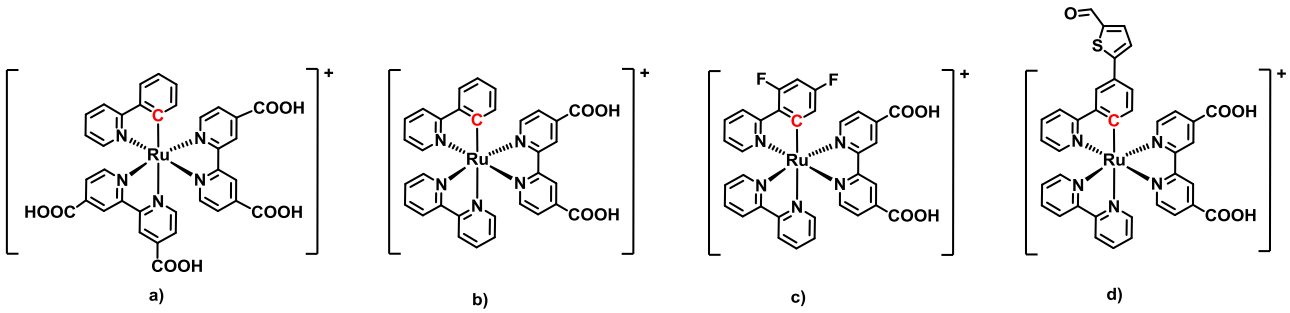

Figure 3. Cyclometalated Ru(II) photosensitizers developed for the dye sensitized solar cell (DSSC).[18-19]

Due to their visible light absorption properties, cyclometalated Ru(II) complexes are also promising for photocatalytic materials, for example in the field of solar fuel production. A class of materials that have gained increasing interest as heterogeneous catalysts, and in particular photocatalysts, is metal-organic frameworks (MOFs). Although the reported cyclometalated Ru(II) complexes could fit into the porous structures of MOFs, no complexes of this type have been developed for proper chemical incorporation into MOF materials.

1.2. Metal-Organic Frameworks (MOFs)

Metal-organic frameworks (MOFs) are materials which consist of metal ions, or more often, inorganic clusters, that are linked by organic ligands to form a two- or three-dimensional network structure that contains potential voids, or pores.[25] Most of the MOFs developed in recent years are crystalline and porous. The inorganic clusters, also called secondary building units (SBUs), typically consist of several metal cations and have various numbers of points of connection, usually between four and twelve. The organic ligands that connect the metal clusters are called *linkers*, and they can have two or more coordinating groups. The number of coordinating groups (topicity) and their relative geometry leads to a large variety of possible MOF structures. The most widely used coordinating group is carboxylates, since these anionic species form stable bonds with the cationic metal ions and coordinate in a bidentate manner, usually bridging two metal centres. The rest of the linker structure is often based on aromatic rings, as these are stable and rigid moieties.

In 2008, Lillerud and co-workers discovered the first MOFs based on Zr SBUs.[26] These MOFs consist of $Zr_6O_4(OH)_4^{12+}$ clusters that are coordinated by 12 carboxylates (COO^-). The six Zr^{4+} cations in each cluster are arranged in an octahedron. The linkers (in their protonated form) are terephtalic acid (H_2bdc), biphenyl-4,4'-dicaboxylic acid (H_2bpdc) and *p*-terphenyl-4,4''-dicaboxylic acid (H_2tpdc), which creates the materials UiO-66, UiO-67, and UiO-68, respectively (Figure 4). They are remarkably chemically, thermally, and mechanically stable, which is attributed to the strong bonds between the Zr^{4+} cations and the carboxylate groups, and the high connectivity number (12) of the cluster.[26-31] These MOFs have the same framework topology (face-centered cubic, fcu) because they have the same SBUs and the same linear geometry of the linkers. The only difference between them is the length of the linkers and the resulting available pore space. This illustrates how MOFs can be designed through the choice of SBU and linker, a strategy known as reticular synthesis.[32-33]

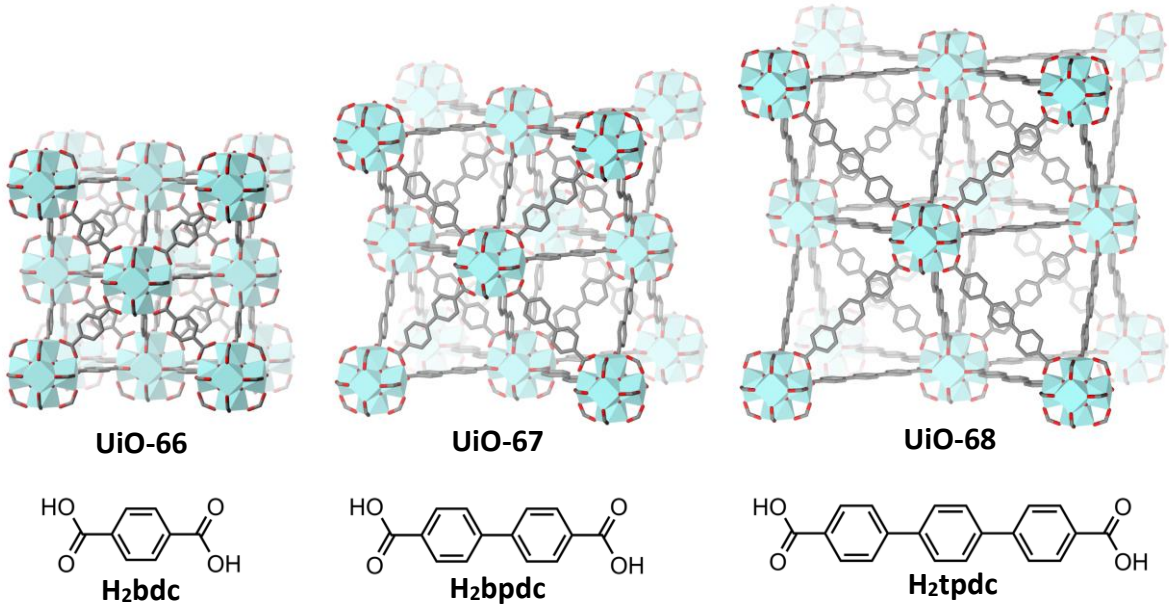

Figure 4. Unit cells of UiO-66, UiO-67, and UiO-68, and molecular structures of their respective linkers terephtalic acid (H_2bdc), biphenyl-4,4'-dicaboxylic acid (H_2bpdc) and *p*-terphenyl-4,4''-dicaboxylic acid (H_2tpdc). Zr atoms are represented as cyan square antiprisms, C and O atoms as grey and red sticks, respectively. H atoms are omitted for clarity.

As can be understood from the available pore space in these materials, they are promising candidates for gas adsorption, and therefore the storage of gases like methane, hydrogen and carbon dioxide.[34-37] Since it is possible to design the size of the MOF pores via reticular synthesis, gas separation is another application area.[38]

The size of the pores is not the only factor that determines the way guest molecules interact with the MOF structure; the organic linkers can be functionalized in order to be chemically repellent, attractive, or even reactive toward certain species. If the functionalized MOF regains its initial structure after the reaction and allows the reaction to be cycled, then it is per definition a heterogeneous catalyst.[39-40] A popular strategy for functionalizing a MOF for catalytic applications is to incorporate metal complexes as part of the MOF structure. This is often done by using 2,2'-bipyridine-5,5'-dicarboxylic acid (H_2bpydc) as linker (or a fraction of the linkers) because it can function as a chelating ligand in a variety of metal complexes. Examples of such complexes are $Pt(H_2bpydc)Cl_2$,[41] $[Ru(H_2bpydc)(bpy)_2]^{2+}$,[12] and $Re(H_2bpydc)(CO)_3Cl$[11] (Figure 5). MOFs functionalized with metal complexes have shown catalytic activity for reactions such as water oxidation,[11] organic transformations,[42] and thermal[43] and photocatalytic[44] CO_2 reduction.

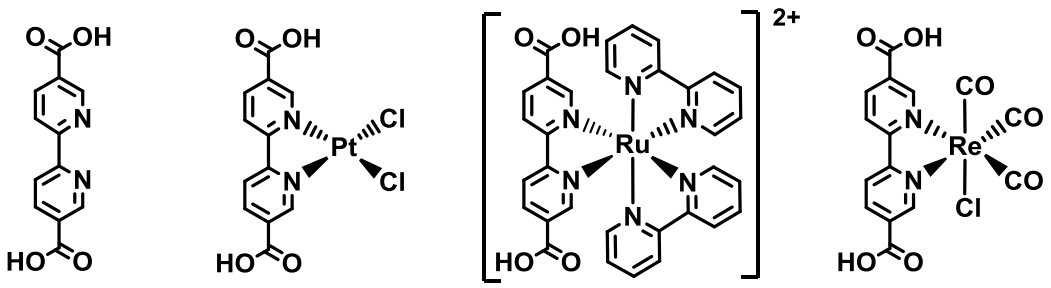

Figure 5. Molecular structures of (from left to right) H_2bpydc, Pt(H_2bpydc)Cl_2, [Ru(H_2bpydc)(bpy)$_2$]$^{2+}$, and Re(H_2bpydc)$(CO)_3Cl$.

Incorporation of metal complexes into MOFs can be achieved through different synthetic strategies. In the literature there are three main methods: premade linker synthesis (PMLS),[11-12, 45-47] postsynthetic functionalization (PSF),[13, 41, 43, 48-50] and postsynthetic linker exchange (PSLE).[51-55] A simplified scheme illustrating these methods is given in Figure 6. Alternative terms for these methods are sometimes used, or the method is not named at all. The term PSM (postsynthetic modification) is used synonymously with PSF, and is also used for pure organic functionalization of MOFs.[49, 56] PSLE is also called PSE (postsynthetic exchange).[51]

In the PMLS method, the metal complex that is to be incorporated into the MOF is synthesized before the MOF synthesis is initiated. The complex has to have at least two coordinating groups (usually on the same ligand), like carboxylic acids (as in H_2bpydc), such that the whole complex can act as a linker in the MOF synthesis. Therefore, this complex can be called the *functionalized linker*. The functionalized linker is then dissolved together with the other reactants necessary for the MOF synthesis: the precursor for the metal clusters in the MOF (usually a metal salt) and the *main linker* for the MOF that is to be functionalized (e.g. H_2bpdc for UiO-67). The solution is then heated for the MOF to assemble. In order for the functionalized linker to fit into the MOF structure, it must have a similar length and relative geometry of the coordinating groups as the main linker. The PMLS method is a facile way to functionalize MOFs, as there is only one MOF synthesis step.

The PSF method is based on a reaction between an already synthesized MOF material, in which a coordinating linker such as bpydc substitutes a fraction of the main linkers, and a dissolved precursor (metal complex). A PSF reaction typically involves exchange of two labile ligands in the precursor with the chelating bpydc linker, in order to produce the functionalized MOF. This method is usually milder than the PMLS method and offers a convenient way to incorporate metal complexes, that otherwise will decompose during synthesis, into MOFs. This is possible

since the harsh conditions (high temperature and acidity of the reaction medium) that are required for PMLS may be omitted when the premade MOF is used as a reactant.

In the PSLE method, an unfunctionalized MOF is suspended in a solution of a functionalized linker (the same as in PMLS) in order for the main linkers in the MOF to be exchanged with the functionalized linkers in the solution. This is a quite direct functionalization method in which a wide range of functionalized linkers could be used that e.g. are not stable under the typical PMLS conditions, or don't have the appropriate reactivity for a PSF reaction to be performed.

Further details about the MOF syntheses in this thesis are provided in section 2.1.

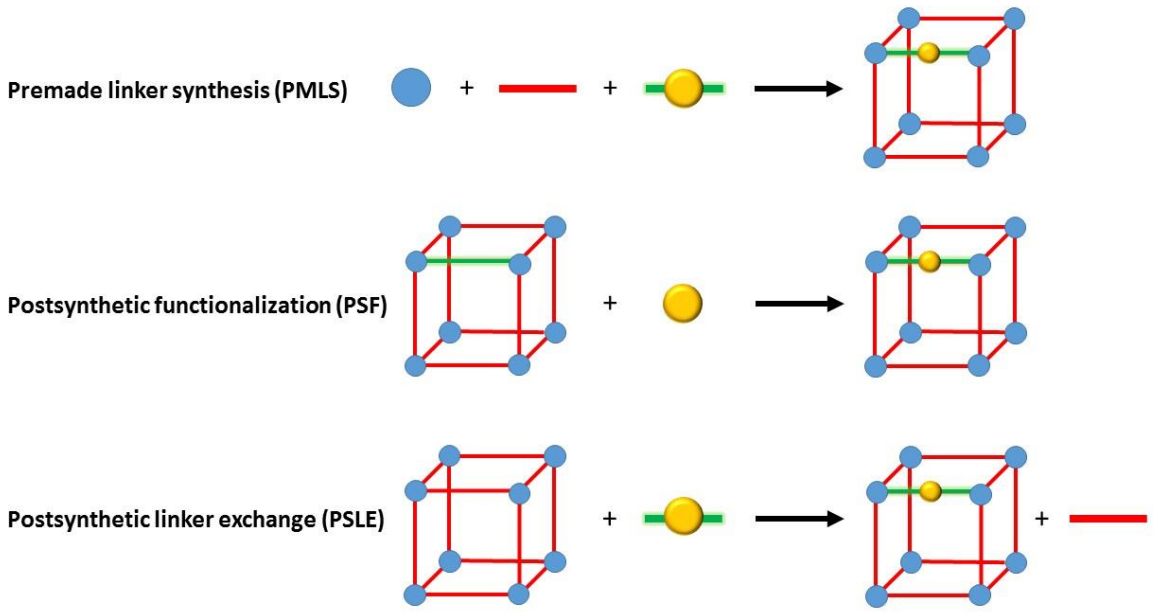

Figure 6. Simplified scheme of the three methods for functionalizing MOFs with metal complexes. Blue balls = metal ions for cluster, yellow balls = metal complex, red lines = main linker, green lines = coordinating linker (e.g. bpydc).

Photocatalysis using MOFs has emerged as an important field of research, and with it the demand for suitable photosensitizers.[44, 57-59] These may either be present as free molecules in solution filling the pores of the MOF material, or be chemically integrated as linkers in the MOF structure. The latter mode of incorporation can be achieved by PMLS, PSF, and PSLE, and has the advantage that the photosensitizer will remain in the structure after isolation and washing of the MOF powder.

Ru(II) complexes with bipyridine (bpy) derived ligands have been studied as photosensitizers both in solution[13, 55, 60-61] and chemically integrated in MOFs.[11-12, 47-48, 62-63] The complex $[Ru(H_2bpydc)(bpy)_2]^{2+}$, or **1-H**, as it will be referred to later in this thesis (Figure 9, page 30), has become a standard photosensitizer as a functionalized MOF linker. **1-H** has been incorporated into MOFs using PMLS,[11-12, 47, 62] PSF,[48, 62] and PSLE.[62] Notably, Yu and Cohen employed all three methods to incorporate this complex into UiO-67.[62]

1.3. MOFs for Photocatalytic CO_2 Reduction

The conversion of CO_2 into useful chemicals is a promising strategy to recycle this readily available greenhouse gas. Moreover, if the conversion process involves reduction to compounds with a high energy content, like methanol, CO_2 would be a source for various fuels. Thus, CO_2 reduction could contribute to the global challenges of both climate change and increasing energy demand. In general, CO_2 reduction can be catalyzed using metal complexes,[64] semiconductors,[65] or hybrid materials,[66] and via either thermal,[43] electrochemical,[67] or photochemical[68] activation. The photocatalytic pathway is the most energy efficient strategy, as sunlight can be directly converted into chemical energy in solar fuels, as mentioned in section 1.1. As heterogeneous photocatalysts for CO_2 reduction, MOFs have the following important advantages over the more thoroughly investigated semiconductor based photocatalysts.[44, 69-71] The inherent porosity of MOFs allows the adsorption and concentration of gas molecules close to catalytic centers. In addition, the possibility to design and modify the linkers in a variety of ways makes MOFs promising as efficient visible light photocatalysts, compared to semiconductors, which are mostly limited to UV light absorption.

The first report on MOFs for photocatalytic CO_2 reduction was published in 2011, in which Lin and co-workers incorporated a Re(I) complex into UiO-67 (Figure 7a).[11] The Re(I)-functionalized MOF photocatalyzed the reduction of CO_2 to CO with a turnover frequency (TOF, with respect to the catalytic Re sites) of 1.2 (6 h reaction time). By the time of writing, at least 30 reports have been published, which are summarized in Table 1.[11, 13, 45-46, 48, 55, 60-61, 63, 72-92] Typically, the reaction system consists of the MOF photocatalyst, CO_2 saturated MeCN, triethanolamine (TEOA, as the reducing agent), and in some cases an additional dissolved photosensitizer. The mixtures are then stirred in a closed reaction cell and illuminated with visible light for some hours. The reduction products are almost invariably CO, sampled from the headspace of the reaction cell, or $HCOOH/HCOO^-$, sampled from the liquid phase.

The CO_2 reduction mechanisms are still not totally understood, although in some cases pathways are proposed. Generally, the photosensitizer (could be the linker itself) is excited by light before it transfers an electron either directly to CO_2 or to the metal cluster, which subsequently reduces CO_2. Regeneration of the photosensitizer occurs via electron transfer from a reducing agent. An example of catalytically active metal clusters is the reduction of Zr^{4+} to Zr^{3+} in a Zr-oxo cluster (UiO-type), which further transfers the electron to CO_2 (Figure 7b).[73] Photocatalysis on the linkers can be achieved by e.g. using an incorporated metal complex with labile ligands (Figure 7c).[13] Some reports suggest a combination of clusters and linkers as active catalytic centers.[78, 83] The reducing agent TEOA is proposed to act as both an electron and a proton (i.e. hydrogen) donor in the system, in which the first reaction step is the formation of a positive radical (Figure 7d).[84] Some good reviews on this field have been published.[44, 69-70]

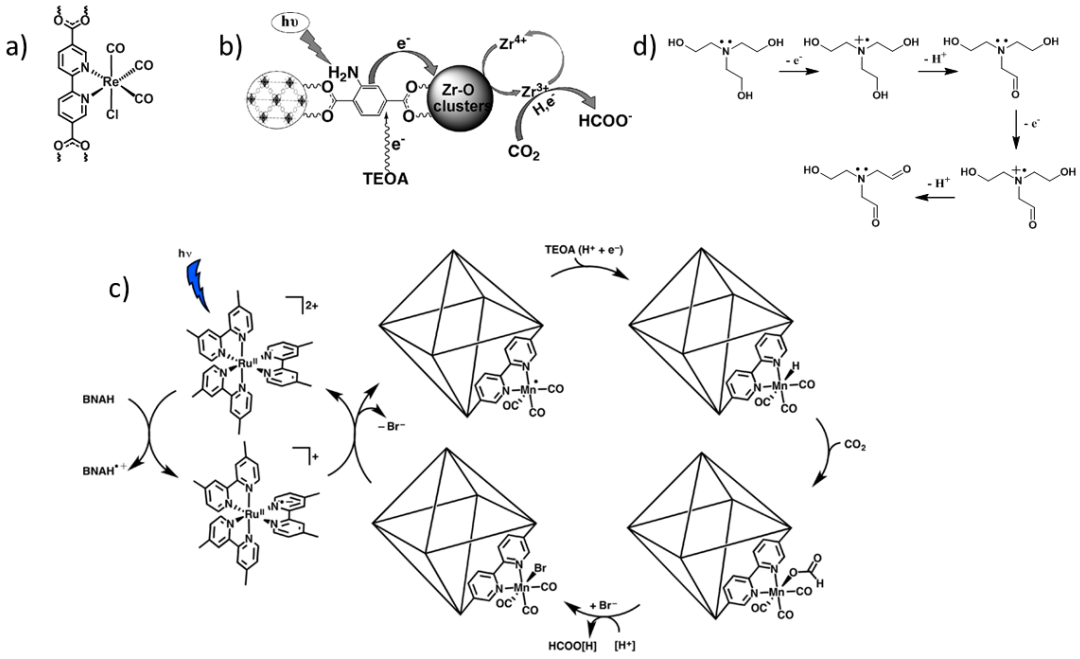

Figure 7. a) The Re(I) complex that was incorporated into UiO-67 in the first report on photocatalytic CO_2 reduction using MOFs,[11] b) proposed mechanism for photoreduction via the Zr_6-cluster in UiO-67-NH_2,[73] c) proposed mechanism for photoreduction on a Mn(I)-functionalized linker in UiO-67,[13] d) Proposed TEOA degradation during the process of photocatalysis.[84]

Table 1. Overview of previous work on photocatalytic CO_2 reduction using MOFs. TOF = turnover frequency, TEA = trietylamine, TEOA = triethanolamine, BNAH = 1-benzyl-1,4-dihydronicotinamide. The unit µmol $g^{-1}h^{-1}$ refer to µmol of product per gram of catalyst per hour of reaction.

Entry	Catalyst	Solution	Product	Product formation rate (µmol $g^{-1}h^{-1}$)	TOF (h^{-1})	Total reaction time (h)	Ref.
1	UiO-67-[$Re(CO)_3$(dcbpy)Cl]	MeCN, TEA	CO	88	1.2	6	11
2	NH_2-MIL-125(Ti)	MeCN, TEOA	$HCOO^-$	16	-	10	72
3	NH_2-UiO-66	MeCN, TEOA	$HCOO^-$	26	-	10	73
4	Cu(II) imidazolate MOF	H_2O, NaOH, Na_2SO_3	MeOH	343	-	5	74
5	Cu(II) porphyrin MOF	H_2O, TEA	MeOH	*262.6 ppm $mg^{-1}h^{-1}$	-	-	75
6	Co-ZIF-9	MeCN, H_2O, TEOA, [$Ru(bpy)_3$] Cl_2	CO	358952	104.5	0.5	76
7	Y[$Ir(ppy)_2$(dcbpy)]$_2$[OH]	MeCN, TEOA	$HCOO^-$	158	-	6	77
8	NH_2-MIL-101(Fe)	MeCN, TEOA	$HCOO^-$	445	-	8	78
9	MOF-253–$Ru(CO)_2Cl_2$-$Ru(bpy)_2$	MeCN, TEOA	$HCOO^-$, CO	121, 46	4.5, 0.9	8	48
10	UiO-66-(Zr/Ti)-$(NH_2)_x$	MeCN, TEOA, BNAH	HCOOH	1052	1	6	79
11	UiO-67-Mn(bpy)$(CO)_3$ Br	DMF, TEOA, BNAH, [$Ru(dmb)_3$] $(PF_6)_2$	$HCOO^-$, CO	5328, 218	6.1, 0.3	18	13
12	(Cd_2[Ru(dcbpy)$_3$]*12 H_2O)$_n$	MeCN, TEOA	$HCOO^-$	77	-	8	80
13	(Cd[Ru(4,4'-dcbpy)$_2$(bpy)]	MeCN, TEOA	$HCOO^-$	72	-	6	63
14	UiO-66-Cr(III)CAT	MeCN, TEOA, BNAH	HCOOH	1724	1.9	6	81
15	PCN-222	MeCN, TEOA	$HCOO^-$	60	-	10	82
16	UiO-67-Ru(bpydc)(terpy)(CO)]$(PF_6)_2$	MeCN, TEOA, [$Ru(bpy)_3$]$(PF_6)_2$	HCOOH, CO	-	5.1, 1.8	6	55
17	NNU-28	MeCN, TEOA	$HCOO^-$	53	-	10	83

18	$Zr_6(O)_4(OH)_4$-$[Re(CO)_3Cl(bpydb)]_6$	MeCN, TEA, H_2O	$HCOO^-$, CO	-	0.04, 1.1	6	45
19	MOF-525-Co	MeCN, TEOA	CO, CH_4	201, 37	-	6	84
20	Ag⊂UiO-67-$[Re(CO)_3(dcbpy)Cl]$	MeCN, TEA	CO	-	0.1	-	46
21	UiO-67-$[Re(CO)_3(dcbpy)Cl]$-NH_2	TEA (gas phase)	CO	1	-	-	85
22	MIL-125-NHR	MeCN, TEOA, mesitylene	$HCOO^-$	-	0.01	120	86
23	TiO_2/NH_2-UiO-66	H_2 (gas phase)	CO	4	-	6	87
24	$Ru(bpy)_3$-$Ru(bpy)(CO)_2(Cl)_2$-bpy-PMO	DMA, H_2O, BNAH	$HCOO^-$, CO	1166, 1666	67, 95	1	88
25	$[Co_3(OH)_3(NTB)(4,4'\text{-}bpy)_{1.5}]$	MeCN, H_2O, TEOA, $[Ru(bpy)_3]Cl_2$	CO	4373	2.6	3	61
26	ZIF-67	TEOA, H_2O, MeCN, $[Ru(bpy)_3]Cl_2$	CO	59200	-	0.5	89
27	Zr-SDCA-NH_2	MeCN, TEOA	$HCOO^-$	39	-	12	90
28	MAF-X27l-OH	TEOA, MeCN, H_2O, $[Ru(bpy)_3]Cl_2$	CO	-	212	10	91
29	ZIF-67	TEOA, H_2O, MeCN, $[Ru(bpy)_3]Cl_2$	CO	3890	0.9	4	60
30	Rh-PMOF-1(Zr)	MeCN, TEOA	$HCOO^-$	-	0.3	18	92

* Another unit was not provided.

2. Experimental Methods

In this chapter, the most important experimental methods for this thesis, and their purpose, are briefly described. Other methods used (MS, DFT, N_2 sorption, and TGA-DSC) are described in the experimental sections of the respective papers. The synthesis procedures for the Ru(II) complexes are quite comprehensive, and are described in the experimental section of **Paper I** and in section 3.1 of this thesis. The photocatalytic experiments are not described elsewhere, thus a detailed experimental description is given in section 2.6.

2.1. MOF Synthesis

The synthesis of pristine UiO-67 is usually performed by dissolving $ZrCl_4$ and biphenyl-4,4'-dicarboxylic acid (H_2bpdc) in dimethylformamide (DMF) containing a small amount of water before heating the solution (solvothermal synthesis). The corresponding reaction equation for the synthesis of UiO-67 is:

$$6\,ZrCl_4 + 8\,H_2O + 6\,H_2bpdc \xrightarrow{\Delta} Zr_6O_4(OH)_4(bpdc)_6 + 24\,HCl$$

Often, a monocarboxylic acid (acting as a so-called *modulator*) is added to the reaction mixture in order to slow down the crystallization and thereby enhance the crystallinity of the resulting MOF material.[93-94]

The functionalization of UiO-67 with Ru(II) complexes (**Paper II**) was achieved using the three methods described in section 1.2: premade linker synthesis (PMLS), postsynthetic functionalization (PSF) and postsynthetic linker exchange (PSLE). These methods were evaluated for their success in incorporation of the different Ru(II) complexes into UiO-67, and for their influence on the properties of the resulting MOF products. Detailed descriptions of the individual synthesis procedures are provided in the experimental section of **Paper II**. The following is a summary of the general procedures for the three methods.

PMLS was performed as outlined above for the synthesis of pristine UiO-67, except that a fraction of the H_2bpdc linkers was replaced by one of the Ru(II)-functionalized linkers shown in Figure 9 (page 30). $ZrCl_4$ (1 equiv.) was dissolved in DMF before water (3 equiv.) was added. Benzoic acid (10 equiv.) was added as a modulator and dissolved, before H_2bpdc (0.9 equiv.) was added and dissolved by heating and stirring on a hotplate for a couple of minutes. Heating

was discontinued before the respective Ru(II) complex (0.1 equiv.) was added as the functionalized linker to the still hot solution and dissolved. The prepared solution was heated at 120 °C in an Erlenmeyer flask (without stirring), loosely capped with a watch glass, for three days. The recovered solid was washed thrice with both DMF and MeOH, before it was dried in air at 100 °C overnight.

For PSF, a sample of UiO-67 was used in which 5 % of the bpdc linkers had been replaced by bpydc (2,2'-bipyridine-5,5'-dicarboxylate). This material (UiO-67-bpy) was suspended in an EtOH solution of either *cis*-$Ru(bpy)_2Cl_2$ or *cis*-$[Ru(ppy)(bpy)(MeCN)_2]PF_6$, and stirred at reflux for 21 h. There were 5 equiv. of the Ru(II) precursor with respect to the amount of bpydc linkers in the MOF. The Ru(II) precursor reacted with the bpydc linkers in UiO-67 to provide the Ru(II)-functionalized MOF product. The recovered solid was washed thrice with DCM, before it was dried in air at 100 °C overnight. UiO-67-bpy (powder and single crystals) was synthesized by Sigurd Øien-Ødegaard.

PSLE was performed by suspending pristine UiO-67 in a DMF/water (1:1) solution of the respective Ru(II)-functionalized linker (1 equiv. with respect to the main bpdc linker in the MOF) before stirring the mixture at 100 °C for three days. The recovered solid was washed thrice with both DMF and MeOH, before it was dried in air at 100 °C overnight. The Ru(II)-functionalized linkers were the same for PSLE as for PMLS. UiO-67 was synthesized by Gurpreet Kaur.

The synthesized MOF samples were given abbreviations based on the respective Ru(II) complex and the functionalization method, e.g. **1-PMLS**, **2-PSF**, etc.

2.2. Nuclear Magnetic Resonance (NMR) Spectroscopy

NMR spectroscopy is a powerful technique for analyzing solutions. It is based on the interaction between electromagnetic radiation (radio waves) and spins of magnetically active nuclei that are aligned with an applied magnetic field. In **Paper I**, ^{1}H and ^{13}C NMR were used to analyze the Ru(II) complexes that were synthesized. This allowed to evaluate the purities and identities of the products.

Moreover, the prepared Ru(II)-functionalized MOFs were digested in 1 M NaOH in D_2O for 24 h before the resulting solutions were analyzed by ^{1}H NMR (**Paper II**). During digestion, the

Zr-carboxylate bonds are hydrolyzed and the linkers (Ru-functionalized and main linkers) are dissolved. In order to obtain clearer spectra, the D_2O solutions were evaporated to dryness before the leftovers were dissolved in CD_3OD for subsequential ^1H NMR analyses. These measurements confirm the presence of the Ru(II) complexes in the MOF structures if their signals are discernible in the digestion solution spectra. This is possible since the Ru(II) complexes are stable under the digestion conditions. In the cases of the MOFs functionalized by PSF, this would also provide evidence of proper chemical incorporation in the MOF structures. The respective Ru(II) complexes are not used as reactants and thus must have been produced during the PSF reaction between the molecular Ru(II) precursors and the bpydc linkers in the MOFs. ^1H NMR could not be used to assess the proportion of incorporation of Ru(II) complexes in the MOFs since H_2bpdc is poorly soluble in CD_3OD.

In addition, ^1H NMR (and ^{13}C NMR in one experiment using $^{13}CO_2$) was employed to analyze the liquid phase (CD_3CN) in the photocatalytic CO_2 reduction experiments.

^1H NMR spectroscopy was performed on Bruker DPX 300 and AVIII400 spectrometers operating at 300 and 400 MHz respectively. ^{13}C NMR was recorded on Bruker AVII600 and AVIII400 spectrometers operating at 151 and 100 MHz respectively. All spectra were recorded at 25 ^oC.

2.3. X-ray Diffraction (XRD)

XRD is based on the scattering of X-rays from long range ordered electron density in materials. Constructive interference occurs when the Bragg condition is satisfied: $n\lambda = 2d\sin\theta$, where λ is the wavelength of the radiation, d is the distance between repeating lattice planes of atoms, and θ is the angle between the lattice planes and the incoming X-rays. In powder XRD (PXRD) the crystallites of the material is randomly oriented, and by changing θ, a one-dimensional diffractogram is obtained, which is characteristic for the material studied. In Single crystal XRD (SC-XRD), is it possible to acquire a three-dimensional diffraction pattern, which, after various corrections and Fourier transform, provides the electron density of the unit cell in real space. From this, detailed crystal structures of molecular compounds and materials can be obtained.

In this thesis, both SC-XRD and PXRD were employed. In **Paper I**, SC-XRD was performed to investigate the molecular structures of the synthesized Ru(II) complexes. Suitable single crystals were obtained by vapor diffusion crystallization.[95] SC-XRD was also performed on

single crystals of Ru(II) functionalized MOFs in **Paper II** to investigate if the Ru atoms were coordinated to the bpydc linkers in the MOFs. Sigurd Øien-Ødegaard performed all SC-XRD measurements and refinements, and made the related figures. In **Paper II**, PXRD was performed in order to identify the main phase of the prepared Ru(II)-functionalized MOFs (by comparing their diffractograms to that of UiO-67) and to assess their crystallinity.

For SC-XRD, a Bruker D8 Venture diffractometer was used, which was equipped with a Photon 100 detector and using Mo Kα radiation (λ = 0.71073 Å). For PXRD, a Bruker D8 Discovery diffractometer was used, which was equipped with a focusing Ge-monochromator, using Cu-Kα radiation (λ = 1.5418 Å) and a Bruker LYNXEYE detector.

2.4. UV-Vis Spectroscopy

This technique is based on the absorption of ultraviolet and visible light by molecules or materials through excitations of electrons to higher energy orbitals. Using a range of wavelengths for the incoming light beam then results in an absorption spectrum. In this thesis, the absorption properties of molecular Ru(II) complexes in solution (**Paper I**) and of solid MOF materials (**Paper II**) were investigated, as these are relevant for potential photocatalytic activity.

For solutions, the absorbance A follows the Beer-Lambert law: $A = \log_{10}(I/I_0) = \varepsilon cL$, in which I_0 is the intensity of the incident light, I is the transmitted intensity, ε is the molar absorptivity, c is the concentration of the absorbing molecule, and L is the path length through the sample. For powders of solid materials, the diffuse reflectance R can be analyzed using the Kubelka-Munk transform: $k/s = (1-R)^2/2R$, in which k is the absorption coefficient and s is the scattering coefficient.

In this work, the solutions of the Ru(II) complexes were measured in transmittance mode using a UV-3600 spectrometer from Shimadzu. The MOFs were measured in diffuse reflectance mode (DR UV-Vis) using a USB2000+ spectrometer from Ocean Optics. All spectra were recorded at 25 ^{o}C.

2.5. Scanning Electron Microscopy (SEM) and Energy Dispersive X-ray Spectroscopy (EDS)

SEM is a technique for obtaining microstructural images and topology information of surface structures, with resolutions as good as under 1 nm.[96] A high-energy electron beam is focused onto the sample and various signals are produced from the interaction between the beam and the sample atoms. For imaging, secondary electrons are mostly detected, which are low energy electrons that are ejected from the surface atoms by inelastic scattering interactions with the beam electrons. Backscattered electrons are also detected, which are higher-energy electrons from the incoming beam that are elastically scattered through interactions with the atom nuclei in the sample.

SEM was used in this work to study the morphology of the crystallites of the prepared Ru(II)-functionalized MOF powders. This was done in order to check if the crystallites had the octahedral shape typical of UiO-67, and to assess if the crystallite surfaces were clean or if other phases were attached to them. Images were obtained with a Hitachi SU8230 field emission scanning electron microscope. The acceleration voltage was set to 2.5 kV and the probe current to 10 μA. In order to reduce sample charging, 1.5 kV deceleration voltage was applied, resulting in an effective voltage ("landing voltage") of 2.5 – 1.5 = 1 kV. In this mode, both secondary and backscattered electrons were collected.

When the electron beam ejects an electron from a sample atom, thereby ionizing it, the resulting vacant state in the atom is reoccupied by a transition of an electron from a higher energy state. This process is accompanied by the emission of an X-ray photon. In a sample, various transitions between different energy states of the atoms occur, leading to characteristic X-ray excitation lines that belong to specific elements. Detection and analysis of these X-ray signals is the basis for EDS. By integrating the intensity of the detected signals, it is possible to obtain the relative concentrations of different elements in the sample.

In this work, EDS was employed to obtain the Ru:Zr ratios in the Ru(II)-functionalized UiO-67 MOFs. This information indicates the success of incorporation of Ru(II) complexes and allows the quantification of other properties of the materials, such as catalytic turnover numbers (TONs) with respect to Ru(II) complexes. In UiO-67 there are one linker per Zr atom. This means that the Ru:Zr ratio corresponds to the proportion of linkers being functionalized with Ru(II) complexes, assuming that all Ru(II) complexes are chemically incorporated into the MOF

structure (compared to simply occupying the MOF pores or being aggregated on the MOF surface).

The same instrument was used for EDS as for the SEM measurements, in which an EDS detector was installed. Samples were prepared as powders or pellets attached to carbon tape. The working distance was 15 mm and the scanned area was ca. 1000 μm^2. The accelerating voltage was set to 10 kV so that both Zr (Lα = 2.042 keV) and Ru (Lα = 2.558 keV) could be quantified. Background subtraction, analysis, and quantification were performed in the software Esprit v. 1.9.4.3535 from Bruker. Repeated measurements resulted in a spread of Ru:Zr ratios, probably due to both variations in sample preparation (powder or pellet) and processing with the quantification software. Thus, the Ru:Zr ratios are reported as ranges rather than single values.

2.6. Photocatalysis

The experimental setup was based on the previous reports on photocatalytic CO_2 reduction with MOFs, as described in section 1.3. An in-house made quartz vessel was used as the reaction cell, which had the inner measures of 30 mm (diameter) and 22 mm (thickness), and a round neck that could be sealed with a septum (Figure 8).

Figure 8. The quartz cell used for photocatalytic CO_2 reduction experiments.

The following procedure was employed for the MOFs **1-PMLS**, **2-PSF**, **3-PSLE**, **4-PMLS**, **4-PSLE**, and pristine UiO-67, as well as for the molecular complex **4-Na**. This is referred to as the standard procedure.

MOF (8 mg) or complex **4-Na** (8 mg) was mixed with CD_3CN (8 mL) in the quartz cell containing a stir bar before the cell was sealed with a septum. This mixture was then purged with a gas mixture of CO_2 (5 mL/min) and H_2 (30 mL/min, the reducing agent) for 1 h while stirring. This was done through two syringes (one into the solution and one that led the gas out from the headspace of the reaction cell). The cell was covered with Al foil during the gas purge to avoid unwanted photoreaction. Ne gas (0.5 mL) was then injected into the headspace as an internal standard using a 1 mL Pressure-Lok® Series A-2 gas tight syringe from VICI®. After one additional hour of stirring the mixture in darkness, the system was ready for photoreaction.

The photoreaction was conducted by irradiating the sealed reaction vessel employing a 300 W ozone free xenon Research Arc Lamp Source (66483-300XF-R22) from Newport. The light

beam was passed through an Air Mass Filter, AM 1.5 Global (81094) from Newport, that gave an intensity of 1 sun at the 14 cm working distance used (measured with a photometer). The irradiation was performed at room temperature for 6 h while stirring. After the photoreaction, the reaction mixture was centrifuged for 10 min at 3000 rpm before the liquid and the solid were separated and stored.

Four experiments were performed with **4-PMLS** employing the standard procedure, but with the following variations:

- The experiment was performed in darkness (the cell was covered with Al foil).
- No CO_2 was bubbled through the system, only H_2 (30 mL/min).
- The isolated sample from a previous catalytic test was directly reused (not washed nor dried).
- Isotopic $^{13}CO_2$ was used instead of normal CO_2.

In addition to the experiments mentioned above, the MOFs **2-PSF** and **4-PMLS** were also tested with TEOA (triethanolamine) instead of H_2 as the reducing agent (this was done twice for **4-PMLS**). These experiments were performed following the standard procedure except that the liquid phase of the reaction consisted of CD_3CN (7 mL) and TEOA (1 mL), and that only CO_2 was purged through the reaction mixture at a flowrate of 20-25 mL/min for 1 h.

In all the experiments, both the headspace of the reaction cell and the reaction solution were analyzed at different times (before, during, and after reaction).

To analyze reaction products in the headspace, samples of 50 µL were withdrawn with a 50 µL Pressure-Lok® Series A-2 gas tight syringe from VICI®. The gas samples were manually injected into an Agilent 6890 gas chromatograph (GC). The columns used were a HP-plot U (30 m, 530 µm, 20 µm) and a CP-molesieve 5A (50 m, 530 µm, 50 µm). The detectors were TCD and FID (coupled in series) and the carrier gas was He. For quantification of produced CO, a reference gas mixture with 0.1 % CO was used.

Gas samples were withdrawn at the following points in time:

- Straight after the purging with CO_2 and H_2 and the injection of the internal standard (corresponding to -1 h irradiation time)
- 1 h in darkness (0 h irradiation time)
- 1 h irradiation
- 2 h irradiation
- 4 h irradiation
- 6 h irradiation

The amounts of produced CO were calculated in units of µmol CO per gram catalyst (hereafter referred to by µmol/g). Table 2 lists the values obtained in the experiments performed in this work, which are plotted in Figure 29 (page 55) and Figure 30 (page 56).

Table 2. Amounts of CO produced in the photocatalytic experiments calculated based on reference measurements of a gas mixture containing 0.1 % CO. The units are µmol CO per gram catalyst (µmol/g). Number of hours refers to time of irradiation. The testing of 1-PMLS, 2-PSF, 3-PSLE, 4-Na employing the standard procedure (see text above), 4-PMLS in darkness, and 2-PSF using TEOA, all gave zero or insignificant amounts of CO and are therefore not included in the table. The amounts in all experiments measured after purging with CO_2/H_2 and after 1 h in darkness were also zero or insignificant. The two experiments with 4-PMLS using TEOA were identical.

Catalyst	**1 h**	**2 h**	**4 h**	**6 h**
4-PMLS	649	990	1304	1578
4-PSLE	357	491	623	821
UiO-67	159	226	457	605
4-PMLS, no CO_2, only H_2	621	972	1301	1555
Reuse of 4-PMLS	328	491	625	792
4-PMLS with TEOA 1	-	913	-	1816
4-PMLS with TEOA 2	457	671	1843	2324

The experiment with **4-PMLS** using isotopic $^{13}CO_2$ was performed in order to investigate the origin of the detected CO. To analyze eventual ^{13}CO, a 100 µL sample was withdrawn with a 100 µL Pressure-Lok® Series A-2 gas tight syringe from VICI®. The sample was injected through a septum into a OmniStar™ mass spectrometer (MS) from Pfeiffer, operating at 70 V ionization voltage. First, the syringe needle was evacuated before the syringe was opened to let the gas sample diffuse into the MS. This was done at the start of the photoreaction (before

irradiation), and at 4 h and 6 h of irradiation. The *m/z* 29 and *m/z* 45 signals, belonging to ^{13}CO and $^{13}CO_2$, respectively, were monitored during the gas pulse. Since CO_2 is partially fragmented into CO in the MS, five reference measurements were performed of an experiment that was identical to the photocatalytic experiment, except that no catalyst was present in the system.

Reaction products in solution were analyzed by taking either 0.1 mL (before and during reaction) or 0.5 mL (after reaction and centrifugation) samples with a Hamilton syringe for ^{1}H NMR (400 MHz). The 0.1 mL samples were diluted to 0.5 mL with CD_3CN before analysis. Liquid samples were withdrawn at the following points in time:

- 1 h in darkness (0 h irradiation time)
- 2 h irradiation
- 4 h irradiation
- 6 h irradiation (and centrifugation)

The solution in the experiment with $^{13}CO_2$ was also analyzed by ^{13}C NMR (100 MHz) at 0 h, 4 h, and 6 h irradiation time.

3. Results and Discussion

3.1. Cyclometalated Ruthenium(II) Complexes

The first part of this thesis consisted of the synthesis and characterization of new Ru(II) complexes capable of functioning as MOF linkers that strongly absorb light in the visible region. This work resulted in **Paper I**: "Cyclometalated Ruthenium Complexes with Carboxylated Ligands from a Combined Experimental/Computational Perspective".[97] Four Ru(II) complexes were synthesized and compared as potential photosensitizers in MOFs (Figure 9). The reference complex was $[Ru(bpy)_2(H_2bpydc)]Cl_2$ (**1-H**, bpy = 2,2'-bipyridine, H_2bpydc = 2,2'-bipyridine-5,5'-dicarboxylic acid), which was first reported in 1999,[98] and has been studied as a linker in MOFs.[11-12, 47-48, 62] This complex, in which the ruthenium atom is only coordinated through dative bonds from nitrogen, absorbs in the UV and blue part of the electromagnetic spectrum. In order to extend the absorbance toward the red end, cyclometalation was chosen as the structural variation. This strategy allows the size of the complex to remain the same as **1-H**, instead of introducing large conjugated groups. In addition to the electromagnetic properties of such complexes, the use of them as MOF linkers has other advantages compared to **1-H**, such as the need for only one counterion (because of the formally anionic charge on the Ru bonded C atom), which has to occupy the MOF pores.

The specific target complexes were structures in which a Ru bonded C atom replaced a N atom in either one of the bpy ligands (**2-Na**) or in the H_2bpydc ligand (**3-Na**). Complex **2-Na** is thus similar to structure b) in Figure 3 (page 10), except that the carboxylate groups are arranged in a linear fashion and, as will be discussed later, the Ru-C bond is *trans* to the carboxylated ligand. In addition, a fourth complex (**4-Na**) was investigated as a reference because of its reported properties as an effective photosensitizer in DSSCs.[16, 18, 23, 99] Unlike the other complexes, it does not contain a ligand with carboxylate groups oriented in a linear fashion, i.e. it is not strictly analogous, neither topologically nor in size, to the bpdc linker in UiO-67. Nevertheless, **4-Na** was included in this work because it can possibly be incorporated into UiO-67 by other means. For example, one or more of its four carboxylate groups might connect at missing linker defects[28, 100-103] in the MOF structure. Alternatively, the complex may bind to the surface of the MOF crystallites, in a similar fashion to the bonding of photosensitizers to TiO_2 particles in DSSCs.[16, 18, 23, 99] It has to be pointed out that two of the four carboxylate groups on **4-Na**, one on each of the substituted ligands, actually are in a linear relative arrangement. However, they

are separated by two pyridine rings and the Ru atom, so that the distance between them do not match the length of the linkers in UiO-67.

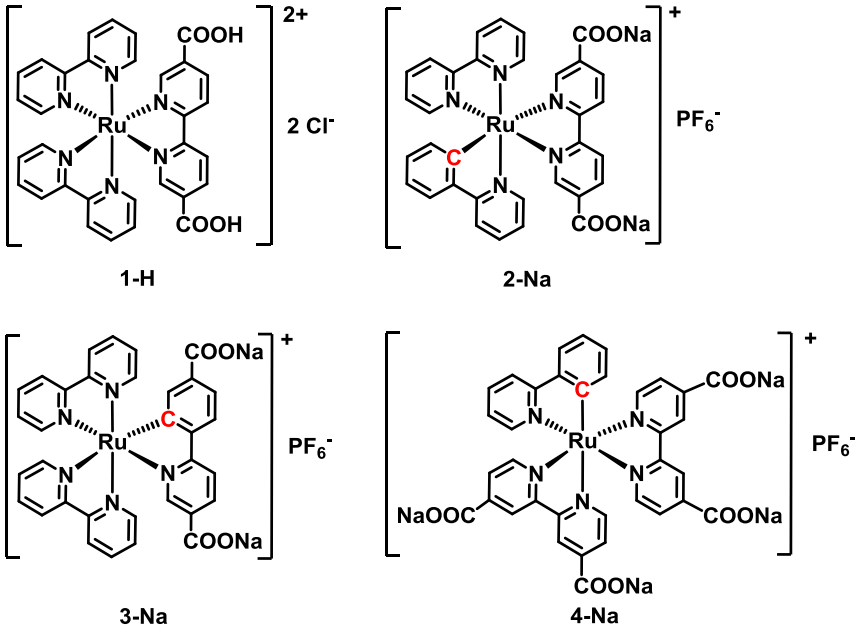

Figure 9. The four Ru(II) complexes that were synthesized and incorporated into the MOF UiO-67.

The synthetic work in **Paper I** resulted in a total of nine new compounds (**2-Et**, **2-Na**, **3-Et**, **3-Na**, **4-Et**, **5-Et**, **6-Et**, **7-Et**, and **7-Na**), which were isolated and characterized by ^{1}H and ^{13}C NMR and HR-MS. The detailed synthetic procedures for these compounds, and the corresponding characterization data, are provided in the experimental section of **Paper I**. Complex **1-H** was synthesized following an earlier reported procedure, in which $RuCl_3$ was reacted with bpy to give $Ru(bpy)_2Cl_2$, which was then reacted with H_2bpydc to yield the final product.[98, 104] The syntheses of the cyclometalated complexes **2-Na**, **3-Na** and **4-Na** proved not to be as straightforward as the synthesis of complex **1-H**. Nevertheless, it was possible to employ similar strategies for some of the synthetic steps, as shown in Scheme 1.[97] The preparation of the ester complexes **2-Et**, **3-Et** and **4-Et** for subsequent hydrolysis using minimum amounts of NaOH proved to be a facile strategy to provide the pure carboxylate complexes **2-Na**, **3-Na** and **4-Na**, respectively. Moreover, the ester complexes **2-Et**, **3-Et** and **4-Et** were easily purified by recrystallization, using dichloromethane and pentane.

Scheme 1. Synthesis routes to Ru(II) complexes 1-H, 2-Na, 3-Na, 4-Na, and 7-Na. $Ru(bpy)_2Cl_2$ was prepared from $RuCl_3$. $[Ru(ppy)(MeCN)_4]PF_6$ and 5-Et were prepared from $RuCl_3$, through $[Ru(C_6H_6)Cl_2]_2$. The detailed synthetic procedures are described in the experimental section of Paper I.

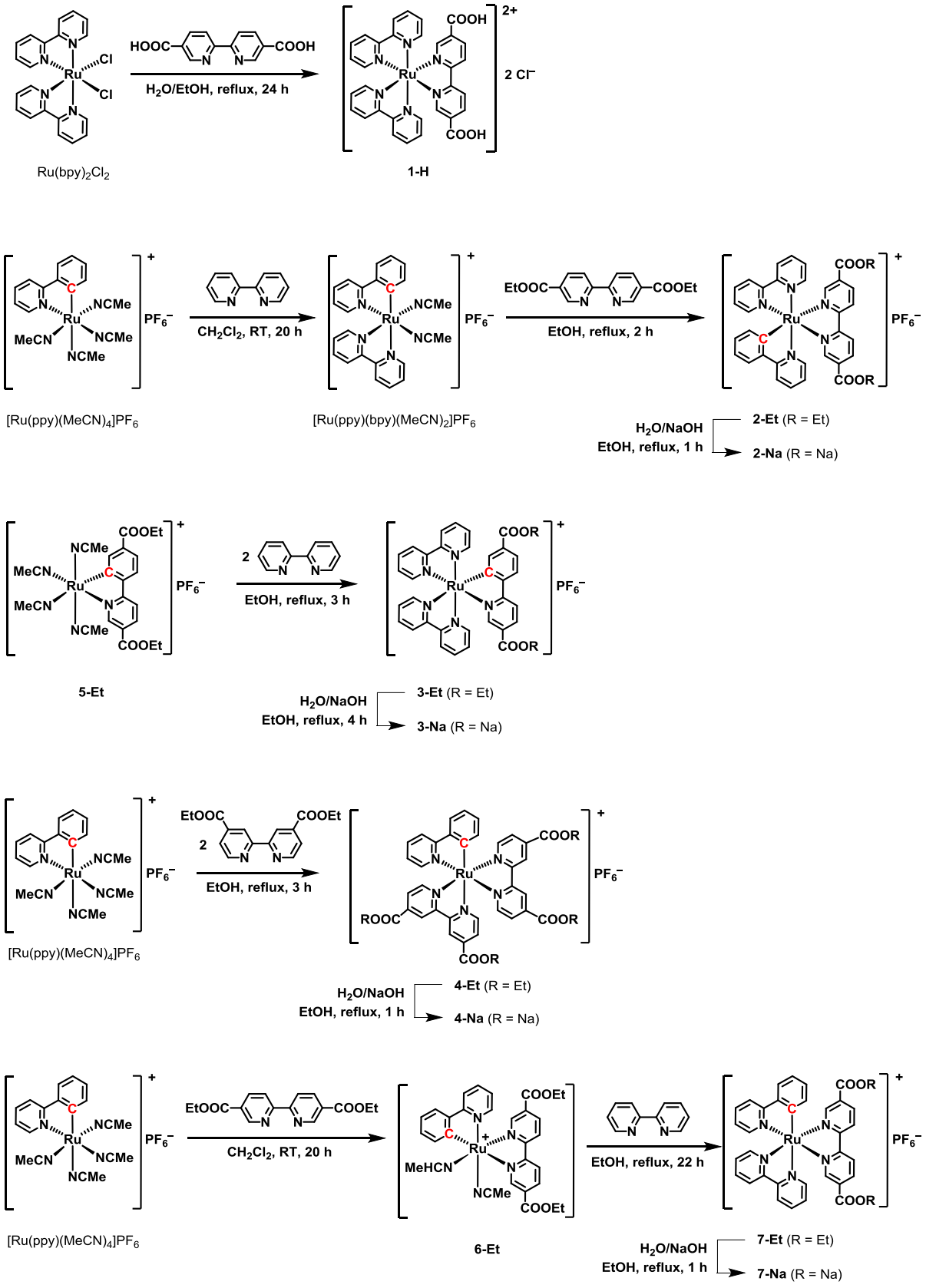

The synthesis of complex **2-Na** involved the intermediate compound $[Ru(ppy)(MeCN)_4]PF_6$, which was prepared from $RuCl_3$, through $[Ru(C_6H_6)Cl_2]_2$, using a slight modification of the literature procedure.[105-106] The use of 10 % excess of phenylpyridine (ppy) and heating at 50 °C in MeCN for 18 h, followed by recrystallization, increased the yield of $[Ru(ppy)(MeCN)_4]PF_6$ from the previously reported 40 % to 59 %. $[Ru(ppy)(MeCN)_4]PF_6$ was then reacted with bpy following the reported procedure to give $[Ru(ppy)(bpy)(MeCN)_2]PF_6$,[107] which was further reacted with diethyl 2,2'-bipyridine-5,5'-dicarboxylate (debpy) in EtOH at reflux to furnish the new complex **2-Et**. The subsequent hydrolysis of **2-Et** to yield **2-Na** was performed with 2 equiv. of NaOH in EtOH/H_2O at reflux for 1 h. Alternative attempts to prepare **2-Na**, including a one-pot stepwise treatment of $[Ru(ppy)(MeCN)_4]PF_6$ with bpy and then H_2bpydc, and reacting $[Ru(ppy)(bpy)(MeCN)_2]PF_6$ with H_2bpydc were not successful.

The preparation of **2-Et** could also be envisioned by changing the order of ligation of bpy and debpy to ruthenium. This was investigated by first reacting $[Ru(ppy)(MeCN)_4]PF_6$ with debpy in DCM at room temperature for 20 h. After filtration through alumina and subsequent recrystallization, complex **6-Et** was isolated, which was then reacted with bpy in refluxing EtOH to afford complex **7-Et**. As shown by ^{1}H NMR spectroscopy, complexes **2-Et** and **7-Et** are not identical (Figures S2 and S10 in the SI of **Paper I**). This indicates that the other diastereomer was obtained, which was confirmed by the crystal structure of **7-Et** (*vide infra*). The hydrolysis of **7-Et** to yield **7-Na** was accomplished using the same experimental conditions that were used for the hydrolysis of **2-Et** to give **2-Na**.

The synthesis of **3-Na** started with the preparation of **5-Et**, which is readily available by reaction of $[Ru(C_6H_6)Cl_2]_2$ with ethyl 6-(4-(ethoxycarbonyl)phenyl)pyridine-3-carboxylate (deppy) in MeCN. Reacting **5-Et** with 2 equiv. of bpy in EtOH at reflux for 3 h then provided **3-Et**. For the hydrolysis of **3-Et** to furnish **3-Na**, it was found that a larger excess of NaOH (5.1 equiv.) and a longer reaction time (4 h) was required compared to the corresponding reaction of **2-Et**. This is in agreement with the formally anionic character of the deppy ligand in **3-Et** compared to the neutral debpy ligand in **2-Et**.

The synthesis of complex **4-Na** was based on the same intermediate compound as the synthesis of **2-Na**, i.e. $[Ru(ppy)(MeCN)_4]PF_6$. Ligand exchange was accomplished by a reaction with 2 equiv. of diethyl 2,2'-bipyridine-4,4'-dicarboxylate in EtOH at reflux for 3h to give **4-Et**, and subsequent hydrolysis with 4 equiv. of NaOH furnished pure **4-Na**. This strategy was necessary

because the literature procedure, in which **4-Na** was prepared directly by reaction of $[Ru(ppy)(MeCN)_4]PF_6$ with 2,2'-bipyridine-4,4'-dicarboxylic acid,[18, 23] did not successfully produce pure **4-Na**.

Complexes $[Ru(ppy)(bpy)(MeCN)_2]PF_6$, **1-H**, **2-Et**, **2-Na**, **3-Et**, **3-Na**, **6-Et** and **7-Et** formed high quality crystals using vapor diffusion crystallization,[95] and were suitable for single crystal X-ray diffraction (SC-XRD) structure determination. Their molecular structures are shown in Figure 10. Carbon and nitrogen atoms could be unambiguously distinguished in all cases, and the bonds *trans* to either of them have lengths that are consistent with the stronger *trans* influence of the carbon atom compared to that of the nitrogen atom.

An interesting trend, which is related to the location of the carbon atoms that are bonded to ruthenium, can be seen from these crystal structures. In $[Ru(ppy)(bpy)(MeCN)_2]PF_6$, the carbon atom is *trans* to the bpy ligand, while in **2-Et** and **2-Na**, it is *trans* to the substituted bpy ligands. Moreover, in **6-Et**, the carbon atom is *trans* to debpy, while in **7-Et**, it is *trans* to bpy. Thus, in the two synthetic protocols $[Ru(ppy)(MeCN)_4]PF_6$ → $[Ru(ppy)(bpy)(MeCN)_2]PF_6$ → **2-Et** and $[Ru(ppy)(MeCN)_4]PF_6$ → **6-Et** → **7-Et** (Scheme 1), the carbon atom becomes *trans* to the incoming ligand in each reaction step. This results in **2-Et** (**2-Na**) and **7-Et** (**7-Na**) being diastereomers. In light of these observations, a plausible explanation is that ligand exchange (which involves replacement of two MeCN ligands) occurs stepwise. In the initial step, detachment of one MeCN ligand from ruthenium generates a vacant coordination site. The resulting 5-coordinated Ru(II) complex will have a low barrier for configurational reorganization such that the high *trans* influence C atom occupies the position *trans* to the vacant site. When the incoming ligand (bpy or debpy) coordinates one of its N atoms to Ru, followed by detachment of the second MeCN, the chelate effect will direct the second N atom to occupy the now vacant site before another configurational reorganization has time to take place.

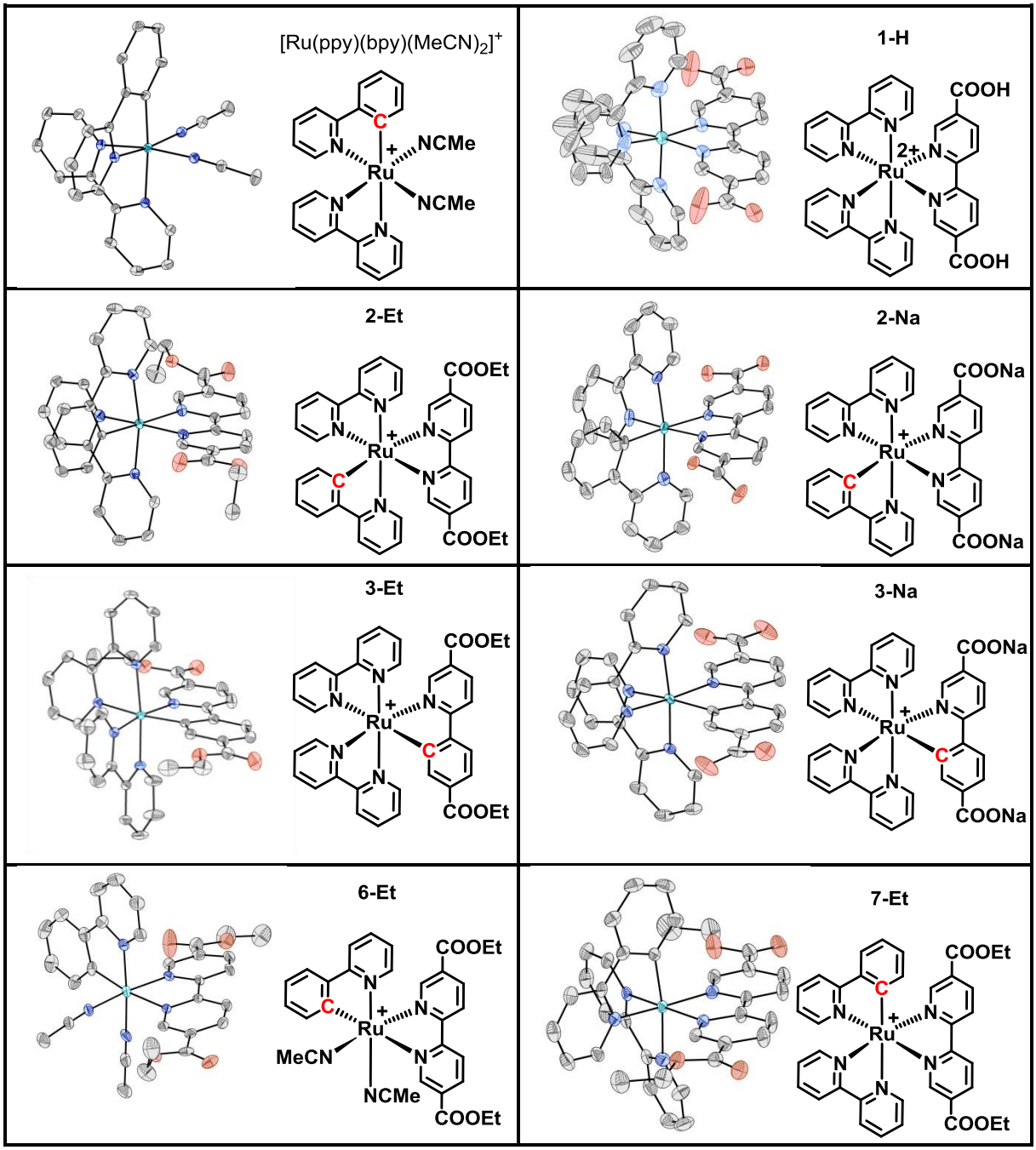

Figure 10. ORTEP plots of the complexes $[Ru(ppy)(bpy)(MeCN)_2]^+$, 1-H, 2-Et, 2-Na, 3-Et, 3-Na, 6-Et and 7-Et determined by single-crystal X-ray diffraction. Hydrogen atoms, counter ions and solvate molecules have been omitted for clarity. Ellipsoids are shown at 50 % probability. In 3-Na, the carboxylated ligand is disordered by symmetry, and the pyridine and phenyl rings occupy equivalent sites with a site occupancy coefficient of 0.5 each. The figure shows one of the possible arrangements.

The light absorption properties of the complexes were investigated by UV-Vis spectroscopy. Figure 11 shows the spectra of **1-Na** (deprotonated for comparison), **2-Na**, **3-Na** and **4-Na** in methanol solution. There is a substantial difference between the non-cyclometalated complex **1-Na** and the cyclometalated complexes **2-Na**, **3-Na** and **4-Na**, in that the latter three show a

bathochromic shift of the lowest-energy absorption band, and also more and broader bands in the visible region. These phenomena arise due to the reduction of both the energy gap and the molecular symmetry, as described in section 1.1. The lowest-energy band of **3-Na** is slightly blue-shifted in comparison to the lowest-energy band of **2-Na**. Complex **4-Na** has a pronounced higher molar absorptivity in the visible region in comparison to the other complexes.

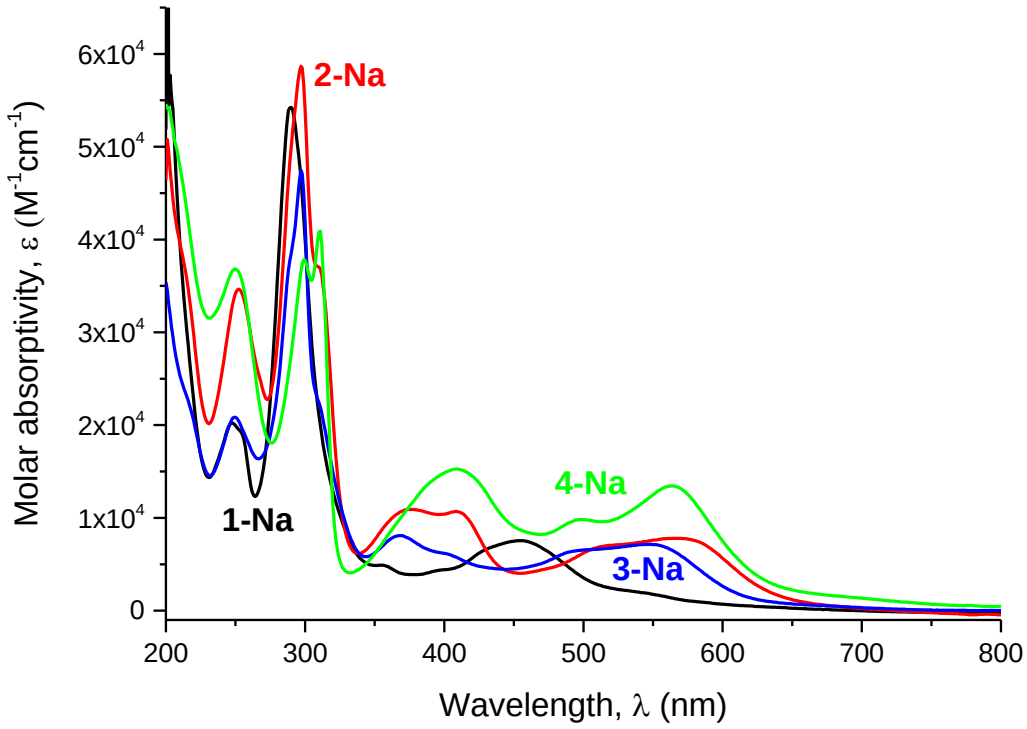

Figure 11. Absorption spectra of complexes 1-Na, 2-Na, 3-Na and 4-Na in methanol, recorded at room temperature.

For the complexes to be useful as photosensitizers, it is important to know how the electron densities in the excited states are distributed in the molecular structures. In order to gain detailed insight into the electronic structures of the complexes, computational investigations were performed. DFT (Density Functional Theory) calculations were carried out to optimize the geometries of the complexes, and TD (Time Dependent)-DFT was then employed to model their absorbance spectra in methanol, using the experimental spectra as reference. The TD-DFT calculations were then used to assign the experimental absorption bands to specific electronic transitions. All calculations were performed by David Balcells.

Figure 12 shows the energies and shapes of the molecular orbitals involved in the key electronic transitions, which are collected in Table 3. All relevant excitations in the visible region can be described as MLCT (metal-to-ligand charge transfer).

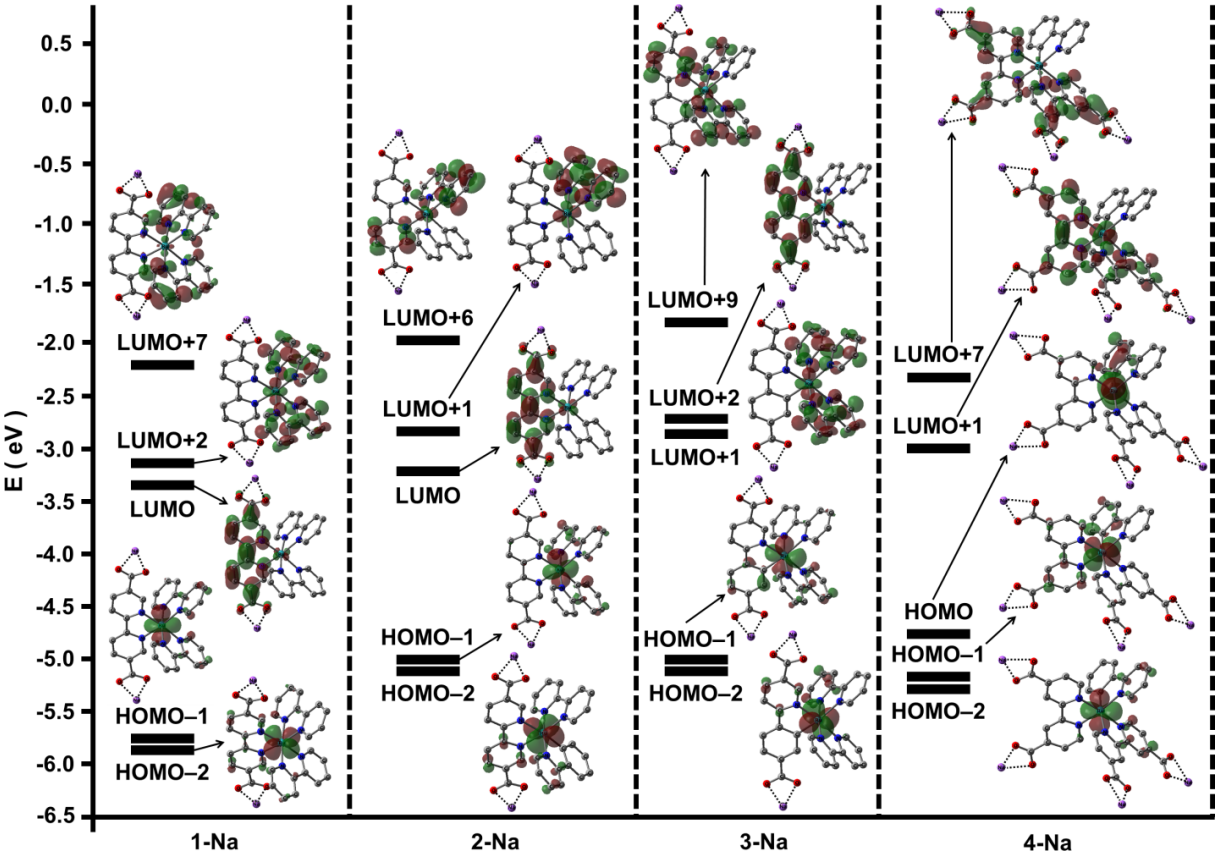

Figure 12. TD-DFT(M11L/6-311G, LANL2TZ(f)) electronic excitations for the complexes. See Table 3 for more details. The 4-Na LUMO+2 orbital is not included for the sake of clarity. All orbitals are shown at an isovalue of 0.04 a.u.**

Table 3. TD-DFT(M11L/6-311G, LANL2TZ(f)) parameters for the complexes, including the wavelength (λ_{Exc}), oscillator strength (f) and molecular orbitals (MOs, see Figure 12) of the main electronic excitations[a]**

Complex	λ_{Exc} (nm)	f	MOs
1-Na	351	0.0502	HOMO-1 → LUMO+7
	452	0.1016	HOMO-2 → LUMO+2
	512	0.0714	HOMO-2 → LUMO
2-Na	406	0.0559	HOMO-1 → LUMO+6
	527	0.0534	HOMO-1 → LUMO+1
	604	0.0707	HOMO-2 → LUMO
3-Na	381	0.0789	HOMO-1 → LUMO+9
	510	0.0481	HOMO-2 → LUMO+1
	515	0.0378	HOMO-1 → LUMO+2
4-Na	423	0.0767	HOMO-2 → LUMO+7
	444	0.0633	HOMO-1 → LUMO+7
	464	0.0560	HOMO-1 → LUMO+2
	493	0.0985	HOMO → LUMO+7
	545	0.0978	HOMO-1 → LUMO+1

[a] Those with the largest coefficient in the CI expansion.

The HOMO-2 and HOMO-1 orbitals in all complexes (and in addition the HOMO of **4-Na**) are metal d-orbitals. These orbitals are positioned at higher energy for the cyclometalated complexes (**2-Na**, **3-Na**, and **4-Na**) than for **1-Na**, because of the additional negative charge introduced by the cyclometalating ligands. This energy increase is significantly smaller for the virtual orbitals, including the LUMO, causing a bathochromic shift of the absorbance bands of the cyclometalated complexes, consistent with the experiments. As seen in Table 3, all complexes have intense excitations to virtual orbitals located on the ligands substituted with carboxylate groups (LUMO in **1-Na** and **2-Na**, LUMO+2 in **3-Na** and both LUMO+1 and LUMO+7 in **4-Na**). This property makes these complexes promising for electron transfer via the carboxylate groups into a potential MOF structure,[72-73, 78, 82-84, 90, 92] similar to the sensitization process in DSSCs.[2]

Due to the different electronic characteristics of the carboxylated ligand in **3-Na** (anionic) and in **2-Na** (neutral), the energy of the virtual orbital on this ligand is higher for **3-Na** (LUMO+2) than for **2-Na** (LUMO). This leads to a smaller energy gap for **3-Na** than for **2-Na**, consistent with the slightly blue-shifted experimental spectrum of the former. In complex **4-Na**, the delocalization of the LUMO and nearby orbitals over two carboxylated ligands leads to more numerous and intense transitions. Moreover, the oscillator strengths of these transitions are significantly larger than those for the other complexes, consistent with the higher molar absorptivity seen in the experiments.

The difference in stereochemistry of complexes **2-Na** and **7-Na**, mentioned above (the Ru-C bond from ppy *trans* to bpydc or bpy, respectively), was further explored by calculation of their respective absorption spectra. Figure 13 shows that these calculated spectra qualitatively agrees with the experimental ones, thus supporting the configurations assigned from the SC-XRD measurements (Figure 10). Moreover, the different absorption profiles of the two isomers in the near-IR region is due to the nature of the electron excitation to the LUMO. In **2-Na**, the electron originates from the HOMO-2, whereas in **7-Na**, it originates from the HOMO-1 (Figure S35 in the SI of **Paper I**).

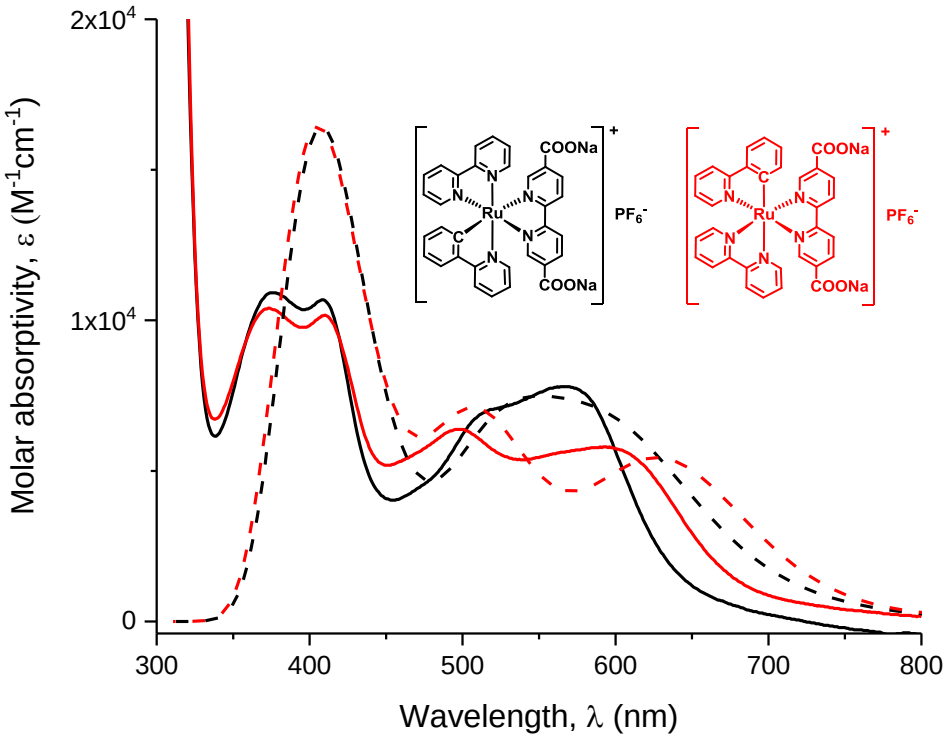

Figure 13. TD-DFT calculations of the electronic absorption spectra of the C-*trans*-bpydc (black dashed line) and C-*trans*-bpy (red dashed line) isomers of the trisheteroleptic Ru(II) complex compared to the experimental spectra of 2-Na (black solid line) and 7-Na (red solid line).

3.2. Incorporation of Ru(II) Complexes into UiO-67

The next step was to incorporate the four Ru(II) complexes into UiO-67. As pointed out earlier, this MOF was chosen due to its high thermal and chemical stability,[26] and the structural similarity between its biphenyl-4,4'-dicaboxylate (bpdc) linkers and the carboxylated ligands in the Ru(II) complexes synthesised in this work (except **4-Na**, as mentioned in section 3.1). By searching the literature, three synthetic strategies emerged as potential candidates for this work. As described in sections 1.2 and 2.1, and illustrated in Figure 14, these were premade linker synthesis (PMLS),[11-12, 45-47] postsynthetic functionalization (PSF),[13, 41, 43, 48-50] and postsynthetic linker exchange (PSLE).[51-55]

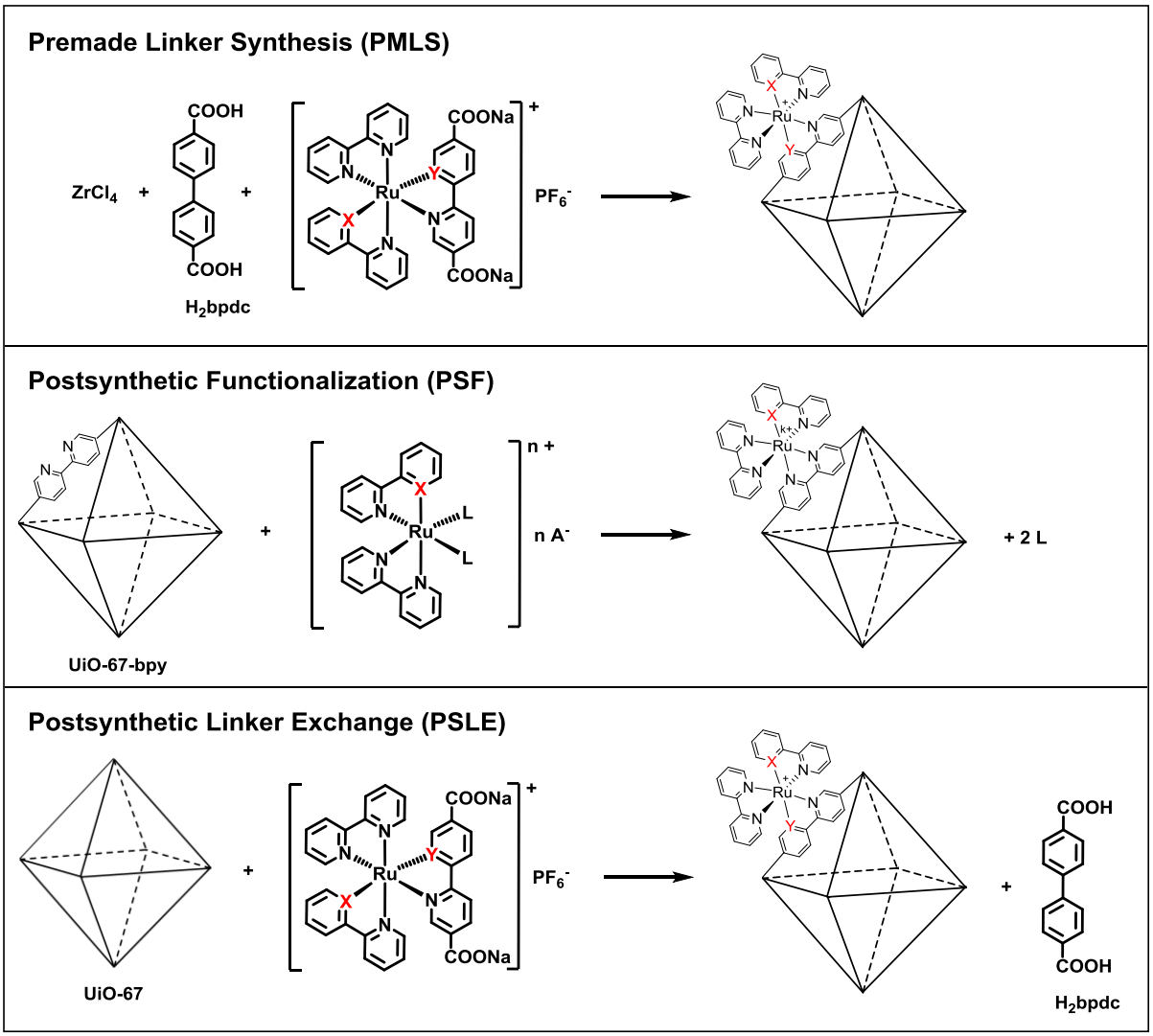

Figure 14. The three functionalization methods used in this work to incorporate cyclometalated Ru(II) complexes into UiO-67. The octahedra represent the octahedral cages in UiO-67. X, Y = C or N. L = Cl^-, n = 0, k = 2 (1-PSF) or L = MeCN, A^- = PF_6^-, n, k = 1 (2-PSF). Further descriptions of the methods are provided in sections 1.2 and 2.1.

Complexes **3-Na** and **4-Na** cannot be incorporated by the PSF method. This is due to the fact that **3-Na** is synthesized via base promoted C-H activation[97] which is not feasible for reaction with the MOF structure, and UiO-67 does not contain linkers that can be substituted for any of the ligands in complex **4-Na,** as mentioned in section 3.1. Thus, the combination of the four Ru(II) complexes in Figure 9 (page 30) and the three functionalization methods resulted in (4·3) – 2 = 10 different Ru(II)-functionalized MOF systems. In the following, these are referred to by a number corresponding to one of the four Ru(II) complexes, and the acronym for the respective functionalization method: **1-PMLS**, **2-PSF**, etc.

The PXRD patterns for each of the Ru(II)-functionalized MOFs are shown in Figure 15. All of them are clearly crystalline and their diffractograms correspond to that of UiO-67. This shows that the synthesis of UiO-67 was not disturbed by the presence of the Ru(II) complexes during PMLS, and that the premade UiO-67 structure remained intact during the PSF and PSLE reactions. These results are not surprising given the high stability of this material.[26] **4-PSLE** is less crystalline than the other MOFs. This could be due to the reaction conditions (DMF/water, 100 °C, 3 d) and the molecular structure of complex **4-Na**, which could interfere with the regular network structure in UiO-67, which is based on linear linkers.

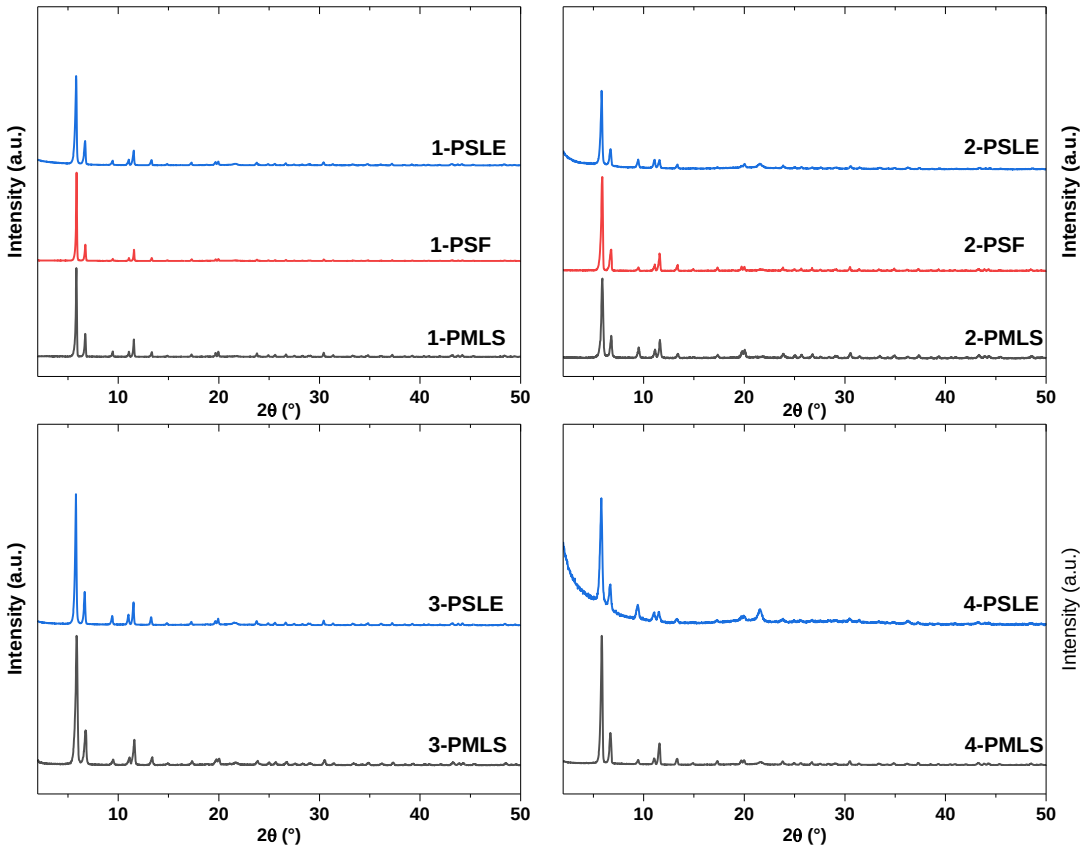

Figure 15. Powder X-ray diffraction patterns for the Ru(II)-functionalized UiO-67 MOFs.

In order to assess the porosity of the prepared MOFs, nitrogen adsorption/desorption measurements were performed. As seen in Table 4, the calculated BET surface areas (A_{BET}) of the Ru(II)-functionalized MOFs obtained from these measurements are reasonable compared to those of pristine UiO-67 and UiO-67-bpy. The incorporation of Ru(II) complexes in the MOF structures, whether as linkers or simply occupying the pores, will naturally lead to lower measured surface areas. This is both because they occupy pore volume and because they

contribute to the total weight that is attributed to the MOF (A_{BET} has a unit of m^2g^{-1}). MOFs **2-PSLE** and **4-PSLE** have the lowest A_{BET}. The low surface area of **4-PSLE** could be explained by the fact that complex **4-Na** may occupy a substantial amount of pore volume as it has four carboxylate groups that could coordinate at defect sites in the MOF structure. **1-PSF** and **3-PMLS** have remarkably high A_{BET}, which could possibly be due to missing linker defects.[108-109] Moreover, the white appearance of **3-PMLS** indicates a very low loading of Ru(II) complexes in the MOF, thus significant occupation of pore volume is not expected.

Table 4. Selected characteristics of the Ru(II)-functionalized MOFs and pristine UiO-67/UiO-67-bpy that were used for the PSLE and PSF reactions, respectively. Pictures of the powders, adsorption/desorption isotherms, and TGA-DSC traces are provided in the Supporting Information of Paper II.

MOF	Color	A_{BET} (m^2g^{-1})	TGA, mass loss range (°C)	SEM, crystallite sizes (μm)	EDS, Ru:Zr ratio
UiO-67	White	2457	480 – 550	0.5 – 2	0
UiO-67-bpy[43]	White	2460	475 – 540	0.5 – 2	0
1-PMLS	Orange	2300	370 – 420	0.5 – 2	0.04 – 0.11
1-PSF	Light orange/brown	2457	380 – 420	0.5 – 2	0.02 – 0.03
1-PSLE	Orange	1694	365 – 415	0.5 – 2	0.03 – 0.05
2-PMLS	Grey	1996	370 – 420	0.2 – 0.5	0.07 – 0.09
2-PSF	Grey/purple	2346	360 – 460	0.5 – 2	0.05 – 0.06
2-PSLE	Dark purple	940	330 – 390	0.5 – 1.5	0.18 – 0.19
3-PMLS	White	2541	450 – 520	0.2 – 0.5	0.01 – 0.03
3-PSLE	Dark maroon	1405	365 – 415	1 – 2	0.21 – 0.23
4-PMLS	Dark purple	1530	370 – 420	0.75 – 3	0.07 – 0.12
4-PSLE	Dark purple	761	280 – 355	0.5 – 2	0.07 – 0.09

The thermal stabilities of the MOFs in air were probed by thermogravimetric analysis (TGA). As can be read from Table 4, the mass loss corresponding to burning of the aromatic linkers appears at around 400 °C for most of the MOFs, which is approximately 100 °C lower than that for pristine UiO-67 or UiO-67-bpy. This difference is probably in part due to increased strain in the MOF structure introduced by the incorporation of the Ru(II) complexes. **3-PMLS** is slightly more stable than the other MOFs, which again can be related to its apparently low

ruthenium content. **4-PSLE** is slightly less stable than the rest, in agreement with the low crystallinity seen from its PXRD pattern.

The morphology of the MOF crystallites was studied with scanning electron microscopy (SEM). Figures 16 - 25 show the SEM images and Table 4 lists the crystallite sizes. It is clear that all the MOFs consist of octahedral crystallites, characteristic of UiO-67. The crystallites of **4-PSLE** (Figure 25) appear to have undergone a degree of erosion. This indicates that the material is partially degraded, which is in agreement with its relatively low crystallinity, surface area, and thermal stability. In **4-PMLS** (Figure 24) and all of the PSLE MOFs (Figures 18, 21, 23, and 25), there are extra phases agglomerated on the surfaces of the crystallites. This could possibly be residual Ru(II) complex phases that were not removed by the washing procedure. These agglomerates might also contribute to the somewhat lower A_{BET} values for these MOFs, in comparison to the rest, by partially blocking the crystallite surfaces for gas diffusion (and by their weight that is attributed to the MOFs). When comparing the SEM images of **4-PMLS** (Figure 24) and **4-PSLE** (Figure 25), it is apparent that there are more agglomerated phases (possibly complex **4-Na**) on the surfaces of the crystallites of **4-PMLS** than on **4-PSLE**. This could indicate that a higher portion of complex **4-Na** is inside the pores, rather than on the surface, of **4-PSLE** compared to **4-PMLS**. This hypothesis is in agreement with both the aforementioned argument concerning lower crystallinity due to incorporation of complex **4-Na**, and the lower A_{BET} for **4-PSLE** (761 m^2g^{-1}) compared to **4-PMLS** (1530 m^2g^{-1}).

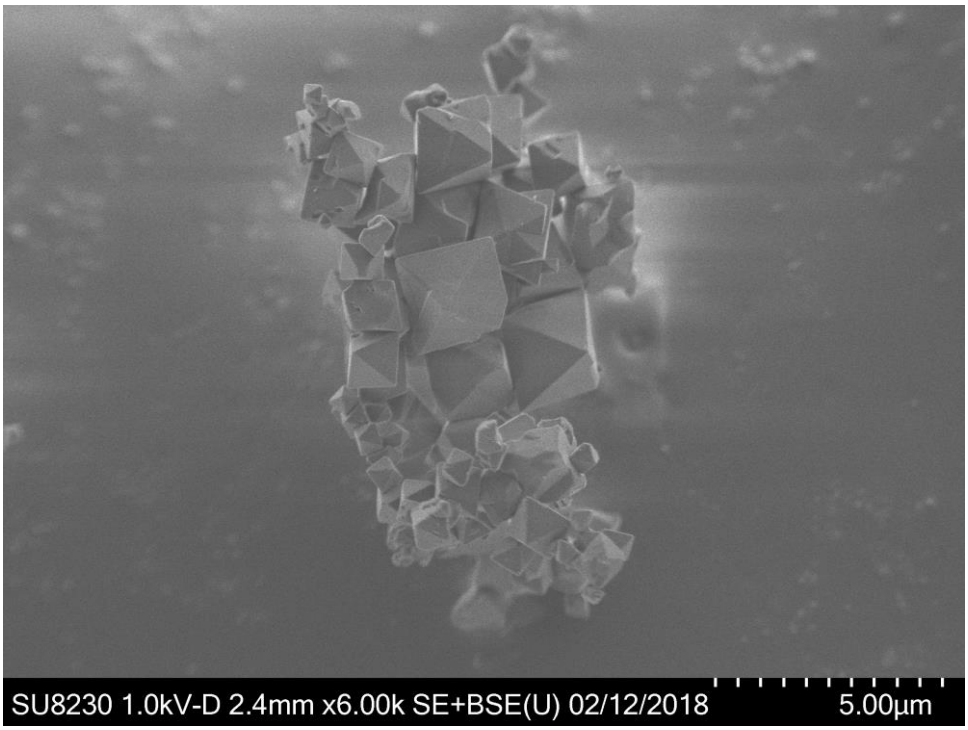

Figure 16. SEM image of 1-PMLS.

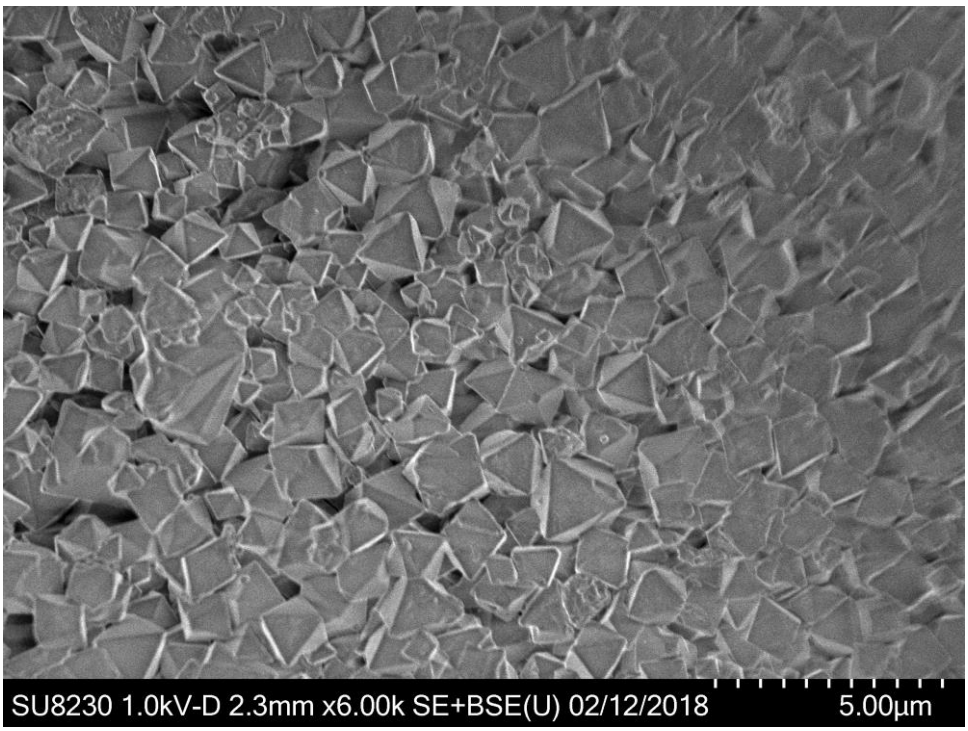

Figure 17. SEM image of 1-PSF.

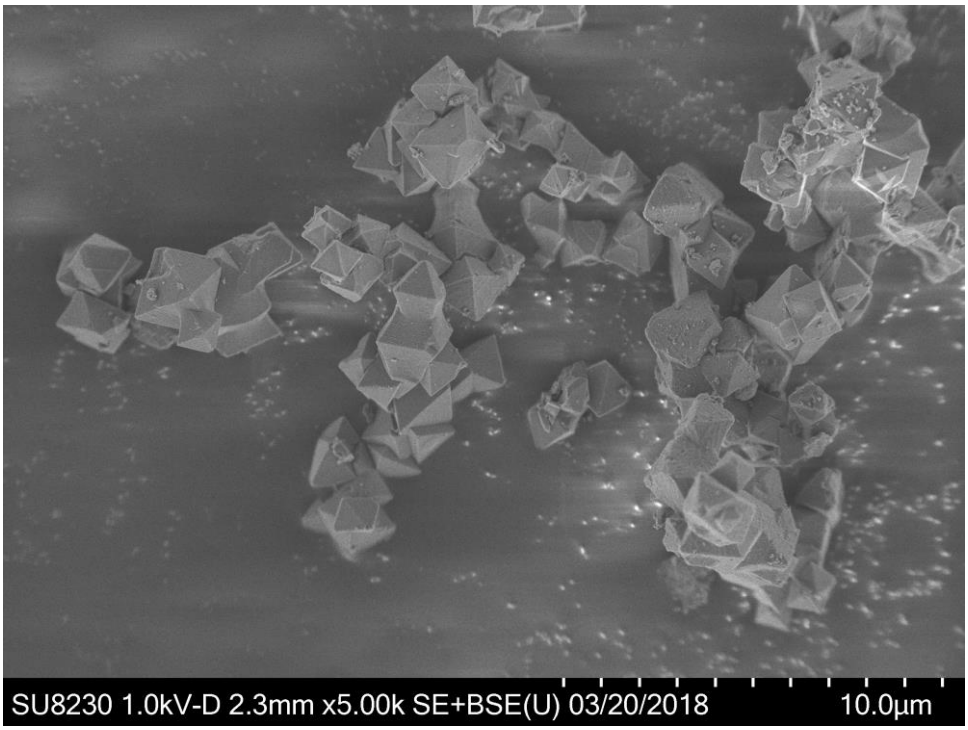

Figure 18. SEM image of 1-PSLE.

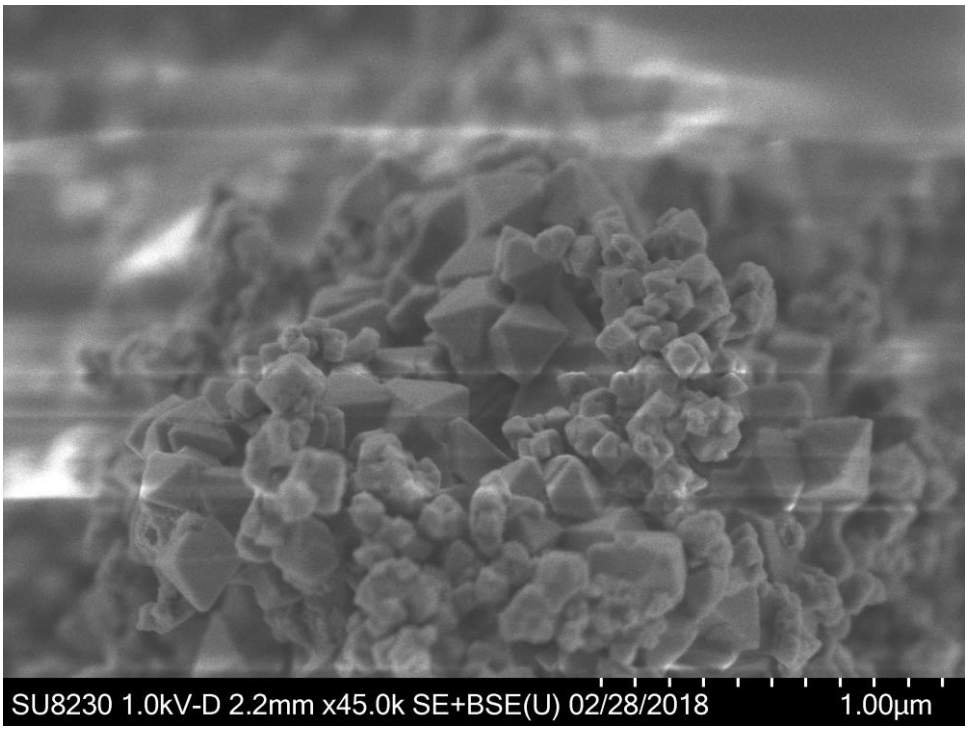

Figure 19. SEM image of 2-PMLS.

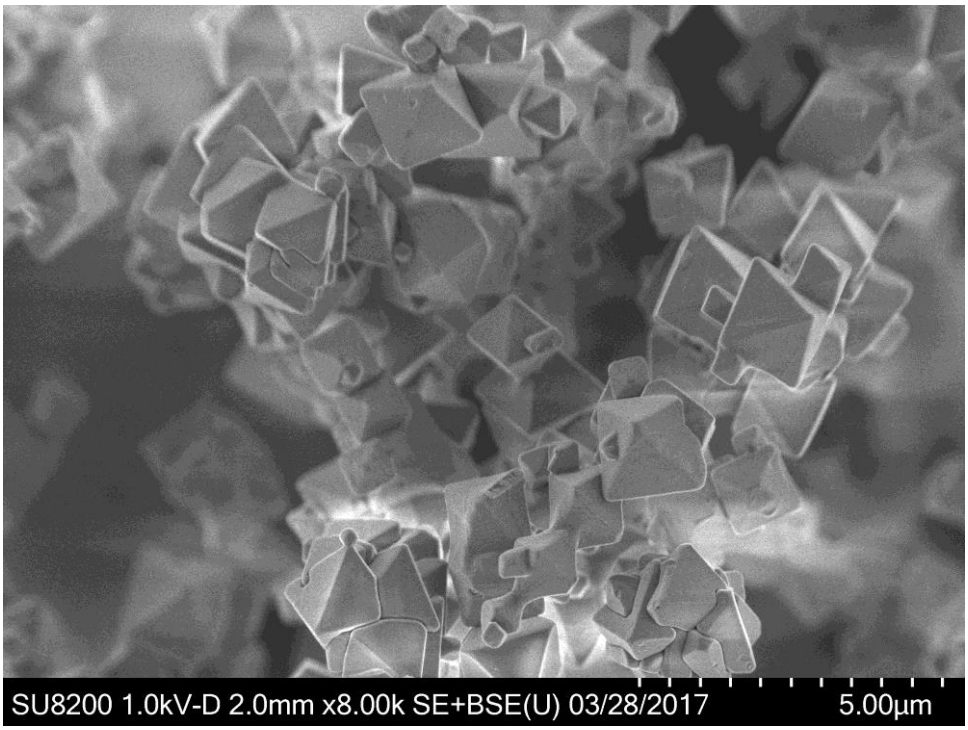

Figure 20. SEM image of 2-PSF.

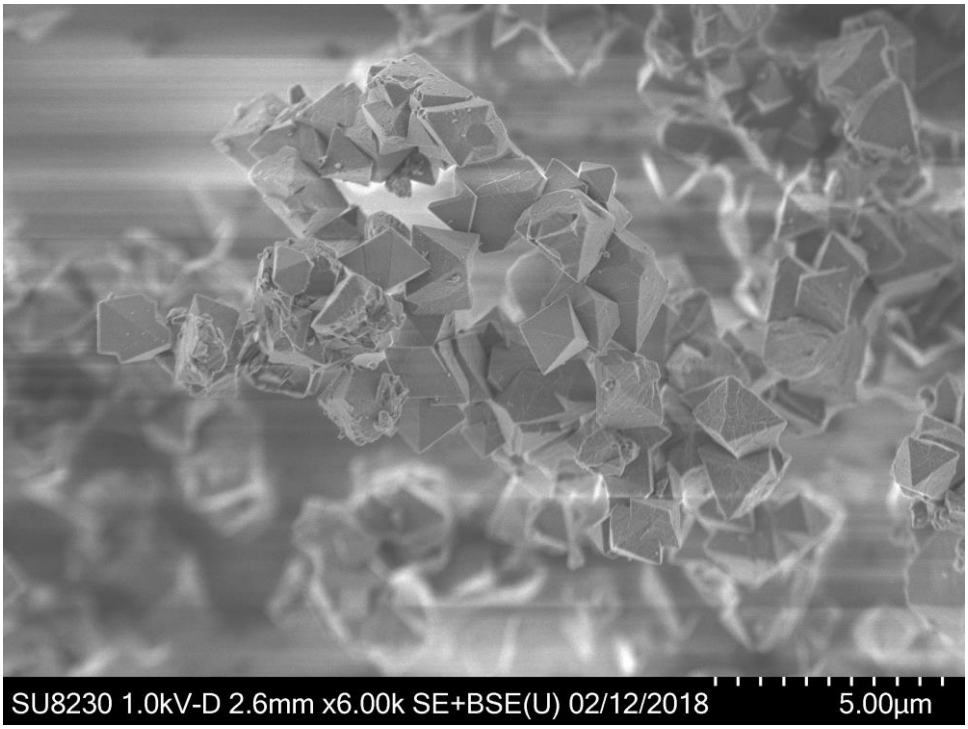

Figure 21. SEM image of 2-PSLE.

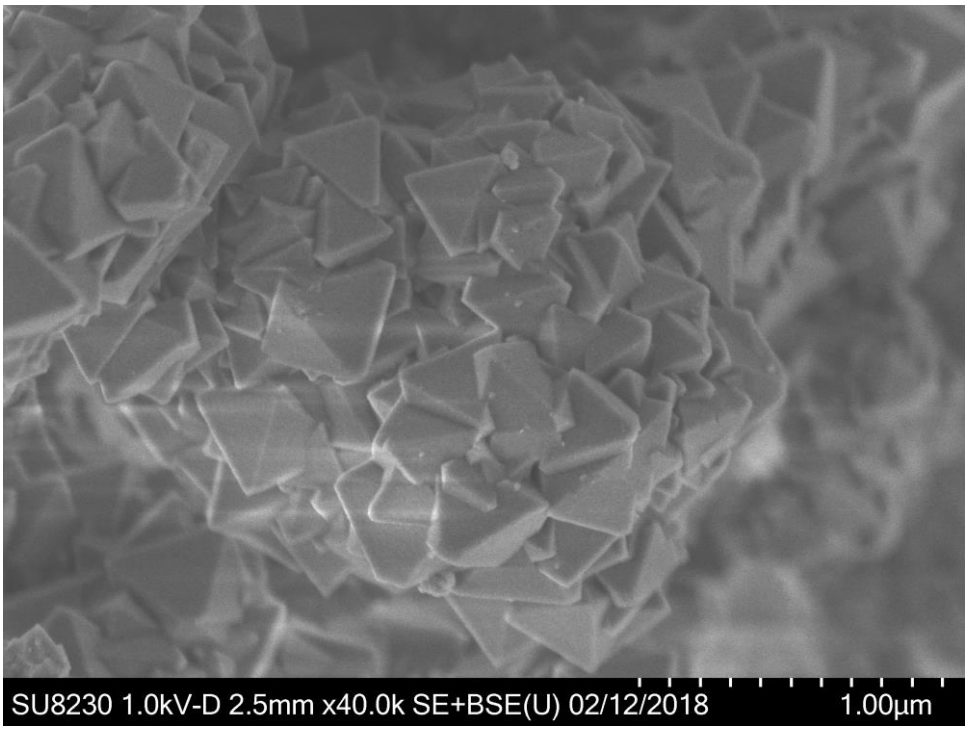

Figure 22. SEM image of 3-PMLS.

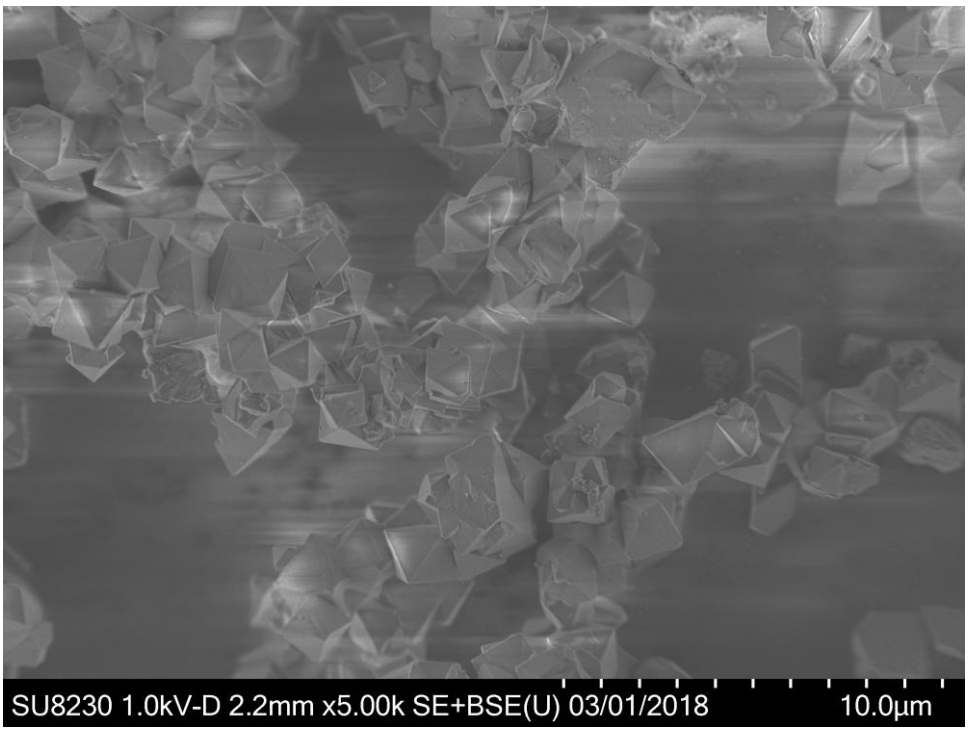

Figure 23. SEM image of 3-PSLE.

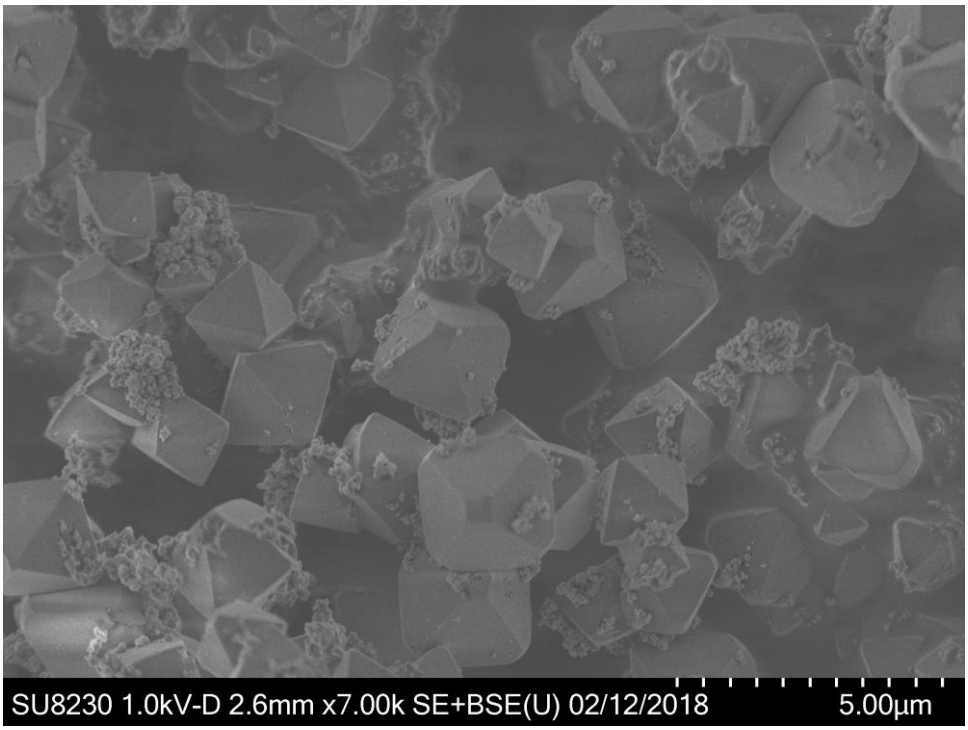

Figure 24. SEM image of 4-PMLS.

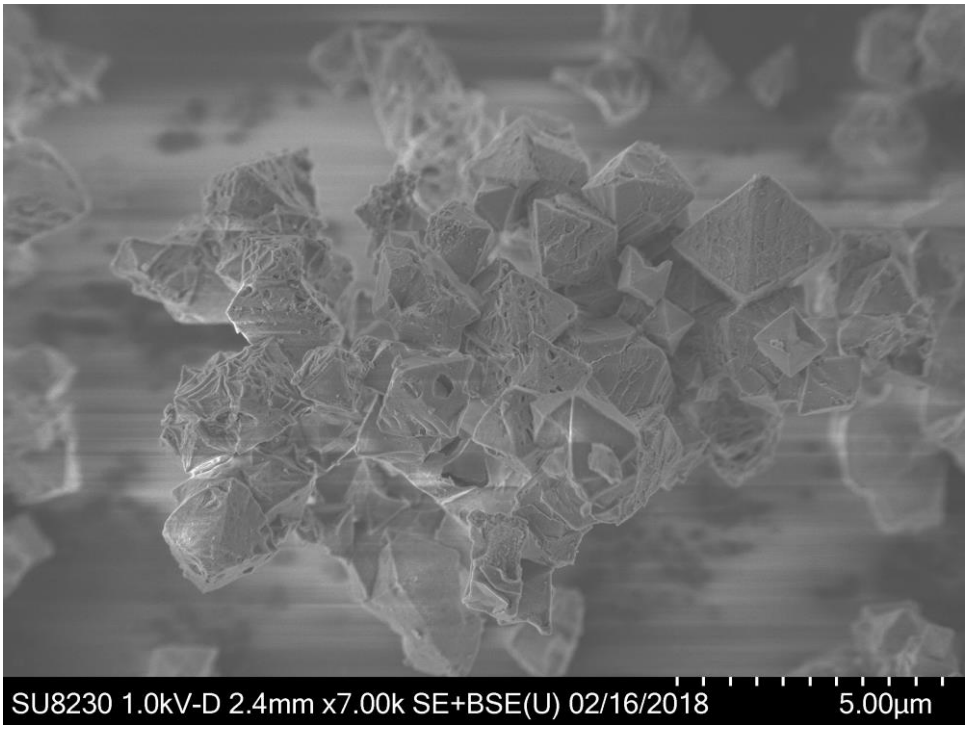

Figure 25. SEM image of 4-PSLE.

In order to estimate the Ru:Zr ratios in the materials, energy-dispersive X-Ray spectroscopy (EDS) was employed. Table 4 lists the ranges of measured ratios. Keeping in mind that in UiO-67 there is one linker per Zr atom, in the case of proper chemical incorporation of the Ru(II) complexes as linkers, the Ru:Zr ratio would correspond to the proportion of the linkers that are functionalized by Ru(II) complexes. For PMLS, 10 % of the linkers used were Ru(II)-functionalized, so the Ru:Zr ratios are within expected values. Ratios higher than 0.1 would indicate that the synthesis system favors the incorporation of the Ru(II)-functionalized linker. The ruthenium content is very low in **3-PMLS**, in accordance with its white appearance, high surface area, and thermal stability, as pointed out above. The Ru:Zr ratios in **1-PSF** (0.02 - 0.03) and **2-PSF** (0.05 - 0.06) are also as expected, since a UiO-67 sample with 5 % bpydc linkers was used in the PSF syntheses. The use of UiO-67 with 10 % bpydc was also attempted for the preparation of **2-PSF**, but this resulted in the same Ru:Zr ratio as when UiO-67 with 5 % bpydc was used. This indicates that steric factors may limit the amount of Ru(II) complex that can be incorporated in this manner. The crystallite sizes, and thus the ratio of surface area to internal pore volume, were approximately the same for the 5 % and 10 % bpydc loaded MOF samples.

2-PSLE and **3-PSLE** have significantly higher Ru:Zr ratios (0.18 – 0.19 and 0.21 – 0.23, respectively) compared to **2-PMLS** and **3-PMLS** (0.07 – 0.09 and 0.01 – 0.03, respectively), which is in agreement with the difference in their respective BET surface areas. The high Ru loading in these PSLE MOFs are as expected since 1 equiv. of Ru(II) complex with respect to bpdc linker was used in the synthesis. However, **1-PSLE** and **4-PSLE** actually have similar or lower Ru:Zr ratios (0.03 – 0.05 and 0.07 – 0.12, respectively) than **1-PMLS** and **4-PMLS** (0.04 – 0.11 and 0.07 – 0.12, respectively). The difference in Ru:Zr ratios between **2-PSLE** and **3-PSLE** on one hand and **1-PSLE** and **4-PSLE** on the other could be due to the difference in the molecular structures of their respective Ru(II) complexes. Complexes **2-Na** and **3-Na** are monocationic and their carboxylate groups are in a linear arrangement, while **1-H** is dicationic (although linear) and **4-Na** have four carboxylate groups in a different arrangement (although monocationic).

As mentioned in section 1.2, complex **1-H** has previously been incorporated into UiO-67 by all of the three methods explored in this work, although with variations in the detailed experimental parameters. In two different studies, **1-PMLS** was reported with a Ru:Zr ratio of 0.02, using ICP-MS[11] and NMR[62] as quantification methods, respectively. In the first report, the synthesis conditions were similar to those in this thesis (including 10 % **1-H**), except that acetic acid was used as the modulator and the reaction temperature was 100 °C.[11] Thus, the use of benzoic acid

and 120 °C as employed herein seems beneficial for the high Ru loadings observed. Details on the synthesis procedure were not provided in the second report.[62] In a third study, a Ru:Zr ratio of 0.01 was reported, quantified by UV-Vis spectroscopy (by digesting the MOF and subsequently recording the optical densities at 448 nm of the solution in order to determine the concentration of the Ru(II) complex).[12] In this report, **1-H** were incorporated simultaneously with $Pt(H_2bpydc)Cl_2$ (8 % of each) using PMLS, thus the low Ru loading could be due to steric limitations. **1-PSF** has been reported with a Ru:Zr ratio as high as 0.15, in which case UiO-67 with as much as 25% bpydc was used for the synthesis.[62] In the same work, **1-PSLE** was reported with a Ru:Zr ratio of 0.01, in which the PSLE reaction was performed in DMF, MeCN, and $EtOH/H_2O$ at 85 °C for 24 h.[62] Thus, the conditions developed in this thesis (DMF/H_2O, 100 °C, 3 d) are probably more appropriate for PSLE with **1-H**, leading to the observed Ru:Zr ratios of 0.03 – 0.05.

Another technique that was utilized in this thesis to investigate the chemical composition of the prepared MOFs was digestion of the materials in base, followed by ^{1}H NMR analysis of the resulting solutions. In the spectra for all the MOFs, except **2-PMLS**, **3-PMLS**, and **4-PMLS**, the signals arising from the respective molecular Ru(II) complexes are clearly apparent (Figures S24-S33 in the supporting information for **Paper II**). This implies that the Ru(II) complexes have remained intact during the functionalization reactions, and that they are part of the MOF materials, either physisorbed or chemically integrated. In the cases of **2-PMLS**, **3-PMLS**, and **4-PMLS**, there are no clear indications of the spectra of the corresponding Ru(II) complexes, which could indicate that the complexes either are not incorporated at all, or that they decompose during MOF synthesis. This is not surprising for **2-PMLS** and **3-PMLS**, which are grey and white, respectively. **4-PMLS**, on the other hand, has the same purple color as the molecular complex **4-Na**.

For the MOFs functionalized by PSF, additional and valuable information can be obtained. In Figure 26 the ^{1}H NMR spectrum of digested **2-PSF** (a) is shown together with the spectra of complex **2-Na** (b), which is the integrated product of the PSF reaction, and of *cis*-$[Ru(ppy)(bpy)(MeCN)_2]PF_6$ (c), which is the molecular Ru(II) precursor for the reaction. The ^{1}H NMR signals arising from complex **2-Na** are clearly distinguishable in the spectrum of the digested MOF, while there is no indication of the reactant *cis*-$[Ru(ppy)(bpy)(MeCN)_2]PF_6$ (the additional signals result from the main bpdc linkers). Since complex **2-Na** was not used as a reactant, it must have been formed during the PSF reaction between the complex *cis*-$[Ru(ppy)(bpy)(MeCN)_2]PF_6$ and the bpydc linkers in the MOF, prior to the digestion

process. These NMR spectra therefore provide good evidence for the proper chemical incorporation of complex **2-Na** as a linker in UiO-67.

Yet another interesting piece of information can be drawn from these spectra. As mentioned in section 3.1, in the precursor *cis*-[Ru(ppy)(bpy)(MeCN)$_2$]PF$_6$ the Ru-bonded C atom of the cyclometalated ppy ligand is located *trans* to a bpy N atom, while in complex **2-Na** this C atom is instead found to occupy a position *trans* to the carboxylated bpy ligand. It was also found that the isomer of **2-Na**, namely **7-Na**, which has the Ru-bonded C atom *trans* to bpy, has a significantly different ^{1}H NMR spectrum than **2-Na**. Hence, it is clear that during the coordination reaction (PSF reaction) that occurs when UiO-67 with 5 % bpydc linkers is reacted with *cis*-[Ru(ppy)(bpy)(MeCN)$_2$]PF$_6$, the same change in stereochemistry is observed at ruthenium as in the corresponding homogeneous reaction.

The ^{1}H NMR spectrum of digested **1-PSF** similarly supported the successful chemical incorporation of complex **1-H** into the MOF (Figure S28 in the supporting information of **Paper II**).

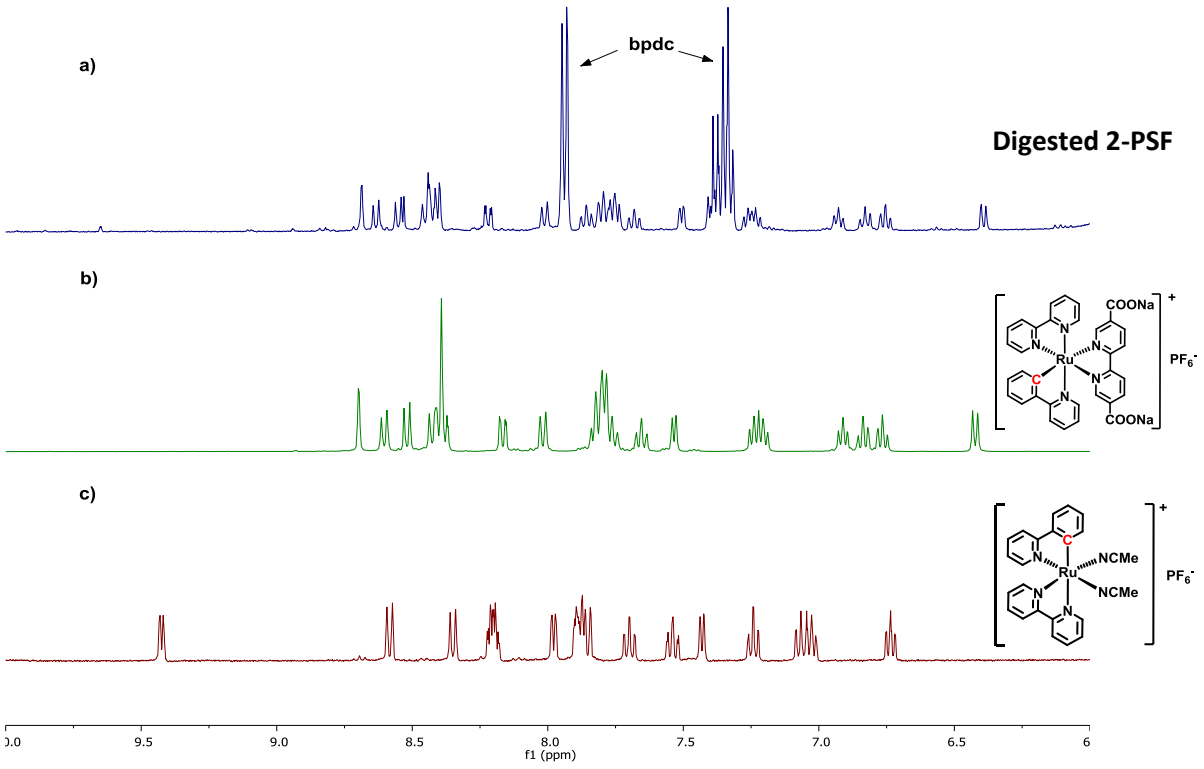

Figure 26. ^{1}H NMR spectra of a) 2-PSF digested in 1 M NaOH, b) complex 2-Na, and c) the Ru(II) precursor *cis*-[Ru(ppy)(bpy)(MeCN)$_2$]PF$_6$. All spectra are recorded in CD$_3$OD.

Ru(II)-functionalized MOF single crystals suitable for SC-XRD were also prepared using the PSF method. In these MOF crystals 3,3'-dimethylbiphenyl-4,4'-dicarboxylic acid was used as main linker (instead of unsubstituted biphenyl dicarboxylic acid) in order to obtain single crystals large enough for measurement on a laboratory source. 10 % of the linkers were substituted by bpydc. In contrast to the PSF reactions on powders, the PSF on single crystals was done in methanol at 60 °C (without stirring) for three days. As can be seen in Figure 27, the Fourier difference maps for both **1-PSF** and **2-PSF** clearly show the presence of an atom in the expected position of ruthenium coordinated to a bipyridine linker. This is, in addition to the NMR results, direct evidence for the chemical incorporation of complexes **1-H** and **2-Na** as linkers in UiO-67.

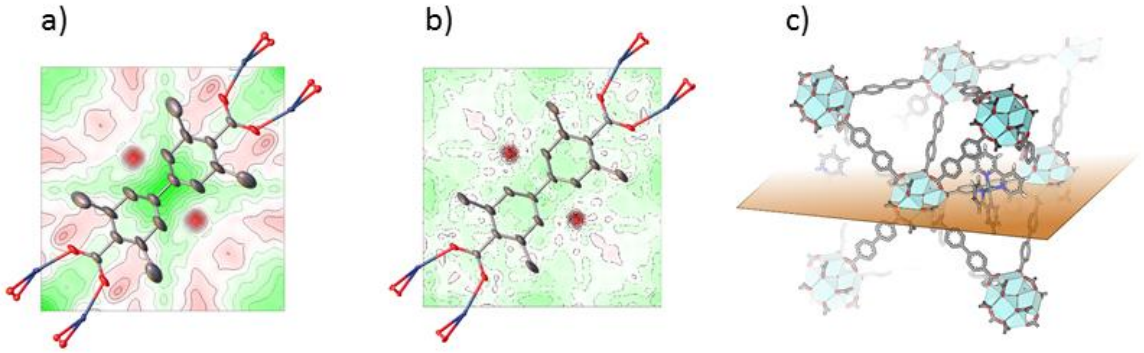

Figure 27. 2D Fourier difference maps of a) 1-PSF and b) 2-PSF, parallel to Miller plane 1 0 0, intersecting the expected position of Ru before including it in the crystal structure refinement. Ru is disordered over two symmetry equivalent positions on each side of the linker's axis of connectivity. c): Representation of the plane used for the Fourier map in the structure of Ru-functionalized UiO-67-Me_2-bpy.

In order to gain detailed information about the electronic properties of the Ru(II)-functionalized MOFs, diffuse reflectance UV-Visible (DR UV-Vis) spectroscopy was employed. The absorbances of the MOFs are shown together with those of the corresponding molecular Ru(II) complexes in methanol solution in Figure 28. It is clear that the MOFs that are functionalized with cyclometalated Ru(II) complexes have absorption bands that extend significantly further into the visible region compared to the MOFs that are functionalized with complex **1-H**. This is the same trend as seen for the molecular complexes (Figure 11, page 35). Qualitatively (with two exceptions), the main features of the absorption profiles of the molecular Ru(II) complexes are apparent in the spectra of the respective Ru(II)-functionalized MOFs. This indicates that the complexes retain their integrity during the functionalization reactions. The two exceptions are **2-PMLS**, which shows a relatively flat absorption profile over the entire visible region, and **3-PMLS**, which absorbs rather weakly in the same region. This is in qualitative agreement with

their grey and white appearances, respectively. Interestingly, the resemblance between the absorption profiles of **2-PSF** and complex **2-Na** indicates that the stereochemistry of the incorporated Ru(II) complex in the MOF is the same as for the molecular complex **2-Na** (ppy-C *trans* to bpydc). This stereochemistry is thus different from that of the precursor *cis*-[Ru(ppy)(bpy)(MeCN)$_2$]PF$_6$ (ppy-C *trans* to bpy), as already discussed for the NMR results.

The MOFs functionalized by PSLE have the highest absorption intensities, compared to those prepared by the other methods. This could be due to a higher portion of the Ru(II) complexes being located on, or close to, the surface of the crystallites as a result of this functionalization method. Indeed, EDS showed that **2-PSLE** and **3-PSLE** have higher Ru:Zr ratios compared to the corresponding MOFs functionalized by PMLS and PSF.

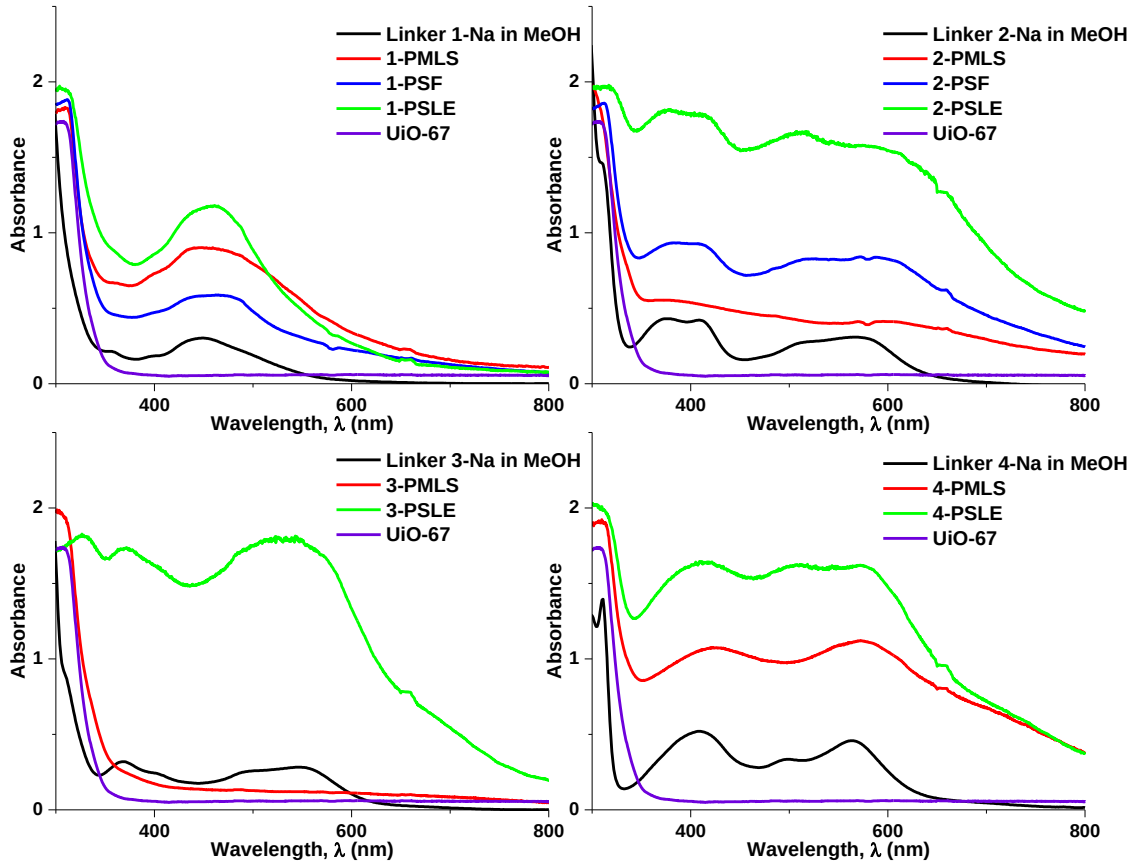

Figure 28. DR UV-Vis spectra of the Ru(II)-functionalized MOFs and the solution spectra of the corresponding Ru(II) complexes in methanol (black lines).

Summarizing this section, UiO-67 can be functionalized with all of the four Ru(II) complexes (**1-H**, **2-Na**, **3-Na**, and **4-Na**) in Figure 9 (page 30). In the following, some conclusions are made about the best methods for incorporation of each of the complexes. These are based on the experimental synthesis conditions, and the resulting material properties observed in this work.

Complex **1-H** could be incorporated utilizing all three functionalization methods, as reported previously.[11-12, 47, 62] However, the premade linker synthesis (PMLS) method is arguably the most promising one for incorporation of this complex. This is because **1-PMLS** showed the highest Ru:Zr ratios (0.04 – 0.11), compared to **1-PSF** (0.02 – 0.03) and **1-PSLE** (0.03 – 0.05), and because **1-PMLS** retains a BET surface area of 2300 m^2g^{-1}, which is significantly higher than that of **1-PSLE** (1694 m^2g^{-1}), and just slightly lower than **1-PSF** (2457 m^2g^{-1}), as seen in Table 4 (page 41).

Attempts of incorporation of complex **2-Na** using the PMLS method led to a grey powder and a flat UV-Vis spectrum (**2-PMLS**, Figure 28). Postsynthetic functionalization (PSF), on the on the other hand, resulted in a defined DR UV-Vis spectrum for **2-PSF**, which was similar to the solution spectrum of complex **2-Na**. For **2-PSF**, it was also possible to directly prove that the Ru(II) complex was really incorporated as a linker in the MOF structure, using ^{1}H NMR analysis of the digestion solution (Figure 26), and SC-XRD (Figure 27). In addition, **2-PSF** showed a higher BET surface area (2346 m^2g^{-1}) than **2-PMLS** (1996 m^2g^{-1}) and **2-PSLE** (940 m^2g^{-1}). Therefore, PSF is the preferred functionalization method for complex **2-Na**.

PMLS was also unsuccessful for the incorporation of complex **3-Na**, as seen from the white appearance and the corresponding UV-Vis spectrum (**3-PMLS**, Figure 28). Postsynthetic linker exchange (PSLE), on the other hand, gave a dark maroon colored MOF (**3-PSLE**) with high Ru:Zr ratios (0.21 – 0.23), which also exhibited a reasonable BET surface area (1405 m^2g^{-1}). Complex **3-Na** is thus preferably incorporated using the PSLE method.

The challenges of incorporating complexes **2-Na** and **3-Na** using PMLS could be due to the complexes not being stable under the synthesis conditions (120 °C and highly acidic solution). Both complexes have a Ru-C bond that may be subject to protolytic cleavage. Thus, further attempts to attain **2-PMLS** and **3-PMLS** were made with (independent) variations to the procedure: 1) heating at 90 °C, 2) stirring while heating, 3) performing the reaction without modulator, and (for **3-PMLS** only), 4) using 0.2 equiv. of complex **3-Na** instead of the standard

0.1 equiv. None of the variations caused discernible changes in the appearance and colours of the MOFs.

Complex **4-Na** was incorporated using both PMLS and PSLE. However, **4-PMLS** showed higher crystallinity, BET surface area, thermal stability, and Ru:Zr ratios, compared to **4-PSLE**. Complex **4-Na** is therefore preferably incorporated using the PMLS method. However, the SEM pictures of **4-PMLS** (Figure 24) indicate that there are Ru(II) complex phases present on the surfaces of the MOF crystallites. This does of course not rule out the possibility that complex **4-Na** is incorporated inside the MOF pores as well.

3.3. Photocatalysis

The culmination of this thesis was the testing of the prepared Ru(II)-functionalized MOFs as photocatalysts for CO_2 reduction. The expected product in the gas phase was CO (based on literature reports, Table 1, page 17), which could be clearly separated using the GC setup described in section 2.6. This gas is a desirable product since it can be further reacted in other catalytic systems to produce a wide range of chemicals, such as methanol and various fuels.[110]

The following discussion is based on experiments that were performed only once each. Therefore, the uncertainties in the amounts of products are unknown. However, the numbers obtained from calculations based on measurements of the reference gas mixture containing 0.1 % CO are given.

The Ru(II)-functionalized MOFs that were tested were **1-PMLS**, **2-PSF**, **3-PSLE**, **4-PMLS**, and **4-PSLE**. All MOFs were tested with H_2 gas as reducing agent, and **2-PSF** and **4-PMLS** were also tested with TEOA (triethanolamine) in initial experiments. The materials that showed significant activity for CO production were **4-PMLS** and **4-PSLE**. For **4-PMLS**, this was achieved with both H_2 and TEOA as reductant. Using H_2, the amount reached 1578 µmol CO per gram catalyst (hereafter referred to by µmol/g) in 6 h (Figure 29, values are given in Table ***2*** on page 27). The two experiments using TEOA (the only duplicate in this work) gave 1816 and 2324 µmol/g in 6 h, respectively. **4-PSLE** produced 821 µmol/g in 6 h using H_2, which is approximately half of the production achieved with **4-PMLS** (Figure 30). To the best of the author's knowledge, this is the first time H_2 gas is used for photocatalytic CO_2 reduction with MOFs in liquid suspension. One previous report used H_2 gas in a solid/gas setup with a TiO_2/UiO-66-NH_2 nanocomposite (Table 1, entry 23, page 17).[87] One advantage of using H_2

instead of TEOA is that the liquid phase can be readily characterized by NMR (avoiding the intense peaks from TEOA in the spectrum) or by GC with liquid injection (TEOA has a boiling point of 335 °C, which makes GC analysis challenging). However, GC analysis of the liquid phase was not performed in this work. Another advantage of H_2 over TEOA is that decomposition products of TEOA that could react with the MOF or the reaction products are avoided.

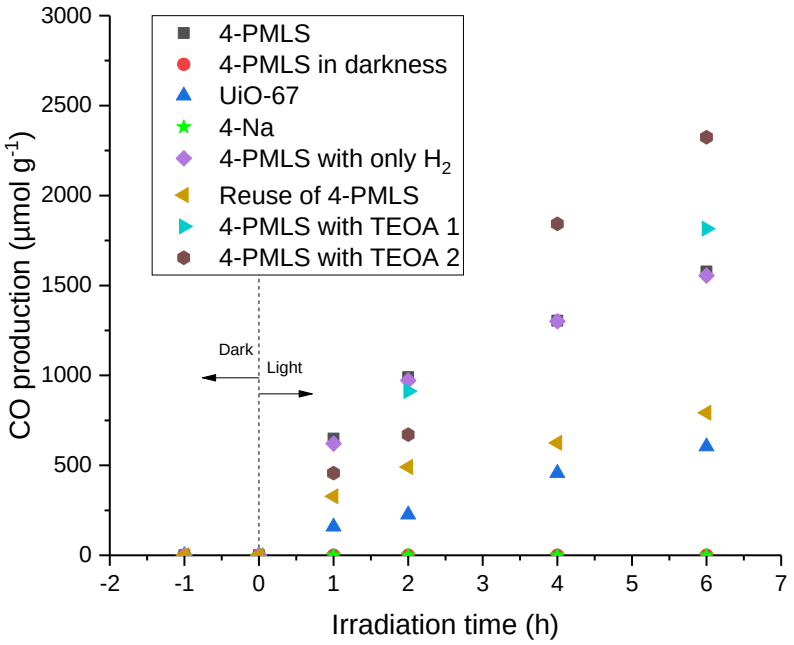

Figure 29. CO production as a function of time for the systems: MOF photocatalyst 4-PMLS in light and in darkness, pristine UiO-67, complex 4-Na, 4-PMLS without purging of CO_2 (only H_2), reuse of 4-PMLS, and 4-PMLS with the use of TEOA (triethanolamine) instead of H_2 (two experiments).

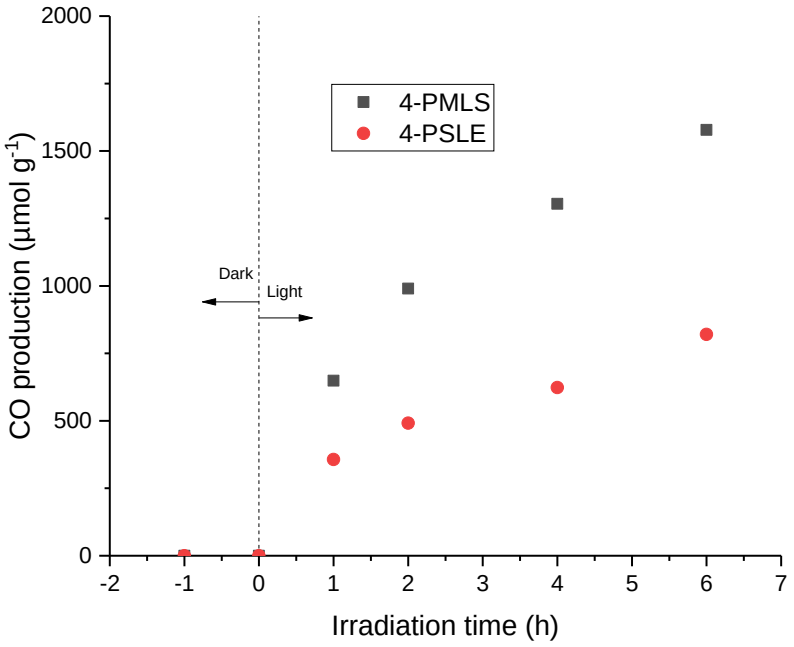

Figure 30. CO production as a function of time for 4-PMLS and 4-PSLE, using H_2 as reductant.

The product formation is reported in units of µmol/g (and not TON) because it is unclear which species is the actual catalytic site, or the amount of it that is available for reaction. It is also possible to calculate the conversion of CO_2 (how many percent of the CO_2 molecules that are reduced to CO) if one assumes that the only reaction product is CO and that this actually originates from the CO_2 added to the system. This is calculated by dividing the percentage of CO in the reaction headspace (calculated based on calibration gas measurements) on the percentage of CO_2 in the gas that is bubbled through the system before reaction (1/7 = 14.3 % when using H_2, 100 % when using TEOA). For **4-PMLS** using H_2, the conversion then becomes 0.216 %. For the two reactions with **4-PMLS** using TEOA, the conversion becomes 0.036 and 0.045 %, respectively. Thus, since the percentage of CO_2 is lower in the experiment using H_2 as reductant than in the experiments using TEOA, the conversion is actually higher in the former.

The origin of the detected CO was investigated using isotopic $^{13}CO_2$ instead of normal CO_2 in the experiment with **4-PMLS** using H_2 as reductant, for analysis by mass spectrometry (MS). The ratios of the integrated areas of the curves of the *m/z* 29 and *m/z* 45 signals over time for the five reference measurements was on average 0.116, with a standard deviation of 0.002. This standard deviation is thus on the same order of magnitude as the estimated conversion of CO_2 to CO. It is therefore no significance in the measured ratios of the *m/z* 29 to *m/z* 45 signals in

the photocatalytic experiments using $^{13}CO_2$. Thus, it is neither proved nor disproved that the produced CO originated from the CO_2 added to the reaction system.

The observed CO production is compared to previous reports by calculating the formation rates in units of μmol/g·h (μmol CO per gram catalyst per hour). At 6 h reaction time, **4-PMLS** produces CO at 263 μmol/g·h with H_2 as reductant, and 303 and 387 μmol/g·h with TEOA as reductant, while **4-PSLE** (with H_2) yields 137 μmol/g·h. The product formation rates in Table ***1*** (page 17) with the same unit for CO production are quite spread. Some of the studies reported values that are not too far from the values in this work: 88 (entry 1), 46 (entry 9), 218 (entry 11), and 201 (entry 19) μmol/g·h. Thus, the CO formation rate catalyzed by **4-PMLS** is in agreement with comparable literature values. Entries 21 and 23 in Table 1 reports 1 and 4 μmol/g·h, respectively. Although these values are much lower than herein and the rest of the literature, these two are the only ones conducted solely in gas phase. There are also some reports with much higher CO production rates (in μmol/g·h) than the rest: 358952 (entry 6), 1666 (entry 24), 4373 (entry 25), 59200 (entry 26), and 3890 (entry 29). It is pointed out that the masses of the MOF catalysts used in these cases were 0.23, 3, 3, 1, and 1 mg, respectively.

The CO production rates for the MOF catalysts in this work decreased with time of reaction, consistent with literature reports (Table 1), and probably due to an approach toward chemical equilibrium.

After centrifugation of the reaction mixtures of all the Ru(II)-functionalized MOFs, the liquid phase was clear (illustrated in Figure 31 for **4-PMLS**). This indicates that no significant amount of their Ru(II) complexes had leached into the solution during the photoreactions.

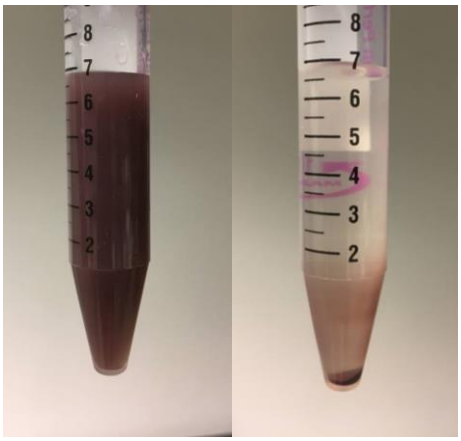

Figure 31. The reaction mixture of 4-PMLS after photoreaction (with H_2 as reductant) before centrifugation (left) and after centrifugation (right).

The experiment with **4-PMLS** using H_2 was repeated in darkness (the reaction cell was wrapped in Al foil), in which no CO was detected. This confirms the photocatalytic nature of the reaction. As additional reference experiments, pristine UiO-67 and complex **4-Na** were tested. UiO-67 produced 605 μmol/g after 6 h of reaction. This indicates that the UV part of the visible light could stimulate excitations in the MOF structure that could reduce CO_2. This result is rather surprising, given that **1-PMLS**, **2-PSF**, and **3-PSLE** did not show any CO production activity. It could be hypothesized that the incorporated Ru(II) complexes in these MOFs hinders the CO_2 molecules from adsorbing on active sites, or that they lead to unfavorable (photo-)chemical processes. Among the reports in Table 1, only four have studied the activity of pristine UiO-67. In entries 1, 20, and 21, no CO_2 reduction was observed. However, in entry 16, UiO-67 was able to photocatalytically reduce CO_2 to both CO and HCOOH, with TONs of 1.1 and 2.9 in 6 h, respectively.[55]

Complex **4-Na** did not give any production of CO. Thus, the combination of UiO-67 and **4-Na** in **4-PMLS** and **4-PSLE** is necessary for the activity seen for these photocatalysts. The activities of **4-PMLS** and **4-PSLE** could arise from the appropriateness of complex **4-Na** as a photosensitizer, as reported for dye sensitized solar cells.[16, 18, 23, 99] It was shown that this complex has several excitations onto the ligands with carboxylate groups (Figure 12, page 36), of which it has four. Thus, a significant amount of electron density could be injected into the MOF structure via the carboxylate groups on **4-Na**.

An experiment with **4-PMLS** without the use of CO_2 (only purging the reaction system with H_2 at 30 mL/min for 1 h) gave surprising results. In this case, almost exactly the same amounts of CO was produced as in the original experiment where CO_2/H_2 (5:30 mL/min) was purged through the system. One explanation for this observation could be that the H_2 purge did not remove all the CO_2 already present in the system. Residues of CO_2 could be adsorbed in the MOF pores and/or dissolved in the MeCN solvent (in which CO_2 is highly soluble). In this case, only very small amounts of CO_2 would be necessary for CO production to occur. This would be interesting for industrial purposes, since the CO_2 gas (e.g. from the atmosphere) would not need to be concentrated before the reduction process. Another explanation for the observed CO production could be that the MOF catalyst decomposes during the photoreaction. For example, the carboxylate groups on complex **4-Na** could detach and subsequently be reduced to CO. Interestingly, the ratios of the peak areas of CO_2 to N_2 in the gas chromatogram are approximately five times higher in this experiment compared to reference measurements of air. This is the case for all the injections, from start to end of the experiment. This rules out the

possibility that all of the CO_2 seen in the chromatogram comes from the needle on the syringe. The ratios of the detected amounts of CO_2 to CO (both were calculated from the same calibration gas mixture) decreased steadily from 16 (start) to 2 (6 h irradiation).

Formation of reduction products without added CO_2 is rarely seen in the literature (Table 1), although some examples are worth noting. In entry 11, both $HCOO^-$ and CO (102 and 40 μmol/g in 18 h, respectively) were detected when only N_2 gas was purged through the system prior to irradiation.[13] In entry 16, it was observed that reducing the concentration of CO_2 from 100 % to 5 % did lead to almost the same production of both HCOOH and CO.[55] This was explained by CO_2 enrichment in the pores of the MOF. In entry 28, the use of dry air (with 400 ppm CO_2) lead to production of CO (TON = 27 in 10 h).[91]

In order to check the catalytic stability of **4-PMLS**, the isolated powder from the first catalytic run was mixed with fresh CD_3CN and purged with CO_2/H_2 (5:30 mL/min) for 1 h. This experiment showed a lower activity (792 μmol/g in 6 h) than the first run. This could be due to incomplete recovery of the catalyst, possible decomposition of the MOF as mentioned above, and/or that the powder was not as well ground as in the first run.

In all of the above-mentioned experiments, the liquid phase was analyzed by ^1H NMR. The expected products, if any, were formic acid (HCOOH) and/or methanol (MeOH). When using **4-PMLS** with TEOA as the reducing agent, photocatalytic activity for the production of both of these compounds was observed. In none of the other testing experiments in this work were any of these products observed, except for **2-PSF** with TEOA, in which traces of HCOOH could be seen after 6 h in light. Figure 32 shows the ^1H NMR spectra of the reaction solution for **4-PMLS** at 1 h in darkness and 2, 4, and 6 h in light. The singlet peak at 8.45 ppm belongs to HCOOH (or $HCOO^-$, since TEOA is basic), which was confirmed by spiking the sample (addition of a small amount of the compound in question). This peak is only visible in the sample taken after 6 h in light, which is the only one that was not diluted with CD_3CN before measurement. Figure 33 shows the same spectra at a different range of chemical shifts. The singlet peak at 3.28 ppm belongs to MeOH, which was also confirmed by spiking the sample. This peak is only visible in the samples that were taken at 4 h and 6 h in light, and the intensity is higher in the latter (corrected for dilution). For the testing of **4-PMLS** using $^{13}CO_2$ and H_2, the liquid phase was also analyzed by ^{13}C NMR. There were no other signals in the spectrum other than those belonging to CD_3CN and $^{13}CO_2$, in agreement with the ^1H NMR analyses of the same solution, and the one using normal CO_2.

To the best of the author's knowledge, **4-PMLS** is the first and only MOF to show photocatalytic production of all three compounds CO, HCOOH, and MeOH.

With respect to the mechanisms for these photocatalytic reactions, some speculations are made, based on previous studies. As mentioned in section 1.3, photocatalytic CO_2 reduction can occur on the metal clusters, the linkers, or both. Several reports have suggested that Zr-oxo clusters can contribute to this reaction, through reduction of Zr^{4+} to Zr^{3+} (entries 3, 15, 17, 27, and 30 in Table 1, page 17).[73, 82-83, 90, 92] Thus, the formation of CO, HCOOH, and MeOH observed in this thesis could possibly be explained by the following mechanistic pathway. First, the photosensitizer (complex **4-Na**) absorbs visible light to form an excited state. This state accepts an electron from TEOA or H_2 into the resulting vacant energy level. The high energy electron in **4-Na** is transferred to the $Zr_6O_4(OH)_4^{12+}$ cluster, so that one Zr^{4+} ion is reduced to Zr^{3+}. The Zr^{3+} ion then transfers an electron to CO_2 to form COO^-. This species could obtain a proton from the cationic radical $TEOA^{+\bullet}$ (Figure 7d), or the proton that resulted from the initial electron transfer from H_2 to complex **4-Na**. Subsequent electron and proton transfers could then lead to the different observed reduction products.

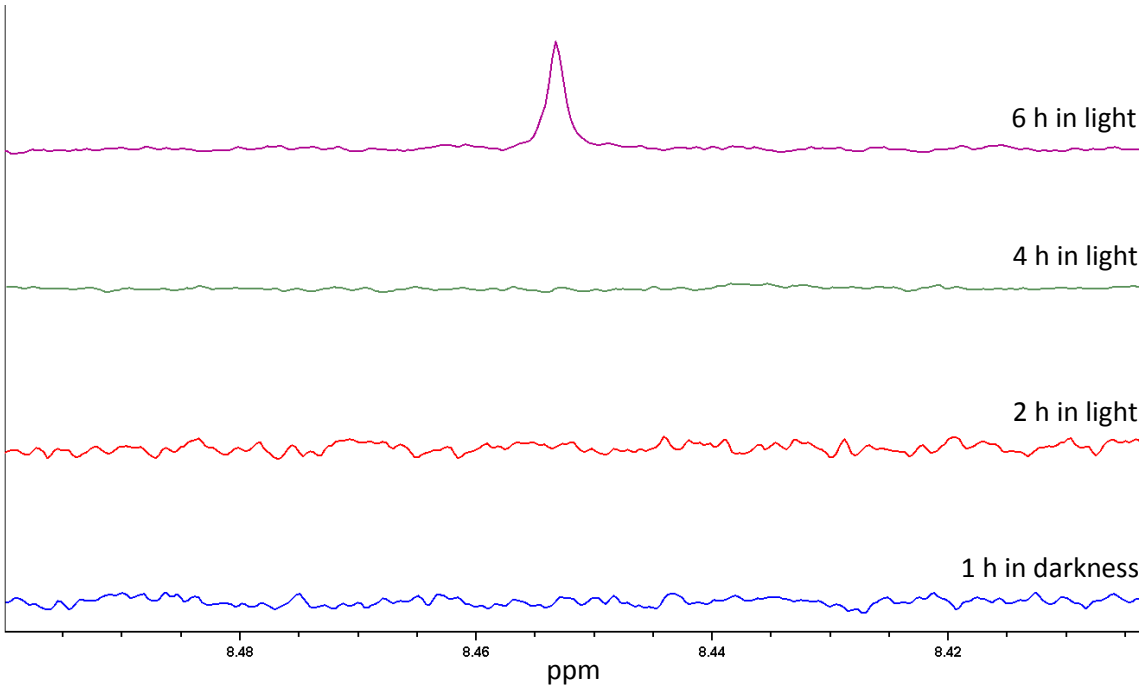

Figure 32. ^{1}H NMR spectra showing the production of HCOOH in the reaction solution of 4-PMLS, using TEOA as reductant, at different times: 1 h in darkness, 2 h in light, 4 h in light, and 6 h in light. The first three samples were diluted fivefold before measurement. CD_3CN, 400 MHz.

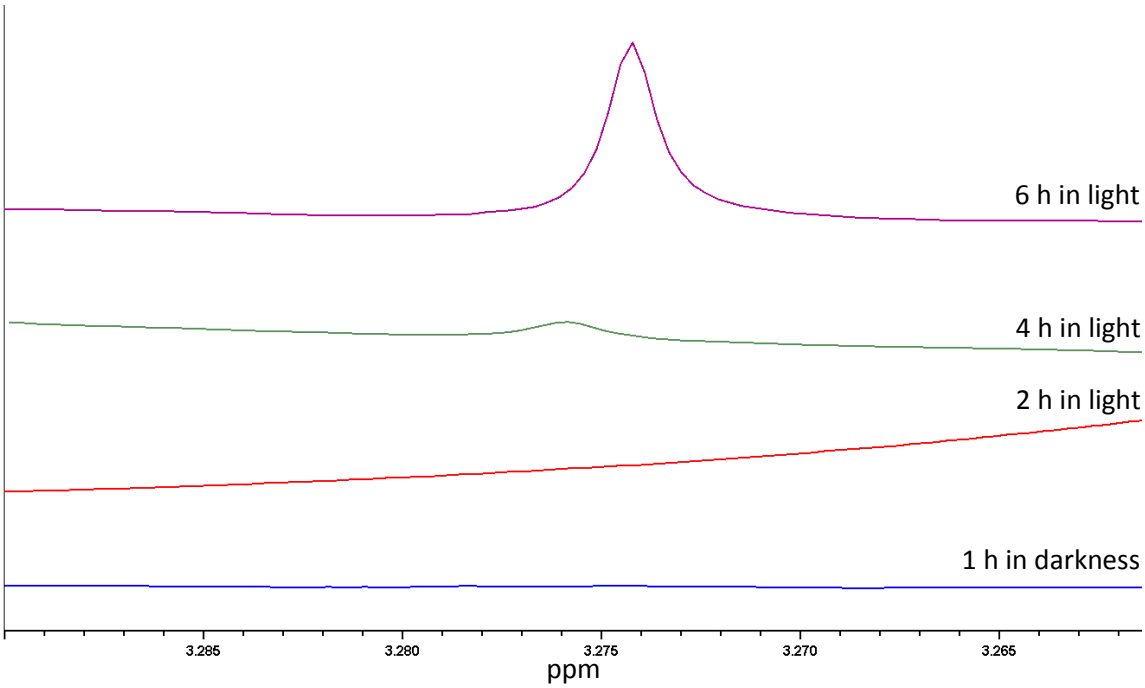

Figure 33. ^{1}H NMR spectra showing the production of MeOH in the reaction solution of 4-PMLS, using TEOA as reductant, at different times: 1 h in darkness, 2 h in light, 4 h in light, and 6 h in light. The first three samples were diluted fivefold before measurement. The baseline of the spectrum measured after 2 h is inclined due to a neighboring peak and its intensity is therefore divided by four. CD_3CN, 400 MHz.

4. Conclusions

This PhD thesis comprises three quite distinct areas of research: organometallic complexes, metal-organic frameworks (MOFs), and catalytic testing. Although they were woven together for the ultimate goal of photocatalytic reduction of CO_2, the work done in each of them provides additional insight that is scientifically interesting in a broader sense.

The study on the synthesis and characterization of the Ru(II) complexes in this work showed that a range of different structures could be isolated through strategic choices of reagents and synthesis conditions (Scheme 1 on page 31). The synthetic routes relied widely on ligand exchange, and some steps included C-H activation with base to form Ru-C bonds (cyclometalated Ru(II) complexes). It proved feasible to use MeCN as labile ligands for further exchange with bipyridine (bpy) ligands or their ester-substituted derivatives. Once these ester-functionalized Ru(II) complexes were isolated, they were readily hydrolyzed into carboxylates using equimolar amounts, or a slight excess, of NaOH (with respect to the total amount of ester groups). It was also found that the order of coordination of the ligands affected the stereochemistry of the product. This was explained by configurational reorganization of a five-coordinated intermediate due to the high *trans* influence of the formally anionic carbon atom bonded to ruthenium.

The electronic properties of the Ru(II) complexes were experimentally investigated by UV-Vis spectroscopy. Specifically, four of them (in which two were previously reported) were studied and compared as potential photosensitizers. As intended, the cyclometalated Ru(II) complexes had absorption profiles that extended further into the visible region compared to the non-cyclometalated Ru(II) complex. This phenomenon was further studied with the use of time dependent density functional theory (TD-DFT), in which the individual electronic energy levels, and the intensities of the transitions between them, were calculated. These calculations were then coupled with the experimental absorption spectra to assign specific electronic transitions to the observed bands. It was shown that all the Ru(II) complexes have electronic excitations to virtual orbitals located on the carboxylated ligands due to absorption of visible light. This makes them promising as photosensitizers in solid materials and/or in homogeneous reactions.

What makes these synthesized Ru(II) complexes especially interesting is the linear arrangement of their carboxylate groups, which makes them suitable for e.g. incorporation into MOFs. In the second part of this thesis, the incorporation of the Ru(II) complexes into the MOF UiO-67 was investigated through three different methods: premade linker synthesis (PMLS),

postsynthetic functionalization (PSF), and postsynthetic linker exchange (PSLE). This resulted in ten different synthesis systems. All of these were, to varying degrees, successful in incorporating the Ru(II) complexes into the MOF, while retaining its integrity (crystallinity, pore volume, thermal stability, and crystallite shape). The only obvious failure was **3-PMLS**, which, with its white appearance and total reflectance of visible light, did not seem to have incorporated any significant amount of Ru(II) complex. In the case of the PSF systems, direct proof of incorporation was offered by ^{1}H NMR analysis of the solutions of the digested MOFs. This was because the signals from the respective Ru(II) complexes, which were not used as reagents in the PSF reactions, were observed in the spectra, while those from the Ru(II) precursors used in the PSF reactions were not observed. Additional evidence of incorporation was provided by single crystal XRD of the MOFs, which showed that ruthenium was chemically bonded to the bpydc linkers. The diffuse reflectance UV-Vis spectroscopic measurements of the Ru(II)-functionalized MOFs qualitatively showed the same absorption profiles as the respective molecular Ru(II) complexes. Thus, these MOFs are potential visible light photocatalysts, either by themselves, or in combination with other components such as molecular catalysts or semiconductors.

The photocatalytic testing experiments led to some interesting results. Even though **1-PMLS**, **2-PSF**, and **3-PSLE** did not show any significant activity for CO_2 reduction, **4-PMLS** was found to catalyze formation of CO, HCOOH, and MeOH, while **4-PSLE** catalyzed formation of CO. Hydrogen gas was utilized as reducing agent for CO formation, which is, to the best of the author's knowledge, the first time this has been reported for photocatalytic CO_2 reduction using a liquid suspension of MOF. Employing mass spectroscopic analysis of an experiment using isotopic $^{13}CO_2$ did neither prove nor disprove that the observed products were actually formed from the CO_2 added to the reaction system. However, it was shown that light was essential for CO formation, and that complex **4-Na** could not catalyze this on its own. Pristine UiO-67, on the other hand, did show some activity. Based on these results, it is evident that UiO-67 represents an interesting platform for further photocatalytic studies.

5. Outlook

There is a lot of further work that could be done in the areas that have been focused on in this thesis. Regarding the synthesis of Ru(II) complexes, a couple of reactions would be interesting to attempt: 1) Reaction between **5-Et** (Scheme 1, page 31) and only 1 equiv. bpy. This could yield a complex that, after hydrolysis of the ester groups, could be integrated into a MOF while still having two labile MeCN ligands coordinated. 2) Coordination of 2-(*p*-Tolyl)pyridine or 4-(3,5-dimethylphenyl)pyridine to Ru(II), e.g. by using them instead of ppy in the synthesis of $[Ru(ppy)(MeCN)_4]PF_6$. This should provide additional electron donation to the Ru(II) center, which again should lead to even larger bathochromic shifts of the absorption profiles.

It would be of further interest to investigate the synthesis of Ru(II) complexes with two Ru-C bonds. This was discarded for this thesis since the only reports on such structures in the literature involved transmetallation reactions with mercury.[111] Thus, the development of more environmentally friendly pathways is desirable.

It would be worth to attempt postsynthetic functionalization (PSF) of UiO-67-bpy with $[Ru(ppy)(MeCN)_4]PF_6$. Ideally, this would lead to a Ru(II)-functionalized MOF product where the integrated Ru(II) complex has two MeCN ligands coordinated. Alternatively, the use of the carboxylate/acid analogue of complex **6-Et** (Scheme 1, page 31) in premade linker synthesis (PMLS) could give the same MOF product. These situations would be similar to using the complex mentioned above (reaction 1) as a linker in PMLS, except that in this case, the Ru-bonded C atom would be located the carboxylated ligand (the linker part of the complex). A MOF functionalized with these complexes could be useful for further catalytic reactions involving the two labile MeCN ligands on Ru(II).

Electrochemical characterization of the Ru(II) complexes and the Ru(II)-functionalized MOFs could be performed to complement the UV-Vis measurements. This could be done both with and without CO_2 in the system in order to study the potential electrocatalytic properties of these complexes and MOFs for CO_2 reduction.

X-ray absorption fine structure (XAFS) analysis could be employed in order to obtain additional insight into the coordination environment of the Ru(II) centers in the complexes and the corresponding functionalized MOFs.

The origin of the observed CO in the photocatalytic CO_2 reduction experiments should be further investigated. Even though significant results were not obtained in this work, the use of a higher catalyst loading could lead to a production high enough for mass spectroscopic analysis.

The liquid phase in the photoreactions could be analyzed by gas chromatography (GC) as it would be advantageous to use the same analysis method for both gas and liquid phase.

Electron paramagnetic resonance (EPR) spectroscopy could be employed to detect possible short-lived species in the MOFs, such as Zr^{3+}, which has been reported in the literature as catalytically active sites for photocatalytic CO_2 reduction.[73]

Other chemical systems would be interesting to test for photocatalytic CO_2 reduction. UiO-67 has been functionalized with a Re(I) complex and NH_2-groups to achieve this reaction.[85] The same been observed for UiO-66-NH_2.[73] Thus, it might be that UiO-67-$(NH_2)_x$ (x = 1 or 2) would be an active photocatalyst for CO_2 reduction. This MOF could also be combined with the Ru(II) complexes in this work in order to achieve supreme light absorption and possibly photocatalytic activity.

TiO_2 is a known photocatalyst for CO_2 reduction,[65] although it is only active in UV light. Several studies have combined nanostructures of TiO_2 with MOFs in order to utilize the properties of both components.[87, 112-114] This could also be investigated for the MOFs in this thesis.

In order to enhance the photocatalytic properties of the Ru(II)-functionalized MOFs in this work, a possible strategy could be to further functionalize them with metal centers like Fe, Mn, Cu, Mg, and Co. Fe(II) and Fe(III) complexes that show fascinating photophysical properties have recently been developed.[115-116] The exchange of the Ru(II) complexes studied herein with such complexes would be interesting due to the higher abundance of Fe than Ru in the earth's crust.

Photocatalytic testing in gas phase should be pursued for the Ru(II)-functionalized MOFs in this work. MOFs are known as effective gas adsorbents, and this setup would pave the way toward industrial utilization of these photocatalysts.

The Ru(II) complexes synthesized in this thesis could also be appropriate structures as photosensitizers in other systems than MOFs. For example, the linear relative arrangement of their carboxylate groups could be beneficial for grafting them between or inside inorganic nanotubes.

6. References

1. O'Regan, B.; Gratzel, M., A low-cost, high-efficiency solar cell based on dye-sensitized colloidal TiO_2 films. *Nature* **1991,** *353* (6346), 737-740.
2. Grätzel, M., Dye-sensitized solar cells. *J. Photochem. Photobiol., C* **2003,** *4* (2), 145-153.
3. Nicewicz, D. A.; MacMillan, D. W. C., Merging Photoredox Catalysis with Organocatalysis: The Direct Asymmetric Alkylation of Aldehydes. *Science* **2008,** *322* (5898), 77.
4. Ischay, M. A.; Anzovino, M. E.; Du, J.; Yoon, T. P., Efficient Visible Light Photocatalysis of [2+2] Enone Cycloadditions. *J. Am. Chem. Soc.* **2008,** *130* (39), 12886-12887.
5. Narayanam, J. M. R.; Tucker, J. W.; Stephenson, C. R. J., Electron-Transfer Photoredox Catalysis: Development of a Tin-Free Reductive Dehalogenation Reaction. *J. Am. Chem. Soc.* **2009,** *131* (25), 8756-8757.
6. Gust, D.; Moore, T. A.; Moore, A. L., Solar Fuels via Artificial Photosynthesis. *Acc. Chem. Res.* **2009,** *42* (12), 1890-1898.
7. Roy, S. C.; Varghese, O. K.; Paulose, M.; Grimes, C. A., Toward Solar Fuels: Photocatalytic Conversion of Carbon Dioxide to Hydrocarbons. *ACS Nano* **2010,** *4* (3), 1259-1278.
8. Adamson, A. W.; Demas, J. N., New photosensitizer. Tris(2,2'-bipyridine)ruthenium(II) chloride. *J. Amer. Chem. Soc.* **1971,** *93* (7), 1800-1.
9. Nazeeruddin, M. K.; De Angelis, F.; Fantacci, S.; Selloni, A.; Viscardi, G.; Liska, P.; Ito, S.; Takeru, B.; Grätzel, M., Combined Experimental and DFT-TDDFT Computational Study of Photoelectrochemical Cell Ruthenium Sensitizers. *J. Am. Chem. Soc.* **2005,** *127* (48), 16835-16847.
10. Grätzel, M., Recent Advances in Sensitized Mesoscopic Solar Cells. *Acc. Chem. Res.* **2009,** *42* (11), 1788-1798.
11. Wang, C.; Xie, Z.; deKrafft, K. E.; Lin, W., Doping Metal–Organic Frameworks for Water Oxidation, Carbon Dioxide Reduction, and Organic Photocatalysis. *J. Am. Chem. Soc.* **2011,** *133* (34), 13445-13454.
12. Hou, C.-C.; Li, T.-T.; Cao, S.; Chen, Y.; Fu, W.-F., Incorporation of a $[Ru(dcbpy)(bpy)_2]^{2+}$ photosensitizer and a $Pt(dcbpy)Cl_2$ catalyst into metal-organic frameworks for photocatalytic hydrogen evolution from aqueous solution. *J. Mater. Chem. A* **2015,** *3* (19), 10386-10394.
13. Fei, H.; Sampson, M. D.; Lee, Y.; Kubiak, C. P.; Cohen, S. M., Photocatalytic CO_2 Reduction to Formate Using a Mn(I) Molecular Catalyst in a Robust Metal–Organic Framework. *Inorg. Chem.* **2015,** *54* (14), 6821-6828.
14. Reference Solar Spectral Irradiance: Air Mass 1.5. National Renewable Energy Laboratory: 2018.
15. Lee, C.; Yum, J.-H.; Choi, H.; Ook Kang, S.; Ko, J.; Humphry-Baker, R.; Grätzel, M.; Nazeeruddin, M. K., Phenomenally High Molar Extinction Coefficient Sensitizer with "Donor−Acceptor" Ligands for Dye-Sensitized Solar Cell Applications. *Inorg. Chem.* **2008,** *47* (7), 2267-2273.
16. Bomben, P. G.; Robson, K. C. D.; Koivisto, B. D.; Berlinguette, C. P., Cyclometalated ruthenium chromophores for the dye-sensitized solar cell. *Coord. Chem. Rev.* **2012,** *256* (15–16), 1438-1450.
17. Robson, K. C. D.; Bomben, P. G.; Berlinguette, C. P., Cycloruthenated sensitizers: improving the dye-sensitized solar cell with classical inorganic chemistry principles. *Dalton Trans.* **2012,** *41* (26), 7814-7829.
18. Bomben, P. G.; Robson, K. C. D.; Sedach, P. A.; Berlinguette, C. P., On the viability of cyclometalated Ru(II) complexes for light-harvesting applications. *Inorg. Chem.* **2009,** *48* (20), 9631-9643.
19. Bomben, P. G.; Theriault, K. D.; Berlinguette, C. P., Strategies for Optimizing the Performance of Cyclometalated Ruthenium Sensitizers for Dye-Sensitized Solar Cells. *Eur. J. Inorg. Chem.* **2011,** (11), 1806-1814.

20. Bomben, P. G.; Gordon, T. J.; Schott, E.; Berlinguette, C. P., A Trisheteroleptic Cyclometalated RuII Sensitizer that Enables High Power Output in a Dye-Sensitized Solar Cell. *Angew. Chem., Int. Ed.* **2011,** *50* (45), 10682-10685.
21. Bessho, T.; Yoneda, E.; Yum, J.-H.; Guglielmi, M.; Tavernelli, I.; Imai, H.; Rothlisberger, U.; Nazeeruddin, M. K.; Grätzel, M., New Paradigm in Molecular Engineering of Sensitizers for Solar Cell Applications. *J. Am. Chem. Soc.* **2009,** *131* (16), 5930-5934.
22. Wadman, S. H.; Kroon, J. M.; Bakker, K.; Lutz, M.; Spek, A. L.; van Klink, G. P. M.; van Koten, G., Cyclometalated ruthenium complexes for sensitizing nanocrystalline TiO_2 solar cells. *Chem. Comm.* **2007,** (19), 1907-1909.
23. Bomben, P. G.; Koivisto, B. D.; Berlinguette, C. P., Cyclometalated Ru complexes of type $[Ru^{II}(N^N)_2(C^N)]^z$: physicochemical response to substituents installed on the anionic ligand. *Inorg. Chem.* **2010,** *49* (11), 4960-4971.
24. Albrecht, M., Cyclometalation Using d-Block Transition Metals: Fundamental Aspects and Recent Trends. *Chem. Rev.* **2010,** *110* (2), 576-623.
25. Batten, S. R.; Champness, N. R.; Chen, X.-M.; Garcia-Martinez, J.; Kitagawa, S.; Ohrstrom, L.; O'Keeffe, M.; Suh, M. P.; Reedijk, J., Terminology of metal-organic frameworks and coordination polymers (IUPAC recommendations 2013). *Pure Appl. Chem.* **2013,** *85* (8), 1715-1724.
26. Cavka, J. H.; Jakobsen, S.; Olsbye, U.; Guillou, N.; Lamberti, C.; Bordiga, S.; Lillerud, K. P., A New Zirconium Inorganic Building Brick Forming Metal Organic Frameworks with Exceptional Stability. *J. Am. Chem. Soc.* **2008,** *130* (42), 13850-13851.
27. Wu, H.; Yildirim, T.; Zhou, W., Exceptional Mechanical Stability of Highly Porous Zirconium Metal–Organic Framework UiO-66 and Its Important Implications. *J. Phys. Chem. Lett.* **2013,** *4* (6), 925-930.
28. Valenzano, L.; Civalleri, B.; Chavan, S.; Bordiga, S.; Nilsen, M. H.; Jakobsen, S.; Lillerud, K. P.; Lamberti, C., Disclosing the Complex Structure of UiO-66 Metal Organic Framework: A Synergic Combination of Experiment and Theory. *Chem. Mater.* **2011,** *23* (7), 1700-1718.
29. Bosch, M.; Zhang, M.; Zhou, H.-C., Increasing the Stability of Metal-Organic Frameworks. *Adv. Chem.* **2014,** *2014*, 8.
30. Feng, D.; Wang, K.; Wei, Z.; Chen, Y.-P.; Simon, C. M.; Arvapally, R. K.; Martin, R. L.; Bosch, M.; Liu, T.-F.; Fordham, S.; Yuan, D.; Omary, M. A.; Haranczyk, M.; Smit, B.; Zhou, H.-C., Kinetically tuned dimensional augmentation as a versatile synthetic route towards robust metal–organic frameworks. *Nat. Commun.* **2014,** *5*, 5723.
31. Devic, T.; Serre, C., High valence 3p and transition metal based MOFs. *Chem. Soc. Rev.* **2014,** *43* (16), 6097-6115.
32. Yaghi, O. M.; O'Keeffe, M.; Ockwig, N. W.; Chae, H. K.; Eddaoudi, M.; Kim, J., Reticular synthesis and the design of new materials. *Nature* **2003,** *423*, 705.
33. Eddaoudi, M.; Kim, J.; Rosi, N.; Vodak, D.; Wachter, J.; O'Keeffe, M.; Yaghi, O. M., Systematic Design of Pore Size and Functionality in Isoreticular MOFs and Their Application in Methane Storage. *Science* **2002,** *295* (5554), 469-472.
34. Vandenbrande, S.; Verstraelen, T.; Gutierrez-Sevillano, J. J.; Waroquier, M.; Van Speybroeck, V., Methane adsorption in Zr-based MOFs: comparison and critical evaluation of force fields. *J. Phys. Chem. C* **2017,** *121* (45), 25309-25322.
35. Øien-Ødegaard, S.; Bouchevreau, B.; Hylland, K.; Wu, L.; Blom, R.; Grande, C.; Olsbye, U.; Tilset, M.; Lillerud, K. P., UiO-67-type Metal–Organic Frameworks with Enhanced Water Stability and Methane Adsorption Capacity. *Inorg. Chem.* **2016,** *55* (5), 1986-1991.
36. Suh, M. P.; Park, H. J.; Prasad, T. K.; Lim, D.-W., Hydrogen Storage in Metal–Organic Frameworks. *Chem. Rev.* **2012,** *112* (2), 782-835.
37. Sumida, K.; Rogow, D. L.; Mason, J. A.; McDonald, T. M.; Bloch, E. D.; Herm, Z. R.; Bae, T.-H.; Long, J. R., Carbon Dioxide Capture in Metal–Organic Frameworks. *Chem. Rev.* **2012,** *112* (2), 724-781.
38. Li, J.-R.; Sculley, J.; Zhou, H.-C., Metal–Organic Frameworks for Separations. *Chem. Rev.* **2012,** *112* (2), 869-932.

39. Lee, J.; Farha, O. K.; Roberts, J.; Scheidt, K. A.; Nguyen, S. T.; Hupp, J. T., Metal-organic framework materials as catalysts. *Chem. Soc. Rev.* **2009,** *38* (5), 1450-1459.
40. Gascon, J.; Corma, A.; Kapteijn, F.; Llabrés i Xamena, F. X., Metal Organic Framework Catalysis: Quo vadis? *ACS Catal.* **2014,** *4* (2), 361-378.
41. Øien, S.; Agostini, G.; Svelle, S.; Borfecchia, E.; Lomachenko, K. A.; Mino, L.; Gallo, E.; Bordiga, S.; Olsbye, U.; Lillerud, K. P.; Lamberti, C., Probing Reactive Platinum Sites in UiO-67 Zirconium Metal-Organic Frameworks. *Chem. Mater.* **2015,** *27* (3), 1042-1056.
42. Yu, X.; Wang, L.; Cohen, S. M., Photocatalytic metal-organic frameworks for organic transformations. *CrystEngComm* **2017,** *19* (29), 4126-4136.
43. Gutterød, E. S.; Øien-Ødegaard, S.; Bossers, K.; Nieuwelink, A.-E.; Manzoli, M.; Braglia, L.; Lazzarini, A.; Borfecchia, E.; Ahmadigoltapeh, S.; Bouchevreau, B.; Lønstad-Bleken, B. T.; Henry, R.; Lamberti, C.; Bordiga, S.; Weckhuysen, B. M.; Lillerud, K. P.; Olsbye, U., CO_2 Hydrogenation over Pt-Containing UiO-67 Zr-MOFs—The Base Case. *Ind. Eng. Chem. Res.* **2017,** *56* (45), 13206-13218.
44. Chen, Y.; Wang, D.; Deng, X.; Li, Z., Metal-organic frameworks (MOFs) for photocatalytic CO_2 reduction. *Catal. Sci. Technol.* **2017,** *7* (21), 4893-4904.
45. Huang, R.; Peng, Y.; Wang, C.; Shi, Z.; Lin, W., A Rhenium-Functionalized Metal-Organic Framework as a Single-Site Catalyst for Photochemical Reduction of Carbon Dioxide. *Eur. J. Inorg. Chem.* **2016,** *2016* (27), 4358-4362.
46. Choi, K. M.; Kim, D.; Rungtaweevoranit, B.; Trickett, C. A.; Barmanbek, J. T. D.; Alshammari, A. S.; Yang, P.; Yaghi, O. M., Plasmon-Enhanced Photocatalytic CO_2 Conversion within Metal-Organic Frameworks under Visible Light. *J. Am. Chem. Soc.* **2017,** *139* (1), 356-362.
47. Yang, S.; Pattengale, B.; Lee, S.; Huang, J., Real-Time Visualization of Active Species in a Single-Site Metal–Organic Framework Photocatalyst. *ACS Energy Lett.* **2018,** *3* (3), 532-539.
48. Sun, D.; Gao, Y.; Fu, J.; Zeng, X.; Chen, Z.; Li, Z., Construction of a supported Ru complex on bifunctional MOF-253 for photocatalytic CO_2 reduction under visible light. *Chem. Commun. (Cambridge, U. K.)* **2015,** *51* (13), 2645-2648.
49. Cohen, S. M., Postsynthetic Methods for the Functionalization of Metal–Organic Frameworks. *Chem. Rev.* **2012,** *112* (2), 970-1000.
50. Kandiah, M.; Usseglio, S.; Svelle, S.; Olsbye, U.; Lillerud, K. P.; Tilset, M., Post-synthetic modification of the metal-organic framework compound UiO-66. *J. Mater. Chem.* **2010,** *20* (44), 9848-9851.
51. Kim, M.; Cahill, J. F.; Su, Y.; Prather, K. A.; Cohen, S. M., Postsynthetic ligand exchange as a route to functionalization of metal-organic frameworks. *Chem. Sci.* **2012,** *3* (1), 126-130.
52. Pullen, S.; Fei, H.; Orthaber, A.; Cohen, S. M.; Ott, S., Enhanced photochemical hydrogen production by a molecular diiron catalyst incorporated into a metal-organic framework. *J. Am. Chem. Soc.* **2013,** *135* (45), 16997-17003.
53. Fei, H.; Shin, J.; Meng, Y. S.; Adelhardt, M.; Sutter, J.; Meyer, K.; Cohen, S. M., Reusable Oxidation Catalysis Using Metal-Monocatecholato Species in a Robust Metal-Organic Framework. *J. Am. Chem. Soc.* **2014,** *136* (13), 4965-4973.
54. Fei, H.; Cohen, S. M., Metalation of a Thiocatechol-Functionalized Zr(IV)-Based Metal-Organic Framework for Selective C-H Functionalization. *J. Am. Chem. Soc.* **2015,** *137* (6), 2191-2194.
55. Kajiwara, T.; Fujii, M.; Tsujimoto, M.; Kobayashi, K.; Higuchi, M.; Tanaka, K.; Kitagawa, S., Photochemical Reduction of Low Concentrations of CO_2 in a Porous Coordination Polymer with a Ruthenium(II)-CO Complex. *Angew. Chem., Int. Ed.* **2016,** *55* (8), 2697-2700.
56. Sun, R.; Liu, B.; Li, B.-G.; Jie, S., Palladium(II)@Zirconium-Based Mixed-Linker Metal-Organic Frameworks as Highly Efficient and Recyclable Catalysts for Suzuki and Heck Cross-Coupling Reactions. *ChemCatChem* **2016,** *8* (20), 3261-3271.
57. Wang, S.; Wang, X., Multifunctional Metal-Organic Frameworks for Photocatalysis. *Small* **2015,** *11* (26), 3097-3112.
58. Li, Y.; Xu, H.; Ouyang, S.; Ye, J., Metal-organic frameworks for photocatalysis. *Phys. Chem. Chem. Phys.* **2016,** *18* (11), 7563-7572.

59. Sun, D.; Li, Z., Robust Ti- and Zr-Based Metal-Organic Frameworks for Photocatalysis. *Chin. J. Chem.* **2017,** *35* (2), 135-147.
60. Wang, M.; Liu, J.; Guo, C.; Gao, X.; Gong, C.; Wang, Y.; Liu, B.; Li, X.; Gurzadyan, G. G.; Sun, L., Metal-organic frameworks (ZIF-67) as efficient cocatalysts for photocatalytic reduction of CO_2: the role of the morphology effect. *J. Mater. Chem. A* **2018,** *6* (11), 4768-4775.
61. Zhao, J.; Wang, Q.; Sun, C.; Zheng, T.; Yan, L.; Li, M.; Shao, K.; Wang, X.; Su, Z., A hexanuclear cobalt metal-organic framework for efficient CO_2 reduction under visible light. *J. Mater. Chem. A* **2017,** *5* (24), 12498-12505.
62. Yu, X.; Cohen, S. M., Photocatalytic metal-organic frameworks for the aerobic oxidation of arylboronic acids. *Chem. Commun. (Cambridge, U. K.)* **2015,** *51* (48), 9880-9883.
63. Zhang, S.; Li, L.; Zhao, S.; Sun, Z.; Luo, J., Construction of interpenetrated ruthenium metal-organic frameworks as stable photocatalysts for CO_2 reduction. *Inorg. Chem.* **2015,** *54* (17), 8375-8379.
64. Elgrishi, N.; Chambers, M. B.; Wang, X.; Fontecave, M., Molecular polypyridine-based metal complexes as catalysts for the reduction of CO_2. *Chem. Soc. Rev.* **2017,** *46* (3), 761-796.
65. N., H. S.; Lukas, S. M.; K., S. J., Photocatalytic Reduction of CO_2 on TiO_2 and Other Semiconductors. *Angew. Chem., Int. Ed.* **2013,** *52* (29), 7372-7408.
66. Suzuki, T. M.; Tanaka, H.; Morikawa, T.; Iwaki, M.; Sato, S.; Saeki, S.; Inoue, M.; Kajino, T.; Motohiro, T., Direct assembly synthesis of metal complex-semiconductor hybrid photocatalysts anchored by phosphonate for highly efficient CO_2 reduction. *Chem. Commun.* **2011,** *47* (30), 8673-8675.
67. Lacy, D. C.; McCrory, C. C. L.; Peters, J. C., Studies of Cobalt-Mediated Electrocatalytic CO_2 Reduction Using a Redox-Active Ligand. *Inorg. Chem.* **2014,** *53* (10), 4980-4988.
68. Gholamkhass, B.; Mametsuka, H.; Koike, K.; Tanabe, T.; Furue, M.; Ishitani, O., Architecture of Supramolecular Metal Complexes for Photocatalytic CO_2 Reduction: Ruthenium−Rhenium Bi- and Tetranuclear Complexes. *Inorg. Chem.* **2005,** *44* (7), 2326-2336.
69. Wang, C.-C.; Zhang, Y.-Q.; Li, J.; Wang, P., Photocatalytic CO_2 reduction in metal–organic frameworks: A mini review. *J. Mol. Struct.* **2015,** *1083*, 127-136.
70. Crake, A., Metal-organic frameworks based materials for photocatalytic CO_2 reduction. *Mater. Sci. Technol.* **2017,** *33* (15), 1737-1749.
71. Neatu, S.; Macia-Agullo, J. A.; Garcia, H., Solar light photocatalytic CO_2 reduction: general considerations and selected bench-mark photocatalysts. *Int. J. Mol. Sci.* **2014,** *15* (4), 5246-5262, 17 pp.
72. Fu, Y.; Sun, D.; Chen, Y.; Huang, R.; Ding, Z.; Fu, X.; Li, Z., An Amine-Functionalized Titanium Metal–Organic Framework Photocatalyst with Visible-Light-Induced Activity for CO_2 Reduction. *Angew. Chem., Int. Ed.* **2012,** *51* (14), 3364-3367.
73. Sun, D.; Fu, Y.; Liu, W.; Ye, L.; Wang, D.; Yang, L.; Fu, X.; Li, Z., Studies on Photocatalytic CO_2 Reduction over NH_2-UiO-66(Zr) and Its Derivatives: Towards a Better Understanding of Photocatalysis on Metal–Organic Frameworks. *Chem. - Eur. J.* **2013,** *19* (42), 14279-14285.
74. Li, J.; Luo, D.; Yang, C.; He, S.; Chen, S.; Lin, J.; Zhu, L.; Li, X., Copper(II) imidazolate frameworks as highly efficient photocatalysts for reduction of CO_2 into methanol under visible light irradiation. *J. Solid State Chem.* **2013,** *203*, 154-159.
75. Liu, Y.; Yang, Y.; Sun, Q.; Wang, Z.; Huang, B.; Dai, Y.; Qin, X.; Zhang, X., Chemical Adsorption Enhanced CO_2 Capture and Photoreduction over a Copper Porphyrin Based Metal Organic Framework. *ACS Appl. Mater. Interfaces* **2013,** *5* (15), 7654-7658.
76. Wang, S.; Yao, W.; Lin, J.; Ding, Z.; Wang, X., Cobalt Imidazolate Metal-Organic Frameworks Photosplit CO_2 under Mild Reaction Conditions. *Angew. Chem., Int. Ed.* **2014,** *53* (4), 1034-1038.
77. Li, L.; Zhang, S.; Xu, L.; Wang, J.; Shi, L.-X.; Chen, Z.-N.; Hong, M.; Luo, J., Effective visible-light driven CO_2 photoreduction via a promising bifunctional iridium coordination polymer. *Chem. Sci.* **2014,** *5* (10), 3808-3813.

78. Wang, D.; Huang, R.; Liu, W.; Sun, D.; Li, Z., Fe-Based MOFs for Photocatalytic CO_2 Reduction: Role of Coordination Unsaturated Sites and Dual Excitation Pathways. *ACS Catal.* **2014,** *4* (12), 4254-4260.
79. Lee, Y.; Kim, S.; Kang, J. K.; Cohen, S. M., Photocatalytic CO_2 reduction by a mixed metal (Zr/Ti), mixed ligand metal-organic framework under visible light irradiation. *Chem. Commun.* **2015,** *51* (26), 5735-5738.
80. Zhang, S.; Li, L.; Zhao, S.; Sun, Z.; Hong, M.; Luo, J., Hierarchical metal-organic framework nanoflowers for effective CO_2 transformation driven by visible light. *J. Mater. Chem. A* **2015,** *3* (30), 15764-15768.
81. Lee, Y.; Kim, S.; Fei, H.; Kang, J. K.; Cohen, S. M., Photocatalytic CO_2 reduction using visible light by metal-monocatecholato species in a metal-organic framework. *Chem. Commun.* **2015,** *51* (92), 16549-16552.
82. Xu, H.-Q.; Hu, J.; Wang, D.; Li, Z.; Zhang, Q.; Luo, Y.; Yu, S.-H.; Jiang, H.-L., Visible-Light Photoreduction of CO_2 in a Metal–Organic Framework: Boosting Electron–Hole Separation via Electron Trap States. *J. Am. Chem. Soc.* **2015,** *137* (42), 13440-13443.
83. Chen, D.; Xing, H.; Wang, C.; Su, Z., Highly efficient visible-light-driven CO_2 reduction to formate by a new anthracene-based zirconium MOF via dual catalytic routes. *J. Mater. Chem. A* **2016,** *4* (7), 2657-2662.
84. Zhang, H.; Wei, J.; Dong, J.; Liu, G.; Shi, L.; An, P.; Zhao, G.; Kong, J.; Wang, X.; Meng, X.; Zhang, J.; Ye, J., Efficient Visible-Light-Driven Carbon Dioxide Reduction by a Single-Atom Implanted Metal-Organic Framework. *Angew. Chem., Int. Ed.* **2016,** *55* (46), 14310-14314.
85. Ryu, U. J.; Kim, S. J.; Lim, H.-K.; Kim, H.; Choi, K. M.; Kang, J. K., Synergistic interaction of Re complex and amine functionalized multiple ligands in metal-organic frameworks for conversion of carbon dioxide. *Scientific Reports* **2017,** *7* (1), 612.
86. Logan, M. W.; Ayad, S.; Adamson, J. D.; Dilbeck, T.; Hanson, K.; Uribe-Romo, F. J., Systematic variation of the optical bandgap in titanium based isoreticular metal-organic frameworks for photocatalytic reduction of CO_2 under blue light. *J. Mater. Chem. A* **2017,** *5* (23), 11854-11863.
87. Crake, A.; Christoforidis, K. C.; Kafizas, A.; Zafeiratos, S.; Petit, C., CO_2 capture and photocatalytic reduction using bifunctional TiO_2/MOF nanocomposites under UV–vis irradiation. *Appl. Catal., B* **2017,** *210*, 131-140.
88. Yusuke, K.; Masato, S.; Kyohei, K.; Yoshifumi, M.; Yasutomo, G.; Soichi, S.; Shinji, I.; Hitoshi, I., Photocatalytic CO_2 Reduction by Periodic Mesoporous Organosilica (PMO) Containing Two Different Ruthenium Complexes as Photosensitizing and Catalytic Sites. *Chem. - Eur. J.* **2017,** *23* (43), 10301-10309.
89. Qin, J.; Wang, S.; Wang, X., Visible-light reduction CO_2 with dodecahedral zeolitic imidazolate framework ZIF-67 as an efficient co-catalyst. *Appl. Catal., B* **2017,** *209*, 476-482.
90. Sun, M.; Yan, S.; Sun, Y.; Yang, X.; Guo, Z.; Du, J.; Chen, D.; Chen, P.; Xing, H., Enhancement of visible-light-driven CO_2 reduction performance using an amine-functionalized zirconium metal-organic framework. *Dalton Trans.* **2018,** *47* (3), 909-915.
91. Wang, Y.; Huang, N.-Y.; Shen, J.-Q.; Liao, P.-Q.; Chen, X.-M.; Zhang, J.-P., Hydroxide Ligands Cooperate with Catalytic Centers in Metal–Organic Frameworks for Efficient Photocatalytic CO_2 Reduction. *J. Am. Chem. Soc.* **2018,** *140* (1), 38-41.
92. Liu, J.; Fan, Y.-Z.; Li, X.; Wei, Z.; Xu, Y.-W.; Zhang, L.; Su, C.-Y., A porous rhodium(III)-porphyrin metal-organic framework as an efficient and selective photocatalyst for CO_2 reduction. *Appl. Catal., B* **2018,** *231*, 173-181.
93. Tsuruoka, T.; Furukawa, S.; Takashima, Y.; Yoshida, K.; Isoda, S.; Kitagawa, S., Nanoporous Nanorods Fabricated by Coordination Modulation and Oriented Attachment Growth. *Angew. Chem., Int. Ed.* **2009,** *48* (26), 4739-4743.
94. Schaate, A.; Roy, P.; Godt, A.; Lippke, J.; Waltz, F.; Wiebcke, M.; Behrens, P., Modulated Synthesis of Zr-Based Metal-Organic Frameworks: From Nano to Single Crystals. *Chem. - Eur. J.* **2011,** *17* (24), 6643-6651.

95. Spingler, B.; Schnidrig, S.; Todorova, T.; Wild, F., Some thoughts about the single crystal growth of small molecules. *CrystEngComm* **2012,** *14* (3), 751-757.
96. *Instruction Manual for SU8200 Series Field Emission Scanning Electron Microscope*. Hitachi.
97. Thoresen, E. M.; Balcells, D.; Øien-Ødegaard, S.; Hylland, K. T.; Tilset, M.; Amedjkouh, M., Cyclometalated ruthenium complexes with carboxylated ligands from a combined experimental/computational perspective. *Dalton Trans.* **2018,** *47* (8), 2589-2601.
98. Xie, P.-H.; Hou, Y.-J.; Zhang, B.-W.; Cao, Y.; Wu, F.; Tian, W.-J.; Shen, J.-C., Spectroscopic and electrochemical properties of ruthenium(II) polypyridyl complexes. *J. Chem. Soc., Dalton Trans.* **1999,** (23), 4217-4221.
99. Grinberg, V. A.; Medved'ko, A. V.; Emets, V. V.; Kurzeev, S. A.; Kozyukhin, S. A.; Baranchikov, A. E.; Ivanov, V. K.; Andreev, V. N.; Nizhnikovskii, E. A., Cyclometalated ruthenium complex as a promising sensitizer in dye-sensitized solar cells. *Russ. J. Electrochem.* **2014,** *50* (6), 503-509.
100. Trickett, C. A.; Gagnon, K. J.; Lee, S.; Gándara, F.; Bürgi, H. B.; Yaghi, O. M., Definitive Molecular Level Characterization of Defects in UiO-66 Crystals. *Angew. Chem., Int. Ed.* **2015,** *54* (38), 11162-11167.
101. Gutov, O. V.; Hevia, M. G.; Escudero-Adán, E. C.; Shafir, A., Metal–Organic Framework (MOF) Defects under Control: Insights into the Missing Linker Sites and Their Implication in the Reactivity of Zirconium-Based Frameworks. *Inorg. Chem.* **2015,** *54* (17), 8396-8400.
102. Øien, S.; Wragg, D.; Reinsch, H.; Svelle, S.; Bordiga, S.; Lamberti, C.; Lillerud, K. P., Detailed Structure Analysis of Atomic Positions and Defects in Zirconium Metal–Organic Frameworks. *Cryst. Growth Des.* **2014,** *14* (11), 5370-5372.
103. Shearer, G. C.; Vitillo, J. G.; Bordiga, S.; Svelle, S.; Olsbye, U.; Lillerud, K. P., Functionalizing the Defects: Postsynthetic Ligand Exchange in the Metal Organic Framework UiO-66. *Chem. Mater.* **2016,** *28* (20), 7190-7193.
104. Sullivan, B. P.; Salmon, D. J.; Meyer, T. J., Mixed phosphine 2,2'-bipyridine complexes of ruthenium. *Inorg. Chem.* **1978,** *17* (12), 3334-3341.
105. Zelonka, R. A.; Baird, M. C., Benzene Complexes of Ruthenium(II). *Canadian Journal of Chemistry* **1972,** *50* (18), 3063-3072.
106. Fernandez, S.; Pfeffer, M.; Ritleng, V.; Sirlin, C., An Effective Route to Cycloruthenated N-Ligands under Mild Conditions. *Organometallics* **1999,** *18* (12), 2390-2394.
107. Ryabov, A. D.; Le Lagadec, R.; Estevez, H.; Toscano, R. A.; Hernandez, S.; Alexandrova, L.; Kurova, V. S.; Fischer, A.; Sirlin, C.; Pfeffer, M., Synthesis, Characterization, and Electrochemistry of Biorelevant Photosensitive Low-Potential Orthometalated Ruthenium Complexes. *Inorganic Chemistry* **2005,** *44* (5), 1626-1634.
108. Shearer, G. C.; Chavan, S.; Ethiraj, J.; Vitillo, J. G.; Svelle, S.; Olsbye, U.; Lamberti, C.; Bordiga, S.; Lillerud, K. P., Tuned to Perfection: Ironing Out the Defects in Metal–Organic Framework UiO-66. *Chem. Mater.* **2014,** *26* (14), 4068-4071.
109. Shearer, G. C.; Chavan, S.; Bordiga, S.; Svelle, S.; Olsbye, U.; Lillerud, K. P., Defect Engineering: Tuning the Porosity and Composition of the Metal–Organic Framework UiO-66 via Modulated Synthesis. *Chem. Mater.* **2016,** *28* (11), 3749-3761.
110. Wender, I., Reactions of synthesis gas. *Fuel Process. Technol.* **1996,** *48* (3), 189-297.
111. Le Lagadec, R.; Alexandrova, L.; Estevez, H.; Pfeffer, M.; Laurinavičius, V.; Razumiene, J.; Ryabov, A. D., Bis-Ruthena(III)cycles $[Ru(C\cap N)_2(N\cap N)]PF_6$ as Low-Potential Mediators for PQQ Alcohol Dehydrogenase (C∩N = 2-phenylpyridinato or 4-(2-tolyl)pyridinato, N∩N = bpy or phen). *Eur. J. Inorg. Chem.* **2006,** *2006* (14), 2735-2738.
112. Maina, J. W.; Schutz, J. A.; Grundy, L.; Des Ligneris, E.; Yi, Z.; Kong, L.; Pozo-Gonzalo, C.; Ionescu, M.; Dumee, L. F., Inorganic Nanoparticles/Metal Organic Framework Hybrid Membrane Reactors for Efficient Photocatalytic Conversion of CO_2. *ACS Appl. Mater. Interfaces* **2017,** *9* (40), 35010-35017.
113. Wang, M.; Wang, D.; Li, Z., Self-assembly of CPO-27-Mg/TiO_2 nanocomposite with enhanced performance for photocatalytic CO_2 reduction. *Appl. Catal., B* **2016,** *183*, 47-52.

114. Li, R.; Hu, J.; Deng, M.; Wang, H.; Wang, X.; Hu, Y.; Jiang, H.-L.; Jiang, J.; Zhang, Q.; Xie, Y.; Xiong, Y., Integration of an Inorganic Semiconductor with a Metal-Organic Framework: A Platform for Enhanced Gaseous Photocatalytic Reactions. *Adv. Mater. (Weinheim, Ger.)* **2014,** *26* (28), 4783-4788.
115. Liu, Y.; Kjær, K. S.; Fredin, L. A.; Chábera, P.; Harlang, T.; Canton, S. E.; Lidin, S.; Zhang, J.; Lomoth, R.; Bergquist, K.-E.; Persson, P.; Wärnmark, K.; Sundström, V., A Heteroleptic Ferrous Complex with Mesoionic Bis(1,2,3-triazol-5-ylidene) Ligands: Taming the MLCT Excited State of Iron(II). *Chem. Eur. J.* **2015,** *21* (9), 3628-3639.
116. Persson, P.; Sundström, V.; Lomoth, R.; Wärnmark, K., Lysande och lovande järnkomplex. *Kemivärlden Biotech med Kemisk Tidskrift* **2017,** (3), 20-21.